

NASA CR-134927



# Solar Electric Geocentric Transfer With Attitude Constraints: Analysis

Lester L. Sackett, Harvey L. Malchow, and Theodore N. Edelbaum  
The Charles Stark Draper Laboratory, Inc., Cambridge, Massachusetts

---

August 1975

## CAVEAT EMPTOR!

This copy of the SECKSPOT (Solar Electric Control Knob Setting Program by Optimal Trajectories) documentation may contain errors in sequencing or with overly clipped margins. Every attempt was made to make the best copy possible using state of the art reproduction equipment. Because the original documents have long since passed into the great landfill beyond, this “copy of a copy” is as close to the original as possible and is the best NASA Glenn Research Center can provide.

Use these documents to understand the workings of the program SEPSPOT. Be aware that this documentation describes an input implementation that does not exist in SEPSPOT. Refer to the “SEPSPOT Inputs” document that Glenn Research Center also distributes for the current input mechanism. What the reader will find here are two documents. One (Solar Electric Geocentric Transfer with Attitude Constraints: Analysis NAS3-18886) describes the theoretical underpinnings of SEPSPOT, the other (Solar Electric Geocentric Transfer with Attitude Constraints: Program Manual Draper Laboratory R-902) describes the program structure. Several pages are missing from the program structure manual. They are merely the source code listings that someone removed from our copy. Should you find an error in these documents especially the theoretical formulation manual, please report them to John P. Riehl or Dr. Leslie R. Balkanyi of Glenn Research Center. Current telephone and email addresses for these individuals can be found at <http://www.grc.nasa.gov/Doc/GRCfind.htm>.

## TABLE OF CONTENTS

### SUMMARY

<u>Section</u>	<u>Page</u>
1 INTRODUCTION	1
2 GENERAL TECHNIQUE	5
2.1 Introduction	5
2.2 Averaging	5
2.3 Optimal and Suboptimal Trajectories	6
2.4 Numerical Methods	12
3 LOW THRUST EQUATIONS	14
3.1 Introduction	14
3.2 Equinoctial Orbital Elements	14
3.3 The State Equations	20
3.4 The Canonical Equations	21
3.5 Geometry and Power	27
3.6 Thrust Direction	31
3.7 Oblateness	40
3.8 The Shadow Effect	41
3.9 Delay in Thrust Start-up after Leaving Shadow	41
3.10 Power and Fluence: The Damage Function	44
3.11 The Flux Equations	45
3.12 Summary of State and Costate Equations	48
3.13 Spacecraft Parameter Output	52
4 RADIATION AND POWER LOSS MODEL	57
4.1 Introduction	57
4.2 1 MEV Equivalent Electron Flux Field Model	59
4.3 Power Loss Model	68
4.4 Conclusions	69

TABLE OF CONTENTS (Cont.)

<u>Section</u>		<u>Page</u>
5	NUMERICAL RESULTS	70
5.1	Examples Without Power Degradations	70
5.2	Examples With Power Degradation	77
5.3	Run Time and Accuracy	92
6	CONCLUDING REMARKS	94
 <u>Appendix</u>		
A	HIGH THRUST EQUATIONS	96
A.1	Introduction	96
A.2	The High Thrust Code	96
A.3	Coupling of High and Low Thrust Code	100
B	THE MATRIX M AND ITS PARTIALS	109
C	AN ALTERNATE FORM OF THE M-MATRIX	115
D	SUN - EARTH RELATION	117
E	WORST CASE EVALUATION OF SUBOPTIMAL APPROXIMATION	119
F	SINGLE-AVERAGED OBLATENESS EQUATIONS	123
G	SHADOW CALCULATIONS	126
	LIST OF REFERENCES	129

## SUMMARY

This report is concerned with development and extension of a computer program for the study of mission performance of spacecraft using solar electric propulsion. The code is designed for analysis of the NASA/Lewis SERT-C design which involves attitude constraints, however, it has been generalized to consider any of the following configurations: (1) yaw motion only (SERT-C), (2) yaw and roll only, (3) unconstrained motion.

The code calculates time optimal or nearly time optimal geocentric trajectories. It uses the method of averaging to reduce computer time by orders of magnitude compared to a precision integrated trajectory. The averaged rates of change of the mean values of the state and costate are found by numerical quadrature. The differential equations for the mean state and costate may then be integrated in large time steps (typically days). A set of nonsingular orbital elements is used to avoid numerical difficulties for eccentricities and inclinations at or near zero. The radiation model is analytic to reduce run time. Included in the code are options for consideration of oblateness, solar motion, shadowing with or without a delay in thruster startup, an analytic radiation and power degradation model, and an initial high thrust stage of one or two impulses of specified  $\Delta V$ .

A costate formulation of the problem yields a two point boundary value problem which is solved by a Newton iteration on the initial costate and value of transfer time. Initial values of the unspecified states and costates and a guess for the transfer time are chosen. An optimal trajectory is then generated by integrating the averaged state and costate using a Runge-Kutta method. A Gaussian quadrature averages the state and costate derivative over an orbit. This will generate an optimal trajectory to the wrong terminal state. A sensitivity matrix is then generated by varying the initial conditions and running a set of neighboring trajectories. A Newton iteration on the initial conditions is then used to drive the terminal errors to within specified bounds. The final converged trajectory is a minimum time trajectory (nearly minimum time for attitude constraints) for the specified velocity increment in the high thrust phase (if included).

The attitude constraint causes power to become a function of thrust direction and sun direction, and the time optimal thrust direction becomes a complex function of primer vector direction. The analysis for the attitude constrained case is considerably more complicated than for the unconstrained case.

For the zero roll and pitch case a suboptimal control is developed which is nearly time optimal, uses less fuel than the time optimal, and is obtained from the solution of a cubic equation. The solution may yield discontinuous changes in the thrust direction. The time delay in thruster startup is modeled as a quadratic function of time in shadow. The proton and electron radiation field is modeled as equivalent 1 MEV particle flux as a function of spacecraft altitude and latitude as well as the solar cell shield thickness. The power loss function is modeled as an analytic function of fluence, cell thickness and base resistivity. Spacecraft parameters such as yaw angle and sun incidence angles may be displayed.

Numerical results were obtained for many SERT-C and other type missions. Attitude constraints increase flight times by a few percent for SERT-C type missions. Power degradation can be quite severe at lower altitudes nearly doubling transfer time, compared to a no degradation case.

## SECTION 1

### INTRODUCTION

The use of time optimal trajectories can save considerable flight time in low thrust missions (days, weeks or even months). As a result there has been considerable use of optimization theory in the analysis of low thrust trajectories and missions. Recent advance in the state of the art have made possible routine calculation of geocentric optimal trajectories considering more representative environmental constraints and influences. It has recently been proposed<sup>(1)</sup> that optimal trajectory computer programs form the basis of a guidance technique.

Most of the geocentric trajectory analyses for solar electric spacecraft have assumed fully articulated spacecraft where the solar array and the thrust vector can both be pointed in their respective optimum direction<sup>(2-5)</sup>. The SERT-C<sup>(6)</sup> spacecraft study performed at NASA-Lewis introduced attitude motion constraints whereby the spacecraft was permitted to rotate only about an axis parallel to the Earth radius vector. This design constrains the thrust vector to lie in a plane perpendicular to the radius vector. The solar panels can rotate about an axis that is orthogonal to both the radius vector and the nominal thrust vector. Although the constraints simplified the SERT-C design and reduced the attitude sensor requirements<sup>(6)</sup>, the constraint couples the power developed to the thrust direction. Most thrust orientations do not allow maximum power to be developed. The flight time is increased both because of this coupling and because of the thrust direction constraint.

The present study, performed for the NASA Lewis Research Center, was undertaken both to provide software for the evaluation of the SERT-C design with attitude constraints and to provide a basis for the proposed guidance scheme. The effort described in this report builds on the work of References 2, 7, and 9. For that effort a computer program was developed which calculated minimum time trajectories for unconstrained solar electric and nuclear electric propulsion. Also an initial high thrust stage of specified  $\Delta V$  with one or two impulses and a final impulse could be included. The low thrust stage uses Kryloff-Bogoliuboff averaging<sup>(10)</sup> of both the state and the costate. The averaged rates of change of the mean values of the state and costate are found by numerical quadrature. The

differential equations for the mean state and costate may then be integrated in large time steps (typically days). A set of nonsingular orbital elements, the equinoctial elements<sup>(11)</sup>, is used to avoid numerical difficulties. The method of averaging has been used extensively in recent years. Edelbaum<sup>(12, 13)</sup> has used averaging to calculate analytic solutions for special cases of optimal low thrust trajectories, and others have used averaging when considering effects such as oblateness, third body perturbations and non-optimal thrusting<sup>(14, 15, 16)</sup>. Jasper<sup>(3)</sup> utilizes equinoctial orbital elements and averaging in recent low thrust optimization work. An interesting feature of his work is numerical comparisons of averaging with integration of the full state and costate. He does not include the effects of perturbing forces, other than thrust, on the costate.

The first stage high thrust optimization is based on a very efficient computer program developed by Huntington Small<sup>(17, 18)</sup>. This program uses a special set of variables and form of the switching conditions developed by Small. The initial orbit is assumed circular with specified semimajor axis and inclination, while the final orbit has specified semimajor axis, eccentricity, and inclination. During the high thrust phase an inverse square gravitational field is assumed. Because the initial orbit is circular, it was possible to constrain the initial costate to the region that yields solutions. This program rapidly calculates either one or two impulse, minimum-fuel, time-open trajectories. Because this transfer always requires less than a full revolution, its time is negligible compared to the low thrust phase and is not considered. A summary of the high thrust analysis is given in Appendix A. The utilization of high and low thrust in combination has been considered by a number of authors<sup>(19, 20, 21, 22, 23)</sup>.

The effect of oblateness is included by analytically adding its associated rate of change of the mean state and costate to that due to thrust. The effects of shadowing are calculated by assuming that thrust is turned off in shadow. The shadow entrance and exit times are calculated analytically by solving a quartic equation. The effects of radiation degradation are calculated by modeling equivalent 1 MEV-electron flux as a function of radius and latitude. The power is then expressed as a function of the total accumulated particle fluence. The model in the first version of the program was valid for one cell and shield thickness. A new model, developed herein, is valid for a variety of cell thickness, shield thicknesses and base resistivities. As for all perturbations, the effect of radiation degradation on the costate as well as the state is calculated.

The overall trajectory is optimized by a shooting method. Initial values of the unspecified states and costates are chosen at the initial time. An optimum high

and low thrust trajectory is then generated by integrating the state and costate through both stages. This will generate an optimal trajectory to the wrong terminal state. A sensitivity matrix is then generated by varying the initial conditions and running a set of neighboring trajectories. A Newton iteration on the initial conditions is then used to drive the terminal errors to within specified bounds. The final converged trajectory is a minimum time trajectory (nearly minimum time for attitude constraints) for the specified velocity increment in the high thrust phase.

The principle modifications and additions performed under this contract to the earlier work are: nearly time optimal trajectories can be generated for the attitude constrained case of zero roll and pitch or zero pitch and free roll as well as the unconstrained case; the shadow model has been modified to include the effect of a delay in thruster turn-on after leaving the shadow; a new, more accurate and more general solar array degradation model is developed; and additional spacecraft parameters may be calculated and displayed. All of the options of the earlier code are included except that the final impulse option has been removed.

The problem, then, which is considered in this report is the calculation of time optimal or nearly optimal geocentric transfers using solar electric spacecraft which may have attitude constraints and an optional initial high thrust stage. For the low thrust phase the initial and final orbits are general ellipses. An inverse square gravity field with oblateness is assumed. Thrust is assumed proportional to power with constant specific impulse and efficiency. The effect on power of solar distance may be included. The thrusters may be assumed to be off while the spacecraft is in Earth's shadow and for a start-up delay time which corresponds to the sum of the time for the solar array to achieve operating temperature and the time for the thruster to achieve full thrust after the solar array power is applied to the power processor. The Van Allen radiation is modeled analytically and its effect on power degradation included.

For the attitude constrained case the class of spacecraft modeled is indicated in Figure 1-1 where the roll axis lies in the orbit plane and is perpendicular to the Earth-spacecraft radius vector; the yaw axis is parallel to the Earth radius vector directed toward the Earth; the pitch axis is perpendicular to the orbit plane and directed south. For the nominal attitude the principle body-centered axes are aligned with this coordinate system. The ion thrusters are mounted on the negative roll face of the spacecraft and directed parallel to the roll axis. The solar arrays are flat panels and are capable of rotation about their longitudinal axis, which is aligned with the spacecraft pitch axis. The required low thrust directions are achieved entirely by the spacecraft attitude rotations.

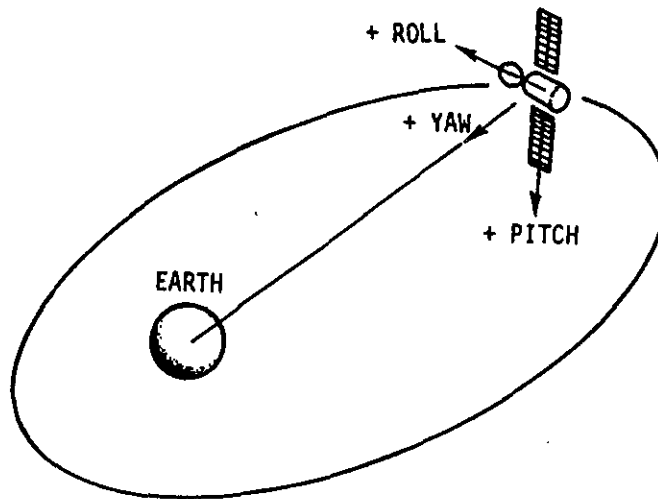


Figure 1-1 Spacecraft Configuration

The thrust vector must have no component along the vector from Earth to spacecraft. The thrust direction is determined by one control variable, the yaw angle. Since pitch and roll are constrained to be zero, the orientation of the axis of the solar panels is determined by the yaw angle. The panels are allowed to rotate about this axis, resulting in one more control variable. Power is assumed to be proportional to the cosine of the angle between the normal to the panels and the line to the sun. The initial state is given and it is desired to reach a final subset of the state at some, unspecified, final time. Although the original aim was to derive the time optimal control, instead, a particular suboptimal control, which is nearly time optimal, is derived. A costate formulation is used along with the method of averaging to set up a two point boundary value problem which can be solved by using a Newton method to iterate on the unknown initial costate and value of the final time in order to meet the desired final conditions on the state and costate.

The computer program developed is used to assess the increase in flight time and fuel consumption due to introducing the attitude constraints and other perturbations. A User's Manual which contains listings and descriptions of the subroutines and a description of the use of the code is published separately<sup>(24)</sup>. Two papers have been presented based on the material in this report<sup>(25, 26)</sup>. Reference 25 has been accepted in modified form to be published in The Journal of Spacecraft and Rockets.

## SECTION 2

### GENERAL TECHNIQUE

#### 2.1 Introduction

Three areas of general technique are discussed in this section. One is the method of averaging, essential to the running of a program which generates many trajectories in a reasonable amount of computer time. Second is discussed the method of generation of the final trajectory. A time optimal or nearly optimal trajectory is desired. A state and costate formulation is used which results in a two point boundary value problem which can be solved by a Newton iteration procedure. Finally some comments on numerical techniques are made. Later sections give details of the dynamical equations, calculation of the control, and the effects of perturbations on an individual trajectory.

#### 2.2 Averaging

A great savings in computer time can be effected by considering a first approximation to the state and costate. Short period variations in the state and costate are eliminated by the averaging technique. When low thrust propulsion is utilized and the other perturbations to the inverse square motion are small and when the state includes the five slowly varying orbital elements which indicate the size, shape and orientation of an orbit and possibly other slowly varying quantities, then averaging may be used. Spacecraft mass and the accumulated particle fluence (both slowly varying) were also averaged. The orbital element indicating the position of the spacecraft in the orbit is eliminated by the averaging process.

The averaged Hamiltonian can be defined as

$$\tilde{H} = \frac{1}{T} \int_{t-\frac{T}{2}}^{t+\frac{T}{2}} H dt \quad (2.1)$$

where  $H$  is the unaveraged Hamiltonian and  $T$  is the orbital period. When calculating this integral the state and costate are held fixed. The motion of the spacecraft is assumed to vary in a manner described by Kepler's equation over the averaging integration. The approximate state and costate satisfy the canonical equations

$$\underline{\dot{\bar{x}}}^T = \frac{\partial \tilde{H}}{\partial \bar{\lambda}} \quad (2.2)$$

$$\underline{\dot{\bar{\lambda}}}^T = - \frac{\partial \tilde{H}}{\partial \bar{x}} \quad (2.3)$$

where the overbar indicates the approximate quantities.

In what follows the averaging integral for oblateness ( $J_2$ ) is solved analytically; otherwise a numerical quadrature formula is used. The differential equations can then be solved numerically using a time step which is much larger than but unrelated to the number of orbital revolutions.

### 2.3 Optimal and Suboptimal Trajectories

The original aim was to calculate time optimal trajectories for the constrained problem as well as the unconstrained problem. However in the course of the analysis, which is described more fully in Section 3, it was decided to use a slightly suboptimal control for the constrained case of zero roll and pitch. The suboptimal control chosen is nearly time optimal, saves on fuel, and it is easier to calculate. The controls considered for the zero pitch but free roll case and the unconstrained case are time optimal. Transversality conditions for the time optimal control are used for all cases. In the following discussion the words "optimal trajectory" will be used to refer to both the optimal and suboptimal trajectories. In all cases the method used to generate a low thrust trajectory is to develop the Hamiltonian, to calculate a control (the thrust direction), either optimal or suboptimal, and to write the canonical equations for the state and costate. Some or all of the initial state and costate are specified. Application of transversality conditions for the time optimal problem yield additional specifications on the state and costate. Thus a two point boundary value problem results which must be solved to obtain the requisite trajectory. When these equations are solved, an extremal trajectory will result which is usually locally optimal. No attempt is made to investigate generalized Jacobi-type conditions to establish local sufficiency. Also, in common with other nonlinear problems, there may be more than one extremal meeting the same end conditions. The very difficult question of global optimality is not considered.

The single trajectory generation portion of the code is coupled with a Newton iterator to solve the two point boundary value problem. The unknown initial conditions and value of the final time are iterated on in order to meet the final conditions which are functions of the final state and costate (usually a specified

semimajor axis, eccentricity, and inclination and the appropriate transversality conditions). The partial derivative matrix of final conditions with respect to the initial costate is obtained numerically by calculating neighboring trajectories to a nominal.

When only low thrust is included the initial orbit is specified as well as the mass of the spacecraft. A seventh state variable, the equivalent 1 MEV electron fluence is also specified. At the unknown final time either five orbital elements can be specified or three: the semimajor axis,  $a$ , the eccentricity,  $e$ , and the inclination,  $i$ . Transversality conditions require that the adjoint to the mass and fluence be zero at the final time. If the final line of nodes ( $\Omega$ ) and argument of perigee ( $\omega$ ) are free, then their adjoints are zero ( $\lambda_{\Omega} = 0, \lambda_{\omega} = 0$ ). In either case the final value of the Hamiltonian must be unity.

If initial high thrust is included, the necessary conditions for minimum time low-thrust transfer with specified high thrust velocity increments can be derived by considering each phase separately as a variational problem. The cost of each phase can then be expressed as a function of its terminal states and costates. The proper interface conditions for each phase can then be derived by considering the parameter optimization problem of minimizing the time of the low thrust phase for fixed velocity increments in the high thrust phases. This minimization is carried out over all the free states and costates at the interfaces between high and low thrust

The flight time for the high thrust stages is assumed to be negligible compared to the low thrust stage flight time. At the beginning of the first high thrust stage  $a, e, i$  are assumed given (eccentricity is set to zero). Transversality conditions then require  $\lambda_{\Omega} = 0$  and  $\lambda_{\omega} = 0$ .

For the high thrust phases only an inverse square gravity field is assumed.  $\lambda_{\Omega}$  is a constant of the motion and therefore  $\lambda_{\Omega}$  remains zero during the initial high thrust phase if  $\Omega$  is fixed. A single extremal is generated in the following fashion (it does not necessarily reach the desired final conditions). Values for  $\lambda_a, \lambda_e, \lambda_i$ , and  $\omega$  are picked. Values for  $\lambda_m, \lambda_N, t_f$  are also picked but not used until after the first high thrust stage. Since the initial orbit is circular we are assuming that the first impulse occurs at  $u = f + \omega$  where  $f = 0$  and so  $\omega$  just indicates the location in the orbit of the first impulse. From the standpoint of maximizing the primer vector magnitude, the location on the orbit at which an impulse occurs is arbitrary, since for a circular orbit one position cannot be distinguished from another. Optionally, the user may specify the initial line of nodes. There is then an impulse in the direction of the primer vector. The magnitude of the  $\Delta V$  will be equal to the maximum for an optimal one impulse transfer if that maximum is less than the specified total initial  $\Delta V$ , or otherwise equal to the specified total initial  $\Delta V$ . If

the maximum one impulse  $\Delta V$  is less than the total  $\Delta V$  available, then a second impulse occurs at the next maximum of the Hamiltonian, again in the direction of the primer vector. The program requires that all remaining initial high thrust  $\Delta V$  be used for this impulse. This may not be optimal, as one or more additional impulses may be optimal. Generally, for practical cases one or two impulses will be optimal.

After the one or two initial impulses there is a resultant orbit  $a, e, i, \Omega, \omega$  and values for  $\lambda_a, \lambda_e, \lambda_i, \lambda_\Omega, \lambda_\omega$ . The high thrust program scales the costate so that the magnitude of the primer vector is 1 at the impulses. At the beginning of the low thrust stage they may need to be rescaled so that final transversality conditions will be met. This scaling factor, the picked values of  $\lambda_m, \lambda_N$  and the values of  $\lambda_a, \lambda_e, \lambda_i, \lambda_\Omega, \lambda_\omega$  from the high thrust stage are then used as input to the low thrust equations of motion. These are essentially Eqs. (2.2) and (2.3). They are integrated to the picked final time,  $t_f$ . The final orbit is then reached. This is an extremal trajectory, though possibly not arriving at the desired final orbit.

We desire to reach a specified  $a, e, i$ . Transversality conditions require that  $\lambda_\Omega, \lambda_\omega, \lambda_m, \lambda_N$  be zero and that  $H = 1$ . If we have not met these final conditions a Newton iteration on the free initial conditions and time of flight is used in order to meet the final conditions to within some tolerance.

The actual calculations of the initial high thrust stage uses code developed by H. Small<sup>(12, 13)</sup> which uses a special set of variables. (See Appendix A.) The low thrust code uses equinoctial orbital elements rather than classical orbital elements. This stage is discussed in detail in Section 3.

The Newton method works by first guessing values for the iteration parameters, call them  $\underline{x}$  and  $t_f$ , and then running a nominal trajectory which will yield final conditions  $\underline{y}$  which in general are not equal to the desired final conditions,  $\underline{y}_d$ . Revised values for  $\underline{x}, t_f$  may then be obtained by calculating a sensitivity matrix or partial derivative matrix,  $A$ , which is generated by varying slightly, one at a time, each of the iteration parameters,  $\underline{x}$ , and running a new, neighboring, trajectory. Differencing the resulting values of the final conditions with the nominal values yields a  $\Delta y$  for each  $\Delta x_i$ . In addition  $\frac{\partial y}{\partial t_f}$  can be calculated analytically except perhaps for  $\frac{\partial H}{\partial t_f}$  which can be approximated numerically by varying  $t_f$  slightly and evaluating the corresponding  $H$ , differencing this with the nominal  $H$  and dividing by  $\Delta t_f$ . Then  $A$  is an approximation for the partial of  $\underline{y}$  with respect to  $\underline{x}, t_f$ .

$$A = \begin{bmatrix} \frac{\Delta y^T}{\Delta x} \\ \frac{\partial y^T}{\partial t_f} \end{bmatrix} \quad (2.4)$$

A revised estimate of the iteration parameters can then be obtained by the formula

$$\begin{bmatrix} \underline{x} \\ t_f \end{bmatrix}_{\text{NEW}} = \begin{bmatrix} \underline{x} \\ t_f \end{bmatrix}_{\text{OLD}} - A^{-1}(\underline{y} - \underline{y}_d) \quad (2.5)$$

A new nominal trajectory can then be generated and the procedure continued until the final conditions are met to within some tolerance. In the event that the new  $\underline{x}$ ,  $t_f$  do not yield a reduction in the norm of the final condition errors, the change in  $(\underline{x}, t_f)$  is reduced in magnitude by factors of 2. Also there is an option of using a modified Newton-Raphson procedure wherein the A matrix is not always recalculated at each iteration by running neighboring trajectories, but instead a new A may be approximated using the old A and the values of the changes in  $\underline{x}$ ,  $t_f$ .

We will now specify more precisely the initial and final conditions. Since the low thrust code uses equinoctial elements, they will be defined here in terms of the classical elements,

$$\begin{aligned} a &= a \\ h &= e \sin(\omega + \Omega) \\ k &= e \cos(\omega + \Omega) \\ p &= \tan\left(\frac{i}{2}\right) \sin \Omega \\ q &= \tan \frac{i}{2} \cos \Omega \end{aligned} \quad (2.6)$$

These are five of the seven state variables. The other two are mass,  $m$ , and particle radiation fluence,  $N$ .

The Newton iteration scheme iterates on a vector  $\underline{x}$  to drive a vector  $\underline{y}$  to zero, where now we are using  $\underline{y}$  to mean  $\underline{y} - \underline{y}_d$  as used above. Separately coded is the iteration variable  $t_f$ , the final time.  $\underline{x}$  is a function of the unknown state or co-state elements at the initial time;  $\underline{y}$  is the error in the final conditions, a function of the state and costate at the final time and the Hamiltonian at the final time.

Two final conditions options are considered. In the first, all five orbital elements are specified at the final time. Thus,

$$\underline{y} = \begin{bmatrix} a(t_f) - a_d \\ h(t_f) - h_d \\ k(t_f) - k_d \\ p(t_f) - p_d \\ q(t_f) - q_d \\ \lambda_m(t_f) \\ \lambda_N(t_f) \\ H(t_f) - 1 \end{bmatrix} \quad (2.7)$$

where the subscript  $_d$  indicates the desired value.

For the second option only three orbital elements (a, e, i) are specified. The adjoints to  $\Omega(t_f)$  and  $\omega(t_f)$  must then be driven to zero. They are given in terms of the equinoctial state and costate.

$$\lambda_{\Omega} = \lambda_{\omega} + q\lambda_p - p\lambda_q \quad (2.8)$$

$$\lambda_{\omega} = k\lambda_h - h\lambda_k \quad (2.9)$$

The eccentricity and inclinations are given by

$$e = \sqrt{h^2 - k^2} \quad (2.10)$$

$$i = 2 \tan^{-1} \sqrt{p^2 + q^2} \quad (2.11)$$

For this case, then, let

$$\underline{y} = \begin{bmatrix} a(t_f) - a_d \\ \sqrt{h^2(t_f) - k^2(t_f)} - e_d \\ \sqrt{p^2(t_f) + q^2(t_f)} - \tan \frac{i_d}{2} \\ h(t_f)\lambda_k(t_f) - k(t_f)\lambda_h(t_f) \\ p(t_f)\lambda_q(t_f) - q(t_f)\lambda_p(t_f) \\ \lambda_m(t_f) \\ \lambda_N(t_f) \\ H(t_f) - 1 \end{bmatrix} \quad (2.12)$$

When  $i_d = 0$  driving the above  $\underline{y}$  to zero is equivalent to driving p and q to zero and not considering  $p\lambda_q - k\lambda_p$ . When calculating small errors near  $i_d = 0$ , the above  $\underline{y}$  expression cannot distinguish between positive or negative inclinations. This can lead to numerical problems, so when  $i_d = 0$ , the code sets the third component of  $\underline{y}$  to  $p(t_f)$  and the fifth component to  $q(t_f)$  in the SEP code. A similar situation exists if  $e_d = 0$ , so in this case the second component is  $h(t_f)$  and the fourth component  $k(t_f)$ . If both  $e_d = 0$  and  $i_d = 0$ , then both options are equivalent in the SEP code.

For low thrust only, the initial state must be specified, and therefore  $\underline{x}$  is just the initial costate. When initial impulses are included either  $\omega$  and  $\Omega$  are free or just  $\omega$  is free. Since the initial orbit is circular for this case,  $\omega$  indicates the location of the first impulse. Thus  $\lambda_\omega(t_0) = 0$ . If  $\Omega(t_0)$  is free,  $\lambda_\Omega(t_0) = 0$ . It is shown in Appendix A that for the  $\Omega(t_0)$  specified case, setting the initial  $\omega$  determines the initial  $\lambda_\Omega$ . Thus  $\omega$  is used as the iteration variable. The high thrust code requires special input variables and these variables must be within specific bounds if a circular parking orbit is assumed (Appendix A). Taking into account these bounds let  $\xi_1, \xi_2, \xi_3$  be the first three iteration parameters where Small's special variables are given by

$$T = \frac{\pi}{2} \frac{\xi_1}{\sqrt{1 + \xi_1^2}} \quad (2.13)$$

$$k = \cos T \left( .75 + .25 \frac{\xi_2}{\sqrt{1 + \xi_2^2}} \right) \quad (2.14)$$

$$j = (1 + k \cos T) \sqrt{\frac{\cos T - k}{\cos T + k}} \frac{\xi_3}{\sqrt{1 + \xi_3^2}} \quad (2.15)$$

This transformation allows  $\xi_1, \xi_2,$  and  $\xi_3$  to be unbounded.

In order to interface the high and low thrust stages a correspondence or scale factor is needed to relate the respective costates where

$$c = \frac{\partial t_f}{\partial \Delta V_{\text{HIGH}}} \quad (2.16)$$

and  $t_f$  and  $\Delta V_{\text{HIGH}}$  refer to the respective costs for the two stages. Then

$$\lambda_z \Big|_{\text{LOW}} = c \lambda_z \Big|_{\text{HIGH}} \quad (2.17)$$

The iteration parameters are then

$$\underline{x} = \begin{bmatrix} \xi_1 \\ \xi_2 \\ \xi_3 \\ c \\ \Omega \text{ or } \omega \\ \lambda_m \\ \lambda_N \end{bmatrix} \quad (2.18)$$

and recall that the initial  $a$ ,  $e$ ,  $i$ ,  $\lambda$ ,  $\omega$  and  $\Omega$  are specified.

If roll is free so that the panels can always face the sun and if shadowing is not included, then the perturbations on the spacecraft are axially symmetric. The perturbations modeled are oblateness and the Van Allen radiation. The latter was forced to be axial symmetric by the particular model used. Therefore,  $\lambda$  is theoretically constant and varying  $\Omega$  at the initial time will only affect  $\Omega$  at the final time. Thus if  $\Omega$  at the final time is not specified, the sensitivity matrix will be singular. For this case the  $\Omega$  should be specified.

The sensitivity matrix is calculated by varying each  $x_i$  by a small amount and comparing the resulting error in the final conditions with the nominal.

$$\frac{\partial \underline{y}}{\partial x_i} \approx \frac{\underline{y}(\underline{x} + \Delta \underline{x}) - \underline{y}(\underline{x})}{\Delta x_i} \quad (2.19)$$

Except for  $\frac{\partial(H-1)}{\partial t_f}$  the partial of  $\underline{y}$  with respect to  $t_f$  can be calculated analytically since the derivatives of the state and costate are known at the final time. For example -

$$\frac{\partial y_2}{\partial t_f} = \dot{h}(t_f) \quad (2.20)$$

The other partials are obtained similarly except for the partial of the Hamiltonian.

For SEP the time dependence of the Hamiltonian derives from the shadow effect and solar distance and direction and therefore an analytical evaluation is difficult. Therefore, the partial was obtained numerically by varying  $t_f$  slightly and re-evaluating the state derivative (holding the state and costate constant) and then evaluating the Hamiltonian. Thus

$$\frac{\partial H(t_f)}{\partial t_f} \approx \frac{\underline{\lambda}^T(t_f) (\underline{x}(t_f + \Delta t_f) - \dot{\underline{x}}(t_f) \Delta t_f)}{\Delta t_f} \quad (2.21)$$

## 2.4 Numerical Methods

A Newton-Raphson iterator is used which calculates the sensitivity matrix by running neighboring trajectories by changing slightly the initial values of the iteration parameters, one at a time. The size of the change in the iteration variables is chosen by the user and can affect the accuracy of the matrix. A Modified Newton-Raphson iterator uses basically the same technique but many of the iterations make use of a modified sensitivity matrix rather than calculating a new one by running neighboring trajectories at each iteration.

The low thrust differential equations are integrated using a fourth order Runge-Kutta method. The time step is selected by the user. This is fixed for one subroutine supplied or may internally be changed if the IBM Scientific Subroutine version is used<sup>(27)</sup>, in which case error weights and an upper error bound must be supplied by the user. Cutting the size of the time step can increase the accuracy of the trajectory but rapidly increase run time.

Numerical averaging utilizes a Gaussian quadrature. The number of points sampled on an orbit can largely be determined by the user. Again, more points increase accuracy at the expense of run time.

## SECTION 3

### LOW THRUST EQUATIONS

#### 3.1 Introduction

This section develops most of the new analytic results. Some of these new results are based on previous work, which is included in summary form, often in appendices. The new results include the derivation of the attitude constrained thrust control, the effect of a delay in thruster turn-on after leaving the shadow, the new solar array degradation model and the calculation of several spacecraft parameters.

#### 3.2 Equinoctial Orbital Elements

By using equinoctial orbital elements the singularities that occur for zero eccentricity or inclinations of zero or ninety degrees when using classical orbital elements are avoided. (For inclinations near  $180^\circ$  retrograde equinoctial orbital elements can be used, although we will not consider that case in this report.) The formulas given in this section are taken from Reference 16 except for the costate transformations.

The direct equinoctial orbital elements are defined in terms of the classical orbital elements,  $a$ ,  $e$ ,  $i$ ,  $\Omega$ , and  $\omega$  by the formulas

$$\begin{aligned} a &= a \\ h &= e \sin(\omega + \Omega) \\ k &= e \cos(\omega + \Omega) \\ p &= \tan\left(\frac{i}{2}\right) \sin \Omega \\ q &= \tan\left(\frac{i}{2}\right) \cos \Omega \end{aligned} \tag{3.1}$$

In Reference 16 the sixth orbital element is the mean longitude at epoch. In this paper we will consider the eccentric longitude,  $F$ , as the sixth element, defined by

$$F = E + \omega + \Omega \tag{3.2}$$

where  $E$  is the eccentric anomaly. This element will be eliminated from the dynamical equations by the averaging process.

The inverse relationships are defined by

$$\begin{aligned}
 a &= a \\
 e &= (h^2 + k^2)^{1/2} \\
 i &= 2 \tan^{-1} \left( \sqrt{\frac{p^2 + q^2}{p^2 + q^2}} \right) \\
 \Omega &= \tan^{-1}(p/q) \\
 \omega &= \tan^{-1}(h/k) - \tan^{-1}(p/q)
 \end{aligned} \tag{3.3}$$

The equinoctial coordinate frame is defined by the basis vectors  $\hat{f}$ ,  $\hat{g}$ ,  $\hat{w}$ , which are given below with respect to an earth equatorial coordinate frame.

$$\begin{aligned}
 \hat{f} &= \frac{1}{1 + p^2 + q^2} \begin{bmatrix} 1 - p^2 + q^2 \\ 2pq \\ -2p \end{bmatrix} \\
 \hat{g} &= \frac{1}{1 + p^2 + q^2} \begin{bmatrix} 2pq \\ 1 + p^2 - q^2 \\ 2q \end{bmatrix} \\
 \hat{w} &= \frac{1}{1 + p^2 + q^2} \begin{bmatrix} 2p \\ -2q \\ 1 - p^2 - q^2 \end{bmatrix}
 \end{aligned} \tag{3.4}$$

This coordinate frame is illustrated in Figure 3-1 where  $\hat{w}$  is normal to the orbital plane.

The equinoctial orbital elements can be calculated from position and velocity. The semimajor axis is given by

$$a = \left( \frac{2}{|r|} - \frac{|\dot{r}|^2}{\mu} \right)^{-1} \tag{3.5}$$

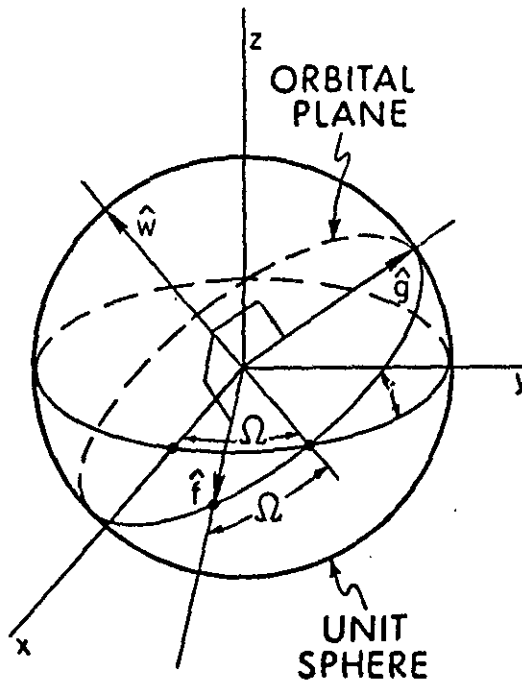


Figure 3-1. The equinoctial coordinate frame.

The eccentricity vector is given by

$$\underline{e} = -\frac{\underline{r}}{|\underline{r}|} - \frac{(\underline{r} \times \dot{\underline{r}}) \times \dot{\underline{r}}}{\mu} \quad (3.6)$$

The vector normal to the orbital frame is given by

$$\hat{\underline{w}} = \frac{\underline{r} \times \dot{\underline{r}}}{|\underline{r} \times \dot{\underline{r}}|} \quad (3.7)$$

Then

$$p = \frac{\hat{w}_x}{1 + \hat{w}_z} \quad (3.8)$$

$$q = \frac{-\hat{w}_y}{1 + \hat{w}_z} \quad (3.9)$$

From the values of  $p$  and  $q$  and Eq. (3.4)  $\hat{f}$  and  $\hat{g}$  may be computed. Then

$$\begin{aligned} h &= \underline{e} \cdot \hat{g} \\ k &= \underline{e} \cdot \hat{f} \end{aligned} \quad (3.10)$$

Further relationships include the position coordinates  $X_1, Y_1$  with respect to the  $\hat{f}, \hat{g}, \hat{w}$  frame,

$$\begin{aligned} X_1 &= \underline{r} \cdot \hat{f} \\ Y_1 &= \underline{r} \cdot \hat{g} \end{aligned} \quad (3.11)$$

and the eccentric longitude,  $F$ , where

$$\begin{aligned} \cos F &= k + \frac{(1 - k^2 \beta) X_1 - hk \beta Y_1}{a \sqrt{1 - h^2 - k^2}} \\ \sin F &= h + \frac{(1 - k^2 \beta) Y_1 - hk \beta X_1}{a \sqrt{1 - h^2 - k^2}} \end{aligned} \quad (3.12)$$

where

$$\beta = \frac{1}{1 + \sqrt{1 - h^2 - k^2}} \quad (3.13)$$

The mean longitude is defined by

$$\lambda = M + \omega + \Omega \quad (3.14)$$

The eccentric longitude,  $F$ , was defined in Eq. (3.2). Kepler's equation in terms of  $\lambda$  and  $F$  is then given by

$$\lambda = F - k \sin F + h \cos F \quad (3.15)$$

We will not make use of the true longitude

$$L = v + \omega + \Omega \quad (3.16)$$

M, E, v are the mean, eccentric, and true anomalies, respectively.

Position and velocity are given by

$$\underline{r} = X_1 \hat{f} + Y_1 \hat{g} \quad (3.17)$$

$$\underline{\dot{r}} = \dot{X}_1 \hat{f} + \dot{Y}_1 \hat{g} \quad (3.18)$$

where

$$X_1 = a[(1-h^2\beta) \cos F + hk\beta \sin F - k] \quad (3.19)$$

$$Y_1 = a[(1-k^2\beta) \sin F + hk\beta \cos F - h] \quad (3.20)$$

$$\dot{X}_1 = \frac{na^2}{r} [hk\beta \cos F - (1-h^2\beta) \sin F] \quad (3.21)$$

$$\dot{Y}_1 = \frac{na^2}{r} [(1-k^2\beta) \cos F - hk\beta \sin F] \quad (3.22)$$

and

$$n = \sqrt{\frac{\mu}{a^3}} \quad (3.23)$$

$$\frac{r}{a} = 1 - k \cos F - h \sin F \quad (3.24)$$

$\mu$  is the earth gravitational constant.

The adjoints to the classical and the equinoctial orbital elements are related. Let  $\underline{\lambda}$  represent the adjoints to a, h, k, p and q, and let  $\underline{\psi}$  represent the adjoints to a, e, i,  $\Omega$  and  $\omega$ . Then

$$\begin{bmatrix} \lambda_a \\ \lambda_h \\ \lambda_k \\ \lambda_p \\ \lambda_q \end{bmatrix} = \begin{bmatrix} 1 & 0 & 0 & 0 & 0 \\ 0 & \sin(\omega+\Omega) & 0 & 0 & \cos(\omega+\Omega)/e \\ 0 & \cos(\omega+\Omega) & 0 & 0 & -\sin(\omega+\Omega)/e \\ 0 & 0 & 2\sin\Omega \cos^2 \frac{i}{2} & \cos\Omega / \tan \frac{i}{2} & -\cos\Omega / \tan \frac{i}{2} \\ 0 & 0 & 2\cos\Omega \cos^2 \frac{i}{2} & -\sin\Omega / \tan \frac{i}{2} & \sin\Omega / \tan \frac{i}{2} \end{bmatrix} \begin{bmatrix} \psi_a \\ \psi_e \\ \psi_i \\ \psi_\Omega \\ \psi_\omega \end{bmatrix} \quad (3.25)$$

This can be written in terms of equinoctial orbital elements

$$\begin{bmatrix} \lambda_a \\ \lambda_h \\ \lambda_k \\ \lambda_p \\ \lambda_q \end{bmatrix} = \begin{bmatrix} 0 & 0 & 0 & 0 & 0 \\ 0 & \frac{h}{\sqrt{h^2+k^2}} & 0 & 0 & \frac{k}{h^2+k^2} \\ 0 & \frac{k}{\sqrt{h^2+k^2}} & 0 & 0 & \frac{-h}{h^2+k^2} \\ 0 & 0 & \frac{2p}{\sqrt{p^2+q^2}(1+p^2+q^2)} & \frac{q}{p^2+q^2} & \frac{-q}{p^2+q^2} \\ 0 & 0 & \frac{2q}{\sqrt{p^2+q^2}(1+p^2+q^2)} & \frac{-p}{p^2+q^2} & \frac{p}{p^2+q^2} \end{bmatrix} \begin{bmatrix} \psi_a \\ \psi_e \\ \psi_i \\ \psi_\Omega \\ \psi_\omega \end{bmatrix} \quad (3.)$$

Note that some of the elements of this matrix are undefined if e or i are zero.

The inverse relationship can also be written. In terms of classical orbital elements, the classical costate is given in terms of the equinoctial costate by the following relation,

$$\begin{bmatrix} \psi_a \\ \psi_e \\ \psi_i \\ \psi_\Omega \\ \psi_\omega \end{bmatrix} = \begin{bmatrix} 1 & 0 & 0 & 0 & 0 \\ 0 & \sin(\omega+\Omega) & \cos(\omega+\Omega) & 0 & 0 \\ 0 & 0 & 0 & \frac{1}{2} \sec^2 \frac{i}{2} \sin \Omega & \frac{1}{2} \sec^2 \frac{i}{2} \cos \Omega \\ 0 & e \cos(\omega+\Omega) & -e \sin(\omega+\Omega) & \tan \frac{i}{2} \cos \Omega & -\tan \frac{i}{2} \sin \Omega \\ 0 & e \cos(\omega+\Omega) & -e \sin(\omega+\Omega) & 0 & 0 \end{bmatrix} \begin{bmatrix} \lambda_a \\ \lambda_h \\ \lambda_k \\ \lambda_p \\ \lambda_q \end{bmatrix} \quad (3.)$$

or in terms of equinoctial orbital elements

$$\begin{bmatrix} \psi_a \\ \psi_e \\ \psi_i \\ \psi_\Omega \\ \psi_\omega \end{bmatrix} = \begin{bmatrix} 1 & 0 & 0 & 0 & 0 \\ 0 & \frac{h}{\sqrt{h^2+k^2}} & \frac{k}{\sqrt{h^2+k^2}} & 0 & 0 \\ 0 & 0 & 0 & \frac{1}{2} p \frac{(1+p^2+q^2)}{\sqrt{p^2+q^2}} & \frac{1}{2} q \frac{(1+p^2+q^2)}{\sqrt{p^2+q^2}} \\ 0 & k & -h & q & -p \\ 0 & k & -h & 0 & 0 \end{bmatrix} \begin{bmatrix} \lambda_a \\ \lambda_h \\ \lambda_k \\ \lambda_p \\ \lambda_q \end{bmatrix} \quad (3.)$$

Certain elements are undefined if e or i are zero.

### 3.3 The State Equations

The unaveraged state differential equations are

$$\dot{\underline{z}} = \frac{2P}{mc} M(\underline{z}, F) \quad (3.29)$$

$$\dot{m} = -\frac{2P}{c^2} \quad (3.30)$$

where  $\underline{z}$  represents the five equinoctial orbital elements (a, h, k, p, q), m is spacecraft mass, P is thruster beam power, which is assumed given by

$$P = \eta P_0 D(N) \frac{1}{R_s^2} \cos \phi \quad (3.31)$$

where  $P_0$  is a constant initial maximum array power at 1 A.U.,  $\eta$  is the total constant power efficiency factor,  $D(N)$  is a damage factor which is a function of the fluence, N, and has a maximum value of 1 (this function is derived in Section 4.3),  $R_s$  is the distance to the sun in A.U.'s and  $\phi$  is the angle that the normal to the panels makes with the spacecraft - sun vector. For the unconstrained attitude case  $\cos \phi = 1$ . For the attitude constrained case it is a function of spacecraft position and the thrust direction. The constant exhaust velocity is given by

$$c = I_{sp} g_0 \quad (3.32)$$

where  $I_{sp}$  is the specific impulse and  $g_0$  is the acceleration of gravity at the equator. The thrust direction is given by the unit vector  $\hat{u}$ . We define the 5x3 matrix

$$M(\underline{z}, F) = \frac{\partial \underline{z}}{\partial \dot{\underline{z}}} \quad (3.33)$$

The elements of this matrix are listed in Table B-1 of Appendix B. In addition to the quantities defined in Section 3.2 the partials of  $X_1$  and  $Y_1$  with respect to h and k are required. These are listed in Table B-2. These partials differ from Reference 16 since we consider F as an orbital element rather than as a function of h and k; thus when partials are taken, F is held constant. This assumption also affects the appearance of the expressions given in Table B-1 when compared with Table 3 of Reference 16. However, if the expressions are written out in detail they are seen to be identical. The code utilized the form shown in Ref. 16.

That form of  $M$  was also used when calculating and coding  $\frac{\partial M}{\partial z}$  for the costate equations. An algebraically simpler form of this matrix is given in a later work<sup>(28)</sup> but was not utilized in the coding of our program, although a variation of it is discussed in Appendix C.

The high energy particle fluence is also included as the seventh state variable. It is a function of position, but the exact form is developed in Section 4.2. For the present discussion assume

$$\dot{N} = f(\underline{z}, F) \quad (3.34)$$

When mass flow rate is given by Eq. (3.30) and exhaust velocity is constant, for arbitrary power history, the  $\Delta V$  is given by

$$\Delta V = c \ln \left( \frac{m_0}{m(t)} \right) \quad (3.35)$$

### 3.4 The Canonical Equations

To simplify the analysis we will first consider only the costate elements  $\underline{z}$ ,  $m$ . The effect of fluence can be considered later. For simplicity also assume that in Eq. (3.31) that  $\eta = 1$  and  $R_s = 1$ . Then beam power is given by

$$P = P_0 \cos \phi \quad (3.36)$$

The method used to get the canonical equations is to form a Hamiltonian,  $H$ , then average it, from which a first order approximation to the actual state and costate is obtained. (This does not necessarily yield the averaged costate.)

Let  $H$  represent the unaveraged Hamiltonian and  $\underline{x}$  the full state, then the averaged Hamiltonian is

$$\bar{H}(\bar{x}, \bar{\lambda}, \bar{t}) = \frac{1}{T_0} \int_{t-\frac{T_0}{2}}^{t+\frac{T_0}{2}} H(\bar{x}, \bar{\lambda}, \bar{t}, F(t), \underline{u}(F(t))) dt = \frac{1}{T_0} \int_{-\pi}^{\pi} H(\bar{x}, \bar{\lambda}, \bar{t}, F, \underline{u}(F)) \frac{dt}{dF} dF \quad (3.37)$$

where  $T_0$  is the orbital period, and the overbar indicates approximate quantities. The  $\bar{t}$  dependence refers to time dependence which is independent of spacecraft motion such as Earth motion around the sun. In practice integration with respect to  $F$  is more convenient. The expression  $\frac{dt}{dF}$  can be obtained from the equinoctial version of Kepler's equation (Eq. (3.15)). It is given by

$$\frac{dt}{dF} = \frac{T_0}{2\pi} (1 - \bar{k} \cos F - \bar{h} \sin F) \quad (3.38)$$

For convenience define

$$s(\underline{z}, F) = \frac{1}{T_0} \frac{dt}{dF} \quad (3.39)$$

Then the canonical equations for the approximation to the state and costate are given by

$$\dot{\underline{x}} = \frac{\partial \tilde{H}^T}{\partial \underline{\lambda}} = \int_{-\pi}^{\pi} \frac{\partial H^T}{\partial \underline{\lambda}} s \, dF \quad (3.40)$$

$$\dot{\underline{\lambda}} = -\frac{\partial \tilde{H}^T}{\partial \underline{x}} = -\int_{-\pi}^{\pi} \left( \frac{\partial H^T}{\partial \underline{x}} s + H \frac{\partial s^T}{\partial \underline{x}} \right) dF \quad (3.41)$$

Note that inside the averaging integral the state and costate are held constant. From the definition of  $s$  the only non-zero elements of  $\frac{\partial s}{\partial \underline{x}}$  are

$$\begin{aligned} \frac{\partial s}{\partial \bar{h}} &= -\frac{1}{2\pi} \sin F \\ \frac{\partial s}{\partial \bar{k}} &= -\frac{1}{2\pi} \cos F \end{aligned} \quad (3.43)$$

$\frac{\partial H}{\partial \underline{\lambda}}$  is just the unaveraged state equations with the dependence on the state and costate held constant over the averaging interval. The expression  $-\frac{\partial H}{\partial \underline{x}}$  is just the unaveraged costate equation,  $\dot{\underline{\lambda}}$ . Most of the remainder of this section will be involved in obtaining the unaveraged Hamiltonian and its partial derivative with respect to the state for the attitude constrained case. Those equations reduce simply for the pitch constrained or unconstrained cases. Only the state variables  $\underline{z}$  and  $m$  will be included; shadowing and oblateness will not be included.

One method of including the constraints is to write  $\hat{u}$  directly as a function of a single control angle,  $\psi$ , which lies in a plane perpendicular to the radius vector. Let

$$T_1 = [\hat{e}_1, \hat{e}_2] \quad (3.44)$$

where  $\hat{e}_1$  and  $\hat{e}_2$  are any two unit vectors orthogonal to the radius vector and each other (the transformation  $T_1$  is thus dependent on the spacecraft position and thus the orbital elements). Then

$$\dot{\underline{z}} = 2P(\underline{z}, F, \psi) M(\underline{z}, F) T_1(\underline{z}, F) \begin{bmatrix} \cos \psi \\ \sin \psi \end{bmatrix} \quad (3.45)$$

$$\dot{m} = -\frac{2P}{c}(\underline{z}, F, \psi) \quad (3.46)$$

The Hamiltonian is given by

$$H = \underline{\lambda}_z^T \frac{2P}{mc} M T_1 \begin{bmatrix} \cos \psi \\ \sin \psi \end{bmatrix} - \lambda_m \frac{2P}{c^2} \quad (3.47)$$

The costate equations are

$$\dot{\underline{\lambda}}_z = -\frac{\partial P}{\partial \underline{z}} \frac{H}{P} - \underline{\lambda}_z^T \frac{2P}{mc} \left\{ \frac{\partial M}{\partial \underline{z}} T_1 + M \frac{\partial T_1}{\partial \underline{z}} \right\} \begin{bmatrix} \cos \psi \\ \sin \psi \end{bmatrix} \quad (3.48)$$

$$\dot{\lambda}_m = \underline{\lambda}_z^T \frac{2P}{m^2 c} M T_1 \begin{bmatrix} \cos \psi \\ \sin \psi \end{bmatrix} \quad (3.49)$$

The elements of expression  $\frac{\partial M}{\partial \underline{z}}$  are given in Tables B-3 to B-7 of Appendix B along with subsidiary partials in Tables B-8 to B-9.

Another method is to use a constraint formulation (which is the form coded).

Then

$$\dot{\underline{z}} = \frac{2P}{mc} M \hat{\underline{u}} \quad (3.50)$$

$$\dot{m} = -\frac{2P}{c} \quad (3.51)$$

but there is a constraint equation

$$C = \underline{r}^T \hat{\underline{u}} = 0 \quad (3.52)$$

which insures that the thrust direction is orthogonal to the spacecraft radius vector. The Hamiltonian is

$$H = \underline{\lambda}_z^T \frac{2P}{mc} M \hat{\underline{u}} + \mu_r^T \hat{\underline{u}} - \frac{2P}{c} \lambda_m \quad (3.53)$$

with the additional multiplier,  $\mu$ . Then the costate equations are

$$\dot{\lambda}_z = -\frac{\partial P}{\partial z} \left\{ \lambda_z^T \frac{2}{mc} M \hat{u} - \frac{\lambda_m}{c^2} \right\} + \lambda_z^T \frac{2P}{mc} \left\{ \frac{\partial M}{\partial z} + \mu \frac{\partial r^T}{\partial z} \right\} \hat{u} \quad (3.54)$$

$$\dot{\lambda}_m = \lambda_z^T \frac{2P}{m^2 c} M \hat{u} \quad (3.55)$$

Again,  $\frac{\partial M}{\partial z}$  is given in Appendix B. If we assume that  $\underline{r}$  is the radius vector divided by the semimajor axis then the only nonzero partials of  $\underline{r}$  are  $\frac{\partial X_1}{\partial h}, \frac{\partial X_1}{\partial k}, \frac{\partial Y_1}{\partial h}, \frac{\partial Y_1}{\partial k}$ , which are given in Table B-2. Thus the term  $\frac{\partial r^T}{\partial z}$  is a little easier to evaluate than  $\frac{\partial T}{\partial z}$ , and also this form is more useful for the cases of zero pitch but free roll and without constraints. However,  $\mu$  must be evaluated. Rewrite the Hamiltonian

$$H = \left( \lambda_z^T \frac{2P}{mc} M + \mu r^T \right) \hat{u} - \frac{2P}{c^2} \lambda_m = \left( \lambda_z^T \frac{2P}{mc} M + \mu r^T \right) \underbrace{T^T}_{I} \hat{u} - \frac{2P}{c^2} \lambda_m \quad (3.56)$$

where

$$T = [\hat{e}_1 \hat{e}_2 \hat{e}_3] \quad (3.57)$$

and

$$\hat{e}_3 = -\frac{\underline{r}}{|\underline{r}|} \quad (3.58)$$

Now  $T^T \hat{u}$  is just the control in the  $\hat{e}_1, \hat{e}_2, \hat{e}_3$  coordinate system. It can be written

$$\hat{u}_T = \begin{Bmatrix} \cos \psi \cos \xi \\ \sin \psi \cos \xi \\ \sin \xi \end{Bmatrix} \quad (3.59)$$

where  $\xi$  is the angle between  $\hat{u}_T$  and the  $\hat{e}_1 - \hat{e}_2$  plane, and  $\psi$  is the angle between the projection of  $\hat{u}_T$  onto the  $\hat{e}_1 - \hat{e}_2$  plane and  $\hat{e}_1$ . Note that as yet we have not taken into account the constraint equation. Rewriting Eq. 3.56

$$H = \left( \frac{2P \lambda_z^T}{mc} M T + \mu r^T T \right) \hat{u}_T - \frac{2P}{c^2} \lambda_m \quad (3.60)$$

Writing this out in detail

$$H = \frac{2P}{mc} \lambda_z^T M [\hat{e}_1 \cos \psi + \hat{e}_2 \sin \psi] \cos \xi + \left[ \frac{2P}{mc} \lambda_z^T M \hat{e}_3 - \mu |\underline{r}| \right] \sin \xi - \frac{2P}{c^2} \lambda_m \quad (3.61)$$

The longitudinal axis of the panels is parallel to the pitch axis. Therefore, the orientation of the panels can be defined independently of the pitch angle. Thus  $P$  is not a function of pitch. Then to solve for the optimal  $\xi$  set

$$\frac{\partial H}{\partial \xi} = 0 \quad (3.52)$$

or

$$\tan \xi = \frac{\left( \frac{2P}{mc} \lambda_z^T M \hat{e}_3 - \mu |\underline{r}| \right)}{\frac{2P}{mc} \lambda_z^T M [\hat{e}_1 \cos \psi + \hat{e}_2 \sin \psi]} \quad (3.63)$$

Now the constraint can be taken into account. Rewriting Eq. (3.52) as

$$C = \underline{r}^T T T^T \hat{u} = 0 \quad (3.64)$$

since  $T T^T$  is just the identity matrix. From Eqs. (3.57) and (3.59) the constraint reduces to  $\sin \xi = 0$ . So Eq. (3.63) is also zero. Thus

$$\frac{2P}{mc} \lambda_z^T M \hat{e}_3 - \mu |\underline{r}| = 0 \quad (3.65)$$

or (using Eq. (3.58))

$$\mu = - \frac{2P}{mc} \lambda_z^T M \frac{\underline{r}}{|\underline{r}|} \quad (3.66)$$

When roll is free, power is no longer a function of  $\psi$ . For the pitch = 0 case Eq. (3.52) is still valid, and the optimal  $\hat{u}$  is easy to calculate as is  $\mu$ . The Hamiltonian is

$$H = \left( \lambda_z^T \frac{2P}{mc} M + \mu \underline{r}^T \right) \hat{u} - \frac{2P}{c} \lambda_m \quad (3.67)$$

Since  $P$  is not a function of  $\hat{u}$ , to maximize  $H$  set

$$\hat{u} = \frac{\left( \lambda_z^T \frac{2P}{mc} M + \mu \underline{r}^T \right)^T}{\left| \lambda_z^T \frac{2P}{mc} M + \mu \underline{r}^T \right|} \quad (3.68)$$

The constraint  $C = \hat{\underline{u}}^T \underline{r} = 0$  yields

$$\underline{\lambda}_z^T \frac{2P}{mc} M \underline{r} + \underline{\mu}_r^T \underline{r} = 0 \quad (3.69)$$

or

$$\underline{\mu} = -\underline{\lambda}_z^T \frac{2P}{mc} M \frac{\underline{r}}{|\underline{r}|^2} \quad (3.70)$$

the same as Eq. (3.66).

When there is no constraint  $\underline{\mu} = 0$  and

$$\hat{\underline{u}} = \frac{M^T \underline{\lambda}_z}{|M^T \underline{\lambda}_z|} \quad (3.81)$$

is the optimal thrust direction.

In summary the approximating canonical equations are

$$\dot{\underline{z}} = \int_{-\pi}^{\pi} \left( \frac{2P(\underline{z}, \hat{\underline{u}})}{mc} \underline{v}(\underline{z}, F) + \underline{\mu}_r^T \hat{\underline{u}} s(\underline{z}, F) \right) dF \quad (3.72)$$

$$\dot{\underline{m}} = - \int_{-\pi}^{\pi} \frac{2P(\underline{z}, \hat{\underline{u}})}{c^2} s(\underline{z}, F) dF \quad (3.73)$$

$$\begin{aligned} \dot{\underline{\lambda}}_z = & - \int_{-\pi}^{\pi} \left[ \left\{ \frac{\partial P(\underline{z}, \hat{\underline{u}})}{\partial \underline{z}} \left( \underline{\lambda}_z^T \frac{2P(\underline{z}, \hat{\underline{u}})}{mc} M(\underline{z}, F) \hat{\underline{u}} - \frac{2}{c^2} \right) + \underline{\lambda}_z^T \frac{2P(\underline{z}, \hat{\underline{u}})}{mc} \left( \frac{\partial M(\underline{z}, F)}{\partial \underline{z}} \right. \right. \right. \\ & \left. \left. \left. + \underline{\mu} \frac{\partial \underline{r}^T(\underline{z}, F)}{\partial \underline{z}} \right) \hat{\underline{u}} \right\} s(\underline{z}, F) + H(\underline{x}, \underline{\lambda}, \hat{\underline{u}}) \frac{\partial s(\underline{z}, F)}{\partial \underline{z}} \right] dF \end{aligned} \quad (3.74)$$

$$\dot{\underline{\lambda}}_m = \frac{1}{\underline{m}} \int_{-\pi}^{\pi} \underline{\lambda}_z^T \dot{\underline{z}}(\underline{z}, \underline{\lambda}, \hat{\underline{u}}) s(\underline{z}, F) dF \quad (3.75)$$

where

$$\underline{\mu} = -\underline{\lambda}_z^T \frac{2P(\underline{z}, \hat{\underline{u}})}{mc} M(\underline{z}, F) \frac{\underline{r}}{|\underline{r}|^2} \quad (3.76)$$

if pitch is constrained to zero. If there are no constraints,  $\mu = 0$ .  $M$  and  $\frac{\partial M}{\partial \underline{z}}$  are given in Appendix B. Also

$$\frac{\partial \underline{s}}{\partial \underline{z}} = \frac{1}{2\pi} \begin{bmatrix} 0 \\ -\sin F \\ -\cos F \\ 0 \\ 0 \end{bmatrix} \quad (3.77)$$

If  $\underline{r}$  is interpreted as the radius vector divided by the semimajor axis, then in the equinoctial coordinate frame

$$\underline{r} = \begin{bmatrix} X_1/a \\ Y_1/a \\ 0 \end{bmatrix} \quad (3.78)$$

so that

$$\frac{\partial \underline{r}^T}{\partial \underline{z}} = \begin{bmatrix} 0 & 0 & 0 \\ \frac{\partial X_1/a}{\partial h} & \frac{\partial Y_1/a}{\partial h} & 0 \\ \frac{\partial X_1/a}{\partial k} & \frac{\partial Y_1/a}{\partial k} & 0 \\ 0 & 0 & 0 \\ 0 & 0 & 0 \end{bmatrix} \quad (3.79)$$

where the nonzero partials were given in Table B-1.

In the case of free roll,  $P$  is not a function of  $\underline{z}$  and so  $\frac{\partial P}{\partial \underline{z}} = 0$ . For the zero pitch and roll case this partial depends on the actual form of  $P$  which has not yet been specified. For the unconstrained case and for the case with zero pitch but free roll, the canonical equations are completely defined. It remains to calculate the power equation and the control for the zero pitch and roll case.

### 3.5 Geometry and Power

In this section we define a useful coordinate system in which it is convenient to calculate the thrust vector direction and the equation for power. It is shown that we can calculate the panel orientation angle in terms of the thrust direction angle,

thus leaving only one control variable for the problem. Power will then be a function of the thrust angle and the angle between the radius vector and the direction to the sun.

The thrust vector is constrained to a plane which is perpendicular to the radius vector. In this plane the yaw is usually measured from a basis vector in the orbital plane, which it is for the printed output of our program. However, because of the power dependence on sun direction, another coordinate system will be useful. This is the  $\underline{\hat{e}}_1, \underline{\hat{e}}_2, \underline{\hat{e}}_3$  system where

$$\underline{\hat{e}}_3 = -\underline{\hat{r}} \quad (3.80)$$

and  $\underline{\hat{e}}_1$  is in the plane defined by the radius vector and the Earth-sun vector (assumed equivalent to the spacecraft-sun vector). In particular,

$$\underline{\hat{e}}_2 = \underline{\hat{e}}_3 \times \underline{\hat{R}}_s / |\underline{\hat{e}}_3 \times \underline{\hat{R}}_s| \quad (3.81)$$

and

$$\underline{\hat{e}}_1 = \underline{\hat{e}}_2 \times \underline{\hat{e}}_3 \quad (3.82)$$

In this system the sun direction is defined by the angle  $\beta$  where

$$\underline{\hat{R}}_s = \cos \beta \underline{\hat{e}}_3 + \sin \beta \underline{\hat{e}}_1 \quad (3.83)$$

(In the equinoctial system  $\cos \beta = -\underline{\hat{r}}^T \underline{\hat{R}}_s$ .) The thrust acceleration vector direction is constrained to the  $\underline{\hat{e}}_1 - \underline{\hat{e}}_2$  plane and given in terms of the angle  $\psi$  with respect to the  $\underline{\hat{e}}_1$  axis by the unit vector

$$\underline{\hat{u}} = \cos \psi \underline{\hat{e}}_1 + \sin \psi \underline{\hat{e}}_2 \quad (3.84)$$

(See Fig. 3-2).

The power yield of the solar panels is proportional to the cosine of the angle between the normal to the panels and the vector pointing toward the sun. The panels can rotate about an axis which is in the  $\underline{\hat{e}}_1 - \underline{\hat{e}}_2$  plane and is assumed to be perpendicular to  $\underline{\hat{u}}$  (recall Fig. 1-1). The normal to the panels can be defined in terms of  $\psi$  and an angle of rotation,  $\theta$ , about this axis in the  $\underline{\hat{e}}_1 - \underline{\hat{e}}_2 - \underline{\hat{e}}_3$  system, namely:

$$\underline{\hat{N}} = \sin \theta \cos \psi \underline{\hat{e}}_1 + \sin \theta \sin \psi \underline{\hat{e}}_2 + \cos \theta \underline{\hat{e}}_3 \quad (3.85)$$

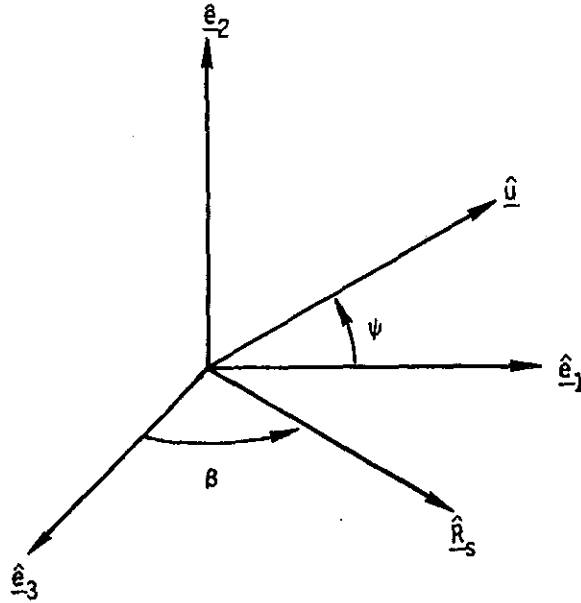


Fig. 3-2 Coordinate and Angle Definition

The cosine of the angle between the normal and the sun vector is given by

$$\cos \phi = \hat{N}^T \hat{R}_s = \sin \beta \sin \theta \cos \psi + \cos \theta \cos \beta \quad (3.86)$$

For a given  $\beta$  it is possible to maximize this expression with respect to  $\theta$  and so eliminate  $\theta$  from  $\cos \phi$ , which will then be a function only of  $\psi$  and  $\beta$ . The maximizing  $\theta$  is given by

$$\sin \theta = \frac{\sin \beta \cos \psi}{\sqrt{\cos^2 \beta + \sin^2 \beta \cos^2 \psi}} \quad (3.87)$$

$$\cos \theta = \frac{\cos \beta}{\sqrt{\cos^2 \beta + \sin^2 \beta \cos^2 \psi}} \quad (3.88)$$

and thus

$$\cos \phi = \sqrt{\cos^2 \beta + \sin^2 \beta \cos^2 \psi} = \sqrt{1 - \sin^2 \beta \sin^2 \psi} \quad (3.89)$$

It is interesting to look in the  $\hat{e}_1 - \hat{e}_2$  plane at the locus of the vector pointing along the thrust direction with magnitude equal to  $\cos \phi$ . For each  $\beta$  there is a curve in the  $\hat{e}_1 - \hat{e}_2$  plane as  $\psi$  varies from 0 to 360 degrees. These curves are symmetric about both axes and repeat for every  $\beta$  interval of 90 degrees. Note that for  $|\cos \beta| < \sqrt{2}/2$  they are convex (see Fig. 3-3). Since power is a function of thrust direction, this curve will be important in determining the desired control angle,  $\psi$ , which specifies the thrust direction.

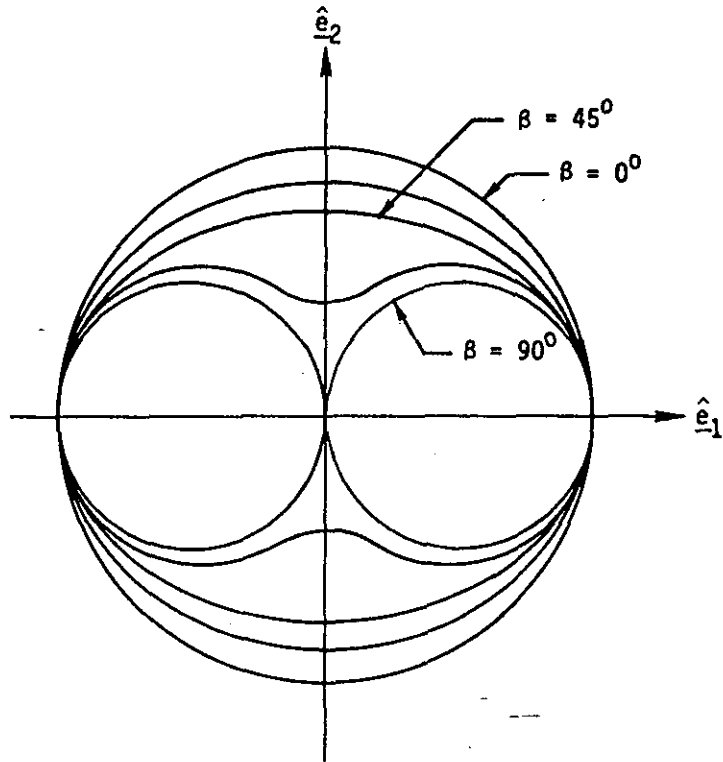


Fig. 3-3  $P/P_0$  Locus

In Eq. (3.74) for the costate derivative we needed  $\frac{\partial P}{\partial \underline{z}}$ . This can now be calculated. Power is given by

$$P = P_0 \cos \phi = P_0 \sqrt{1 - \sin^2 \beta \sin^2 \psi} \quad (3.90)$$

so that

$$\frac{\partial P}{\partial \underline{z}} = -P_0 \left(1 - \sin^2 \beta \sin^2 \psi\right)^{-1/2} \sin^2 \psi \sin \beta \cos \beta \frac{\partial \cos \beta}{\partial \underline{z}} \quad (3.91)$$

But  $\cos \beta = \hat{\underline{e}}_3 \cdot \hat{\underline{R}}_S$ . So

$$\frac{\partial \cos \beta}{\partial \underline{z}} = \frac{\partial \hat{\underline{e}}_3}{\partial \underline{z}} \cdot \underline{R}_S + \hat{\underline{e}}_3 \cdot \frac{\partial \hat{\underline{R}}_S}{\partial \underline{z}} \quad (3.92)$$

where

$$\frac{\partial \hat{\underline{e}}_3}{\partial z_i} = \frac{1}{|\underline{r}|^3} \begin{bmatrix} \left( Y_1^2 \frac{\partial X_1}{\partial z_i} - X_1 Y_1 \frac{\partial Y_1}{\partial z_i} \right) \\ \left( -X_1 Y_1 \frac{\partial X_1}{\partial z_i} + X_1^2 \frac{\partial Y_1}{\partial z_i} \right) \\ 0 \end{bmatrix} \quad (3.93)$$

where the semimajor axis drops out of  $\hat{\underline{e}}_3$  and so we only need the partials of  $X_1$  and  $Y_1$  with respect to  $h$  and  $k$  which are given in Table B-2 of Appendix B.  $\hat{\underline{R}}_S$  is a function of only  $p$  and  $q$  and the partials are given in Appendix D.

### 3.6 Thrust Direction

Let us rewrite the Hamiltonian given in Eq. (3.47) but including dependence of  $P$  on  $\psi$ .

$$H = \frac{2P_0}{c} \sqrt{1 - \sin^2 \beta \sin^2 \psi} \left( \underline{\lambda}_z^T \frac{M T}{m} \begin{bmatrix} \cos \psi \\ \sin \psi \\ 0 \end{bmatrix} - \frac{\lambda_m}{c} \right) \quad (3.94)$$

In the definition of the transformation,  $T$ , we are using the unit vectors defined previously in Eqs. (3.80), (3.81), (3.82). The quantity  $T^T M T \underline{\lambda}_z$  is just the primer vector given in the  $\underline{\hat{e}}_1 - \underline{\hat{e}}_2 - \underline{\hat{e}}_3$  system and will be designated  $\underline{\lambda}_v$  with components  $\lambda_{v1}, \lambda_{v2}, \lambda_{v3}$ . Eq. (3.94) can be rewritten as

$$H = \frac{2P_0}{c} \sqrt{1 - \sin^2 \beta \sin^2 \psi} \left( \frac{\lambda_{v1}}{m} \cos \psi + \frac{\lambda_{v2}}{m} \sin \psi - \frac{\lambda_m}{c} \right) \quad (3.95)$$

For a minimum time solution this Hamiltonian must be maximized with respect to  $\psi$ . If this is done by setting  $\partial H/\partial\psi = 0$  and converting all  $\sin\psi$  to  $\cos\psi$ , a sixth order polynomial in  $\cos\psi$  results. Let

$$\epsilon = -\frac{m\lambda_m}{c\lambda_{v_1}}, \quad \tan\alpha = \frac{\lambda_{v_2}}{\lambda_{v_1}} \quad (3.97)$$

Then

$$H = \frac{2P_0}{cm} \lambda_{v_1} \sqrt{\cos^2\beta + \sin^2\beta \cos^2\psi} (\cos\psi + \tan\alpha \sin\psi - \epsilon) \quad (3.98)$$

This can be maximized with respect to  $\psi$  by setting

$$\frac{\partial H}{\partial\psi} = 0 \quad (3.99)$$

$$\begin{aligned} \frac{\partial H}{\partial\psi} = \frac{2P_0}{cm} \lambda_{v_1} \left\{ -(\cos^2\beta + \sin^2\beta \cos^2\psi)^{-1/2} \sin^2\beta \cos\psi \sin\psi (\cos\psi + \tan\alpha \sin\psi + \epsilon) \right. \\ \left. + (\cos^2\beta + \sin^2\beta \cos^2\psi)^{1/2} (-\sin\psi + \tan\alpha \cos\psi) \right\} = 0 \end{aligned} \quad (3.100)$$

Divide by  $\frac{2P_0 \lambda_{v_1}}{cm(\cos^2\beta + \sin^2\beta \cos^2\psi)^{1/2}}$ , then

$$-\sin^2\beta \cos\psi \sin\psi (\cos\psi + \tan\alpha \sin\psi + \epsilon) + (\cos^2\beta + \sin^2\beta \cos^2\psi)(-\sin\psi + \tan\alpha \cos\psi) = 0 \quad (3.101)$$

or

$$\begin{aligned} -\sin^2\beta \cos^2\psi \sin\psi - \sin^2\beta \tan\alpha \cos\psi \sin^2\psi - \epsilon \sin^2\beta \cos\psi \sin\psi - \cos^2\beta \sin\psi \\ + \cos^2\beta \tan\alpha \cos\psi - \sin^2\beta \cos^2\psi \sin\psi + \sin^2\beta \tan\alpha \cos^3\psi = 0 \end{aligned} \quad (3.102)$$

Rearranging

$$\sin\psi (2\sin^2\beta \cos^2\psi + \cos^2\beta + \epsilon \sin^2\beta \cos\psi) = (\cos^2\beta - \sin^2\beta) \tan\alpha \cos\psi + 2\sin^2\beta \tan\alpha \cos^3\psi \quad (3.103)$$

Squaring

$$\begin{aligned}
 (1-\cos^2\psi)(4\sin^4\beta\cos^2\psi+4\sin^2\beta\cos^2\beta\cos^2\psi+\cos^4\beta+2\epsilon\sin^2\beta(2\sin^2\beta\cos^2\psi+\cos^2\beta)) \\
 +\epsilon^2\sin^4\beta\cos^2\psi = (\cos^2\beta-\sin^2\beta)^2\tan^2\alpha\cos^2\psi+4\sin^2\beta\tan^2\alpha(\cos^2\beta-\sin^2\beta)\cos^4\psi \\
 +4\sin^4\beta\tan^2\alpha\cos^6\psi
 \end{aligned} \tag{3.104}$$

Rearranging, finally,

$$\begin{aligned}
 4\sin^4\beta(\tan^2\alpha+1)\cos^6\psi - 4\epsilon\sin^2\beta\cos^5\psi \\
 +4\left[\sin^2\beta\tan^2\alpha(\cos^2\beta-\sin^2\beta)-\sin^4\beta+\sin^2\beta\cos^2\beta-\epsilon^2\sin^4\beta\right]\cos^4\psi \\
 +\epsilon(4\sin^4\beta-2\sin^2\beta\cos^2\beta)\cos^3\psi \\
 +\left[(\cos^2\beta-\sin^2\beta)^2\tan^2\alpha-4\sin^2\beta\cos^2\beta+\cos^4\beta+\epsilon^2\sin^4\beta\right]\cos^2\psi \\
 +2\epsilon\sin^2\beta\cos^2\beta\cos\psi - \cos^4\beta = 0
 \end{aligned} \tag{3.105}$$

Is the minimum time solution really desirable for this problem? We think not. If power were not a function of the control, the optimal thrust direction would just line up with the projection of the primer vector on the  $\hat{e}_1 - \hat{e}_2$  plane. But for the Hamiltonian of Eq. (3.95)  $\psi$  becomes a function of  $\lambda_m$ . This has the effect of biasing the control so that the thruster is operating in a region on the curves of Fig. 3-3 where  $\cos\phi$  is greater than it would be if  $\lambda_m$  were not included. This reduces the mass of the spacecraft by throwing fuel away in order to reduce the flight time. In fact, if fuel could simply be dumped overboard instead of going through the thruster, the time optimal requirement would be to dump fuel until  $\lambda_m = 0$ . Since the formulation here does not allow separate dumping of mass, a bias on the control is required to reduce mass. Although minimizing time is important, dumping fuel to do so seems undesirable.

So what happens if the part of the Hamiltonian containing  $\lambda_m$  is ignored and instead we maximize

$$H' = \frac{2P_0}{cm} \sqrt{1-\sin^2\beta\sin^2\psi} (\lambda_{v_1}\cos\psi + \lambda_{v_2}\sin\psi) \quad ? \tag{3.106}$$

In the  $\hat{e}_1 - \hat{e}_2$  plane one can see that this is equivalent to maximizing the projection of the vector  $(\cos\psi, \sin\psi)\sqrt{1-\sin^2\beta\sin^2\psi}$  onto the  $\hat{e}_1 - \hat{e}_2$  components of the primer

$(\lambda_{v1}, \lambda_{v2})$ . The locus of the first vector is just that shown in Fig. 3-3. Geometrically, a typical solution is shown in Fig. 3-4. The maximization of  $H'$  can be carried out using analytic geometry by considering the  $\cos\psi$  curve as a parametric function of  $\psi$  and noting that its slope must be the negative of the inverse of the slope of the  $\lambda_{v1} - \lambda_{v2}$  vector. Thus, if

$$\begin{bmatrix} x(\psi) \\ y(\psi) \end{bmatrix} = \begin{bmatrix} \cos\psi \\ \sin\psi \end{bmatrix} \sqrt{1 - \sin^2\beta \sin^2\psi} \quad (3.107)$$

then

$$\frac{dy}{dx} = \frac{\frac{dy}{d\psi}}{\frac{dx}{d\psi}} = -\frac{1}{\tan\alpha} = -\frac{\lambda_{v1}}{\lambda_{v2}} \quad (3.108)$$

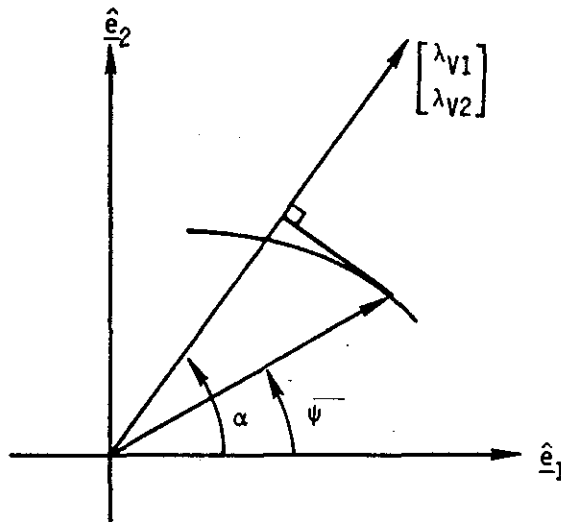


Fig. 3-4 Geometric Calculation of  $\psi$

where

$$\frac{dx}{d\psi} = \frac{(-1 + \sin^2\beta \sin^2\psi - \sin^2\beta \cos^2\psi) \sin\psi}{(1 - \sin^2\beta \sin^2\psi)^{1/2}} \quad (3.109)$$

and

$$\frac{dy}{d\psi} = \frac{(1-2\sin^2\beta\sin^2\psi)\cos\psi}{(1-\sin^2\beta\sin^2\psi)^{1/2}} \quad (3.110)$$

Thus

$$\tan\alpha = \frac{1-\sin^2\beta\sin^2\psi+\sin^2\beta\cos^2\psi}{1-2\sin^2\beta\sin^2\psi} \tan\psi \quad (3.111)$$

Using

$$\sin^2\psi = \frac{\tan^2\psi}{1+\tan^2\psi} \quad (3.112)$$

and

$$\cos^2\psi = \frac{1}{1+\tan^2\psi} \quad (3.113)$$

then

$$\tan\alpha = \frac{1+\sin^2\beta+\cos^2\beta\tan^2\psi}{1+\tan^2\psi-2\sin^2\beta\tan^2\psi} \tan\psi \quad (3.114)$$

or

$$\cos^2\beta\tan^3\psi+(2\sin^2\beta-1)\tan\alpha\tan^2\psi+(1+\sin^2\beta)\tan\psi-\tan\alpha=0 \quad (3.115)$$

Dividing through by  $\cos^2\beta$  yields

$$\tan^3\psi+(\tan^2\beta-1)\tan\alpha\tan^2\psi+(2\tan^2\beta+1)\tan\psi-(1+\tan^2\beta)\tan\alpha=0 \quad (3.116)$$

It is also possible to obtain the control by setting  $\frac{\partial H^1}{\partial\psi}=0$ . The procedure is the same as resulted in Eq. (3.105) and in fact an equation in  $\cos\psi$  can be obtained directly from Eq. (3.105) by setting  $\epsilon=0$ . Thus the coefficients of all odd powers of  $\cos\psi$  are zero. The resulting equation is

$$4\sin^4\beta(\tan^2\alpha+1)\cos^6\psi+4\sin^2\beta(\tan^2\alpha-1)(\cos^2\beta-\sin^2\beta)\cos^4\psi \\ +[(\cos^2\beta-\sin^2\beta)^2\tan^2\alpha-4\sin^2\beta\cos^2\beta+\cos^4\beta]\cos^2\psi-\cos^4\beta=0 \quad (3.117)$$

The cubic equation in  $\tan\psi$  of Eq. (3.115) can be shown to be equivalent to the cubic in  $\cos^2\psi$  of Eq. (3.117) by substituting  $\tan\psi = \frac{\sqrt{1-\cos^2\psi}}{\cos\psi}$  into Eq. (3.115), then removing the square root, rearranging and squaring. Collecting the terms and making certain trigonometric identifications yields Eq. (3.117).

This control does not dump fuel to minimize time, and it is much easier to calculate since the solution to the cubic can be obtained analytically, unlike the solution to the sixth order polynomial. Analysis of the worst case example. (see Appendix E) indicates that the time penalty in using this suboptimal control is small while resulting in a fuel savings. Since it is also much easier to calculate and thus saves computer time, it was decided to use this control law for the present study.

This control law has some interesting characteristics. Fig. 3-5 shows curves of constant  $\alpha$  superimposed on the curves of Fig. 3-3 for one quadrant. Thus for a given  $\beta$  (sun angle) and  $\alpha$  (primer vector angle) the resulting  $\psi$  is just the angle made by the line from the origin to the intersection of the appropriate  $\alpha$  and  $\beta$  curves. Note that in this quadrant  $\psi$  is always less than  $\alpha$  except for  $\beta = 0$  when  $\psi = \alpha$  or for  $\beta < 45^\circ$  and  $\alpha = 90^\circ$  when also  $\psi = 90^\circ$ ; when  $\beta = 90^\circ$ ,  $\psi \rightarrow 45^\circ$  as  $\alpha \rightarrow 90^\circ$ . For  $\beta > 45^\circ$  as  $\alpha$  crosses the  $\hat{e}_2$  axis there is a jump in  $\psi$  to a symmetrical position in the adjoining quadrant. If  $\alpha$  remained aligned with the  $\hat{e}_2$  axis for a finite time a singular arc results. Since it would be nonoptimizing (in terms of  $H'$ ) to operate on the concave portions of the curves, a chattering solution is required as  $\psi$  jumps back and forth in the two quadrants in infinitesimal time yielding a resultant thrust vector along the  $\hat{e}_2$  axis. In practice this solution will probably never be required (as well as being impossible to implement if it were). Jumps in the control direction can and do occur however. The locus of points on Fig. 3-5 at which a jump occurs is given by an arc of a circle of radius  $\sqrt{2}/2$  and center at the origin. This radius represents the minimum power. The  $\psi$  at which a jump occurs is related to  $\beta$  by the relation

$$\cos^2\psi = \frac{\sin^2\beta - \frac{1}{2}}{\sin^2\beta} \quad (3.118)$$

In practice, then,  $\beta$  and  $\alpha$  are calculated and the coefficients of Eq. (3.117) are obtained. The cubic equation can then be solved analytically. Appropriate modifications must be made if the tangents are very large or infinite. There are three roots to the cubic equation and if all three are real they correspond to six possible values of  $\psi$  in a  $360^\circ$  range. These correspond to various maxima and minima. By inspection of the form of

the figures produced by Eq. (3.107) there is apparently only one solution which can lie in the same quadrant as  $\alpha$  and at the same time maximize the projection onto  $(\lambda_{v_1}, \lambda_{v_2})$ . Thus we can obtain the control angle  $\psi$  which can then be substituted into the equations of motion. This calculation must be made at each quadrature point on an orbit.

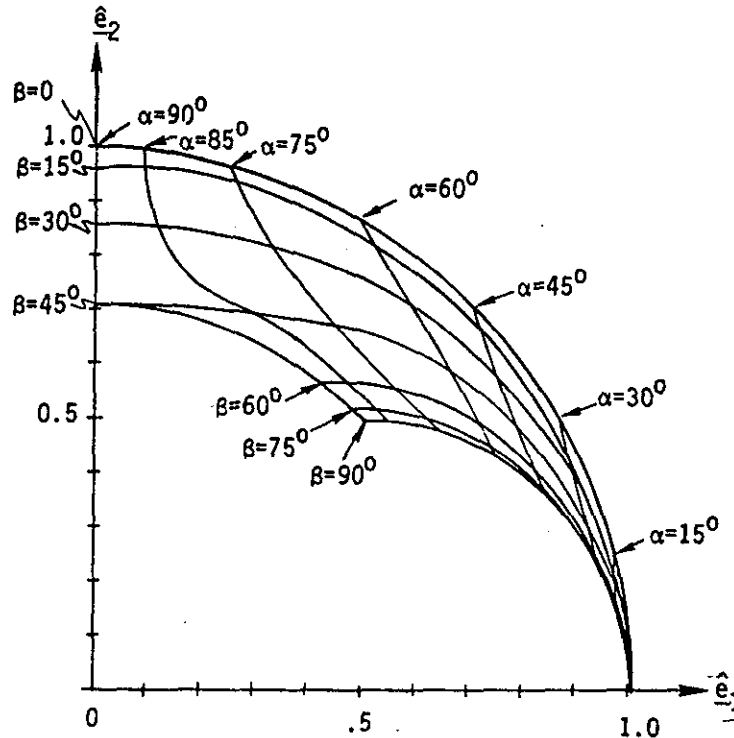


Fig. 3-5 Lines of Constant Primer Angle ( $\alpha$ ) and Sun Angle ( $\beta$ )

There are certain special cases of values of  $\alpha$  and  $\beta$  that must be considered. If  $\tan\alpha = 0$  the cubic reduces to  $\tan^3\psi + (2\tan^2\beta + 1)\tan\psi = 0$ . The correct root is then  $\tan\psi = 0$  and thus  $\psi = \alpha$ . If  $\tan\alpha$  is infinite, first divide Eq. (3.115) through by  $\tan\alpha$ , then set  $\tan\alpha$  equal to infinity, which yields

$$(2\sin^2\beta - 1)\tan^2\psi - 1 = 0 \quad (3.119)$$

or

$$\tan^2 \psi = \frac{1}{2\sin^2 \beta - 1} \quad (3.120)$$

or

$$\cos^2 \psi = \frac{2\sin^2 \beta - 1}{\sin^2 \beta} \quad (3.121)$$

This is valid if  $\sin^2 \beta > \frac{1}{2}$ . Otherwise  $\tan \psi$  equal to infinity is the correct root of Eq. (3.115) and  $\psi = \alpha$  ( $= 90^\circ$  or  $270^\circ$ ). If  $\cos^2 \beta = 0$ , then Eq. (3.115) reduces to

$$\tan \alpha \tan^2 \psi + 2 \tan \psi - \tan \alpha = 0 \quad (3.122)$$

From the binomial theorem

$$\tan \psi = \frac{-1 \pm \sqrt{1 - \tan^2 \alpha}}{\tan \alpha} = \tan \frac{1}{2} \alpha, -\cot \frac{1}{2} \alpha \quad (3.123)$$

If  $-90^\circ < \alpha < 90^\circ$ , the first root is correct and  $\psi = \frac{1}{2} \alpha$ . If  $90^\circ < \alpha < 270^\circ$ , the second root is correct and  $\psi = \frac{1}{2} \alpha + 90^\circ$  if  $90^\circ < \alpha < 180^\circ$  and  $\psi = \frac{1}{2} \alpha - 90^\circ$  if  $180^\circ < \alpha < 270^\circ$ . If  $\cos^2 \beta = 1$  then  $\tan \psi = \tan \alpha$  is the correct root and  $\psi = \alpha$ .

Because of the numerical inaccuracy of using a quadrature over a region which contains a discontinuity in the integrand, it is best to calculate possible jump points and then do separate quadratures between these points. A jump in the thrust direction occurs when the projection of the primer vector onto the  $\hat{e}_1 - \hat{e}_2$  plane passes from one side of  $\hat{e}_2$  to the other. At the time of crossing... the projection is perpendicular to  $\hat{e}_1$ , and also perpendicular to  $\hat{R}_s$ . Thus the condition for a jump can be written

$$\left( M^T \lambda_z^T - (\lambda_z^T M r) \frac{r}{|r|^2} \right)^T \hat{R}_s = 0 \quad (3.124)$$

An actual jump occurs only if the constant  $\beta$  curve is concave, i. e.,  $|\cos \beta| < \frac{\sqrt{2}}{2}$ . For the results given in this report the method used to find the values of  $F$  for which a jump might occur was to divide the  $360^\circ$  range of  $F$  into small equal intervals and then to check to see if there was a sign change of Eq. (3.124) from one side of an interval to the other side. If so, the exact  $F$  within the interval for which Eq. (3.124) was zero was found by using a nonlinear function root finding routine (an IBM scientific subroutine using a Mueller's iteration<sup>(27)</sup>).

The equation for the jump points can be obtained as a sixth order polynomial in  $\cos F$ . This equation is very tedious to derive algebraically and in any case must be solved by an iterative procedure and the roots tested. Thus it seems reasonable to use the search procedure. The sixth order polynomial in  $\cos F$  can be obtained by writing a form of Eq. (3.124) in  $\hat{r}$ ,  $\hat{s}$ ,  $\hat{w}$  coordinates where  $\hat{r}$  is along the spacecraft radius vector,  $\hat{w}$  is perpendicular to the orbit plane and  $\hat{s} = \hat{w} \times \hat{r}$ . If  $\lambda_s$  and  $\lambda_w$  are the components in the  $\hat{s}$  and  $\hat{w}$  directions respectively then

$$\left[ -R_x \frac{Y_1}{r} + R_y \frac{X_1}{r} \right] \lambda_s + R_z \lambda_w = 0 \quad (3.125)$$

where  $\hat{R}_s^T = (R_x, R_y, R_z)$  is the sun's direction in equinoctial coordinates and  $X_1$  and  $Y_1$  are the spacecraft position in the equinoctial frame, and  $r$  is the radial distance. Using the results of Appendix C

$$\lambda_s = \frac{2a\sqrt{1-h^2-k^2}}{nr} \lambda_a - \left( r\dot{X}_1 - \frac{GY_1}{r} \right) \frac{\lambda_h}{\mu} + \left( r\dot{Y}_1 + \frac{GX_1}{r} \right) \frac{\lambda_k}{\mu} \quad (3.126)$$

$$\lambda_w = \frac{(k\lambda_h - h\lambda_k)}{G} (qY_1 - pX_1) + \frac{(1+p^2+q^2)}{G} (\lambda_p Y_1 + \lambda_q X_1) \quad (3.127)$$

The quantities  $X_1$ ,  $Y_1$ ,  $\dot{X}_1$ ,  $\dot{Y}_1$ ,  $r$  all contain  $\cos F$  and  $\sin F$ . Substituting into Eq. (3.125), multiplying through by  $r$  and eliminating  $\sin F$  by rearranging and squaring results in the sixth order polynomial in  $\cos F$ . Three of the roots are introduced by squaring so there will be at most 6 values of  $F$  for which there may be jumps.

If the eccentricity is zero,  $h = k = 0$ , and a quartic results. In that case

$$\lambda_s = 2 \sqrt{\frac{a}{\mu}} \left\{ a\lambda_a + \lambda_h \sin F + \lambda_q \cos F \right\} \quad (3.128)$$

$$\lambda_w = \sqrt{\frac{a}{\mu}} \frac{(1+p^2+q^2)}{2} (\lambda_p \sin F + \lambda_q \cos F) \quad (3.129)$$

There are at most four values of  $F$  at which there may be jumps. If in addition to  $h = k = 0$  also  $\lambda_h = \lambda_k = 0$ , then there is a further simplification and Eq. (3.125) reduces to

$$\tan F = - \frac{K\lambda_q + R_y}{K\lambda_p - R_x} \quad (3.130)$$

where

$$K = \frac{R_z(1+p^2+q^2)}{4a\lambda_a} \quad (3.131)$$

Thus there can be at most two jumps which are 180° apart for this case.

### 3.7 Oblateness

In the previous sections we have considered only perturbations to the inverse square motion caused by thrusting. In this section the effect of oblateness ( $J_2$ ) is considered. Oblateness was considered in Ref. 2 and the equations are included here for convenience. Oblateness does not directly enter the power and mass derivatives so only its effect on the orbital element derivatives will be shown in this section.

The single-averaged perturbing potential due to  $J_2$  has been calculated in terms of equinoctial coordinates in Ref. 16 and is repeated in Appendix F.  $R_e$  is the equatorial radius of the earth and  $J_2$  is set to .001827. These formulas enter the averaged Hamiltonian as coefficients of the costate (outside the integral since the averaging effect has already been accounted for).

If  $\dot{\underline{z}}_a$  indicates the perturbation due to thrust as given in Eq. (3.72), then the Hamiltonian is given by

$$\tilde{H} = \underline{\lambda}^T \dot{\underline{z}}_{J_2} + \underline{\lambda}^T \dot{\underline{z}}_a \quad (3.132)$$

The state equation is

$$\dot{\underline{z}} = \dot{\underline{z}}_{J_2} + \dot{\underline{z}}_a \quad (3.133)$$

The costate equation is

$$\dot{\underline{\lambda}}^T = - \frac{\partial \tilde{H}}{\partial \underline{z}} = - \underline{\lambda}^T \frac{\partial \dot{\underline{z}}_{J_2}}{\partial \underline{z}} - \int_{-\pi}^{\pi} \left[ \underline{\lambda}^T \frac{\partial \dot{\underline{z}}_a}{\partial \underline{z}} s + \underline{\lambda}^T \dot{\underline{z}}_a \frac{\partial s}{\partial \underline{z}} \right] dF \quad (3.134)$$

The partials indicated by  $\partial \dot{\underline{z}}_{J_2} / \partial \underline{z}$  in the above expression are given in Appendix F.

### 3.8 The Shadow Effect

For SEP missions, the thrusting will be shut off while the spacecraft is in the earth's shadow. The entry and exit angles are needed in order to perform the averaging integral. In calculating these angles the following assumptions are made. The shadow is cylindrical; the earth revolves around the sun in an elliptical orbit; and over one spacecraft revolution, the sun's direction is fixed. The time of thruster turn-on can either be immediately upon exit from the shadow or after a delay following the exit from the shadow. The delay time calculation will be considered in the next section. Calculation of the entry and exit eccentric longitudes was considered in Ref. 2. The pertinent equations are summarized in Appendix G.

Let  $F_2$  refer to the eccentric longitude at entry to the shadow and  $F_1$  at exit (or the thruster turn-on time if a delay is included). That part of the Hamiltonian proportional to thrust is then

$$\tilde{H} = \int_{F_1}^{F_2} H s \, dF \quad (3.135)$$

Thus

$$\dot{\tilde{x}} = \int_{F_1}^{F_2} \dot{\tilde{x}} s \, dF \quad (3.136)$$

and by Leibnitz' rule

$$\dot{\tilde{x}} = - \int_{F_1}^{F_2} \left( \frac{\partial H}{\partial \tilde{x}} s + H \frac{\partial s}{\partial \tilde{x}} \right) dF - \left[ \frac{dF}{d\tilde{x}} H s \right]_{F_2} + \left[ \frac{dF}{d\tilde{x}} H s \right]_{F_1} \quad (3.137)$$

The calculation of  $\frac{dF}{d\tilde{x}}$  is discussed in Appendix G and the modification needed if  $F_1$  includes a delay effect is discussed in the next section.

### 3.9 Delay in Thruster Start-Up After Leaving Shadow

Some orbits of the spacecraft may pass through the shadow of the earth. During this period the thrusters are assumed to be turned off. The shadow entry and exit points are derived as the solution of a quartic equation and given in Appendix G under the assumptions of a cylindrical shadow and stationary sun over one orbital period. It was assumed in Ref. 2 that the thrusters were turned on immediately upon leaving the shadow. A more accurate model is to include a delay in turn on time. This delay time is the sum of the time for the solar array to

achieve operating temperature and the time for the thruster to achieve full thrust after the solar array power is applied to the power processor.

The model used is taken from Ref. 29. The thruster start-up time is modeled as a quadratic function of time in shadow. The solar array temperature adjustment is modeled as a constant of 2 minutes. The total delay is then just

$$\tau_T = a\tau^2 + b\tau + c \quad (3.138)$$

where  $\tau$  is the time in shadow. If  $\tau$  and  $\tau_T$  are in minutes, then

$$\begin{aligned} a &= \frac{1}{7700} \\ b &= \frac{-15}{7700} \\ c &= 12 \end{aligned} \quad (3.139)$$

This function is plotted in Fig. 3-6.

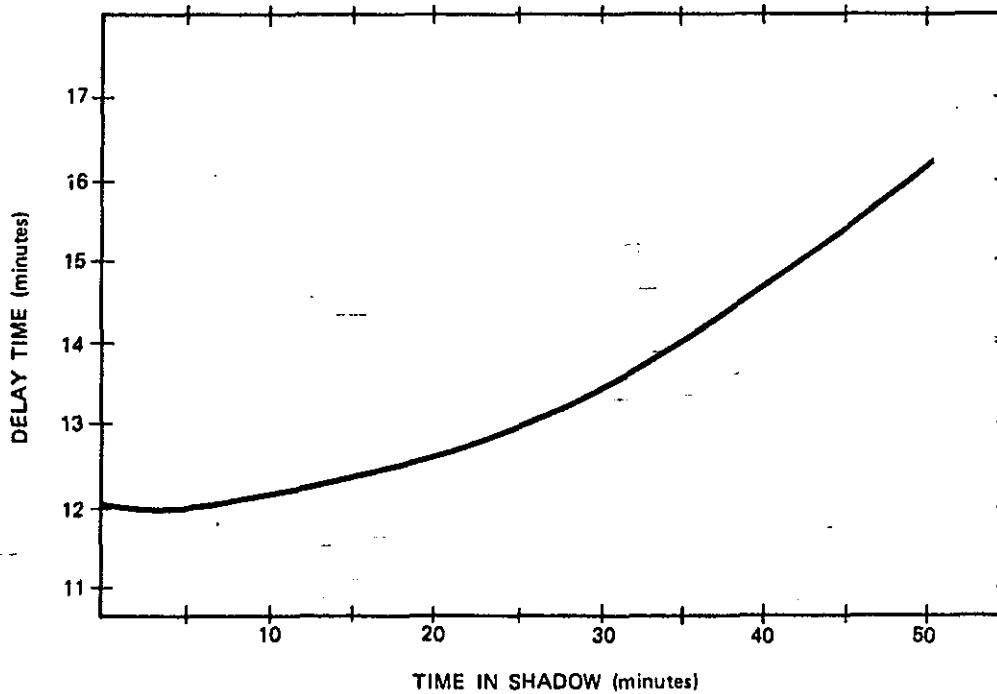


Fig. 3-6 Delay in Thruster Turn-On as Function of Time in Shadow

The shadow entry and exit eccentric longitudes are known. From these the time in shadow is obtained from Kepler's equation. In equinoctial elements the time in shadow is

$$\tau = \left[ (F_{ex} - F_{en}) - k(\sin F_{ex} - k \sin F_{en}) + h(\cos F_{ex} - \cos F_{en}) \right] \frac{1}{n} \quad (3.140)$$

where

$$n = \sqrt{\frac{\mu}{a^3}} \quad (3.141)$$

The shadow delay time can then be calculated. We desire to know the eccentric longitude at which the thrusters are turned on, thus given the exit angle and the delay time, Kepler's equation must be solved for the eccentric longitude  $F_\tau$  at turn-on. If

$$C_o = n\tau_T + F_{ex} - k \sin F_{ex} + h \cos F_{ex} \quad (3.142)$$

Then the required angle satisfies

$$F_\tau = C_o + k \sin F_\tau - h \cos F_\tau \quad (3.143)$$

This transcendental equation can be solved by an iterative procedure. Let

$$F_o = C_o \quad (3.144)$$

$$F_{n+1} = C_o + k \sin F_n - h \cos F_n \quad (3.145)$$

This iteration will converge since  $k^2 + h^2 < 1$ . The iteration can be halted when

$$|F_{n+1} - F_n| < \epsilon \quad (3.146)$$

where  $\epsilon$  is some small number which we set to  $10^{-12}$ . Thus the eccentric longitude at thruster turn-on is obtained.

For the costate equation, Eq. (3.137),  $\frac{dF}{dz}$  is needed at turn-on.  $\frac{dF_{ex}}{dz}$  and  $\frac{dF_{en}}{dz}$  were already obtained (App. G).  $F_\tau$  satisfied Eq. (3.143) so

$$\frac{dF_\tau}{dz} = \frac{1}{1 - k \cos F_\tau - h \sin F_\tau} \frac{dC_o}{dz} \quad (3.147)$$

$$\frac{dC_o}{dz} = \frac{\partial n}{\partial z} t_T + n \frac{\partial t_T}{\partial z} + (1 - k \cos F_{ex} - h \sin F_{ex}) \frac{dF_{ex}}{dz} \quad (3.148)$$

Since  $t_T = a\tau^2 + b\tau + c$

$$\frac{\partial t_T}{\partial z} = (2a\tau + b) \frac{\partial \tau}{\partial z} \quad (3.149)$$

From the definition of  $\tau$  in Eq. (3.140) is obtained

$$\frac{\partial \tau}{\partial z} = \frac{1}{n} \left[ (1 - k \cos F_{ex} - h \sin F_{ex}) \frac{dF_{ex}}{dz} - (1 - k \cos F_{en} - h \sin F_{en}) \frac{dF_{en}}{dz} \right] - \frac{\tau}{n} \frac{\partial n}{\partial z} \quad (3.150)$$

Inserting these partials into Eq. (3.147) yields

$$\frac{dF_t}{dz} = \frac{1}{r_T} \left[ (2a\tau + b + 1) r_{ex} \frac{dF_{ex}}{dz} - (2a\tau + b) r_{en} \frac{dF_{en}}{dz} + (t_T - (2a\tau + b)\tau) \frac{\partial n}{\partial z} \right] \quad (3.151)$$

where

$$r_T = 1 - k \cos F_T - h \sin F_T \quad (3.152)$$

$$r_{en} = 1 - k \cos F_{en} - h \sin F_{en} \quad (3.153)$$

$$r_{ex} = 1 - k \cos F_{ex} - h \sin F_{ex} \quad (3.154)$$

and since  $n$  is only a function of semimajor axis by Eq. (3.141), the only nonzero element of  $\frac{\partial n}{\partial z}$  is

$$\frac{\partial n}{\partial a} = -\frac{3}{2} \frac{n}{a} \quad (3.155)$$

### 3.10 Power and Fluence: The Damage Function

Power degrades as a function of accumulated fluence which is represented by a damage function,  $D(N)$ . This damage function is given in Section 4. To calculate the costate equation, its partial derivative is needed. The damage equation is stated here.

$$D(N) = \exp\{C_1 + C_2(\log_{10}N)^{12}\} \quad (3.156)$$

where  $N$  is the accumulated equivalent 1 MEV electron fluence and  $C_1$  and  $C_2$  are constants for any particular spacecraft, but are functions of cell thickness and base resistivity as indicated in Section 4.3 in Eqs. (4.5) and (4.6). Then

$$\frac{\partial D}{\partial N} = \frac{12 \log_{10} e}{N} C_2 (\log_{10} N)^{11} D(N) \quad (3.157)$$

This form of the damage function can cause numerical difficulties at the initial orbit if the initial  $N(t_0)$  is set at too small a value and the integration time step is large since  $\frac{\partial D}{\partial N}$  looks like a gamma function with very high values for  $N < 10^{10}$ . Typically, a value of  $\Delta N$  for a low orbit would be around  $10^{12}$ , so that it would be reasonable to pick a starting value greater than  $10^{10}$ . In the coding for the program, if the initial  $N$  is zero, then a revised initial  $N$  is calculated which is the "average" of the amount of fluence encountered on the first orbit, i. e.,

$$\bar{N}(t_0) = \frac{\dot{N}(t_0) \cdot T_0}{2} \quad (3.158)$$

where  $T_0$  is the orbital period. Facility also exists for inputting a nonzero initial value for  $N$ .

### 3.11 The Flux Equations

An analytic equation for the flux as a function of spatial coordinates is constructed in Section 4.2. It is repeated here, with slightly different notation.

$$\dot{N} = \exp\left(\sum_{i=1}^5 A_i S^{i-1}\right) \quad (3.159)$$

where flux  $\dot{N}$  is in equivalent 1 MEV particles,

$$S = \ln(R - 1) \quad (3.160)$$

where  $R$  is the radial distance from the Earth's center in units of Earth radii, and

$$A_i = \sum_{j=1}^5 \sum_{m=0}^2 K_{i,j+5m} \text{LAT}^{j-1} \text{SH}^m \quad (3.161)$$

where LAT is geographic latitude in degrees, SH is shield thickness in mils and the  $K_{i,j+5m}$  are coefficients given in Tables 4-4, 4-5. The total flux is a sum of up to four equations like Eq. (3.158), two for the front shielding, two for the back shielding, one of the two for electrons, one for protons. If the back shielding is infinite then the sum will have only two members. If the front and back shielding are equal only one equation like Eq. (3.158) need be calculated for protons and one for electrons and then to get total flux, their sum would be doubled. In the remainder of this section we will consider only a single equation like Eq. (3.158).

Since the shield thickness does not vary for a particular spacecraft the sum involving SH can be done once initially and Eq. (3.161) can be rewritten

$$A_i = \sum_{j=1}^5 \tilde{K}_{ij} w^{j-1} \quad i = 1, \dots, 5 \quad (3.162)$$

where

$$\tilde{K}_{ij} = \left[ \sum_{m=0}^2 K_{i,j+5m} SH^m \right] / (DTR)^{j-1} \quad i = 1, \dots, 5 \quad j = 1, \dots, 5 \quad (3.163)$$

Here  $w$  is latitude in radians, DTR is the degree to radian conversion factor. Thus Eq. (3.159) can be calculated at any point on the spacecraft orbit as a function of latitude, radial distance, and the constant coefficients of Eq. (3.163). The radial distance is just

$$R = \sqrt{X_1^2 + Y_1^2} \quad (3.164)$$

where  $X_1$  and  $Y_1$  were given in Eq. (3.19) and (3.20). The latitude is the arcsine of the angle between the vector pointing through the north pole and the spacecraft radius vector. This is given by

$$w = \sin^{-1} \left( \frac{\hat{f}_3 X_1 + \hat{g}_3 Y_1}{R} \right) \quad (3.165)$$

where  $\hat{f}_3$  and  $\hat{g}_3$  are the third components of the unit vectors given in Eq. (3.4). They are functions only of  $p$  and  $q$  whereas  $X_1$ ,  $Y_1$  (and  $R$ ) are functions of  $a$ ,  $h$  and  $k$ .

In order to calculate the costate equations the partial of flux with respect to the orbital elements must be known.

$$\frac{\partial \dot{N}}{\partial \underline{z}} = N \left\{ \sum_{i=1}^5 \frac{\partial A_i}{\partial \underline{z}} u^{i+1} + \sum A_i u^{i-2(i-1)} \frac{\partial u}{\partial \underline{z}} \right\} \quad (3.166)$$

where

$$\frac{\partial A_i}{\partial \underline{z}} = \sum_{j=2}^5 K_{ij} w^{j-2(j-1)} \frac{\partial w}{\partial \underline{z}} \quad (3.167)$$

Let

$$E_i = \sum_{j=2}^5 \tilde{K}_{ij} w^{j-2(j-1)} \quad (3.168)$$

Then rewriting Eq. (3.166),

$$\frac{\partial \dot{N}}{\partial \underline{z}} = \dot{N} \left\{ \left[ \sum_{i=1}^5 E_i u^{i-1} \right] \frac{\partial w}{\partial \underline{z}} + \left[ \sum_{i=2}^5 A_i u^{i-2(i-1)} \right] \frac{\partial u}{\partial \underline{z}} \right\} \quad (3.169)$$

Now

$$\frac{\partial u}{\partial \underline{z}} = \frac{1}{(R-1)R} \left( X_1 \frac{\partial X_1}{\partial \underline{z}} + Y_1 \frac{\partial Y_1}{\partial \underline{z}} \right) \quad (3.170)$$

For h and k,  $\frac{\partial X_1}{\partial \underline{z}}$  and  $\frac{\partial Y_1}{\partial \underline{z}}$  were given in Appendix B. For the semimajor axis, a,

$$\frac{\partial u}{\partial a} = \frac{R}{(R-1)a} \quad (3.171)$$

Latitude is not a function of a (the a's in the numerator and in the denominator cancel out in Eq. (3.165)) so that  $\frac{\partial w}{\partial a} = 0$ . For the other elements

$$\begin{aligned} \frac{\partial w}{\partial \underline{z}} = & \frac{1}{R \cos w} \left\{ \frac{\partial X_1}{\partial \underline{z}} \hat{f}_3 + \frac{\partial Y_1}{\partial \underline{z}} \hat{g}_3 + X_1 \frac{\partial \hat{f}_3}{\partial \underline{z}} + Y_1 \frac{\partial \hat{g}_3}{\partial \underline{z}} \right. \\ & \left. - \frac{(X_1 \hat{f}_3 + Y_1 \hat{g}_3)}{R^2} \left( X_1 \frac{\partial X_1}{\partial \underline{z}} + Y_1 \frac{\partial Y_1}{\partial \underline{z}} \right) \right\} \quad (3.172) \end{aligned}$$

where  $X_1$  and  $Y_1$  are functions only of  $h$  and  $k$  and the partials of  $\hat{f}$  and  $\hat{g}$  were given in Appendix D. Here the necessary components are

$$\frac{\partial \hat{f}_3}{\partial p} = \frac{2}{1+p^2+q^2} (q \hat{g}_3 + \hat{w}_3) \quad (3.173)$$

$$\frac{\partial \hat{f}_3}{\partial q} = \frac{2p}{1+p^2+q^2} \hat{g}_3 \quad (3.174)$$

$$\frac{\partial \hat{g}_3}{\partial p} = \frac{2q}{1+p^2+q^2} \hat{f}_3 \quad (3.175)$$

$$\frac{\partial \hat{g}_3}{\partial q} = \frac{2}{1+p^2+q^2} (-p \hat{f}_3 + \hat{w}_3) \quad (3.176)$$

This completes the terms given in Eq. (3.105).

### 3.12 Summary of State and Costate Equations

In this section the full seven dimensional state and costate equations are summarized. We will assume that we have analytic functions for flux and the damage function without specifying their exact form. Only thrusting in an inverse square field will be considered. The effect of oblateness is easily included by adding  $\frac{z}{2} J_2$  to the orbital element equations and  $-\lambda^T \frac{\partial z J_2}{\partial z}$  to the orbital element adjoint equations, where these expressions were given in Section 3.7 and App. F.

We can consider a seven dimensional state composed of five orbital elements, mass, and accumulated particle flux.

$$\underline{x} = \begin{bmatrix} z \\ m \\ N \end{bmatrix} \quad (3.177)$$

Since  $m$  and  $N$  are varying slowly the first approximation of these quantities as well as the orbital elements can be considered. The unaveraged state equations are

$$\dot{\underline{z}} = \frac{2P}{mc} (\underline{x}, t, F, \hat{u}) M(\underline{z}, F) \hat{u} \quad (3.178)$$

$$\dot{m} = -\frac{2P}{c} (\underline{x}, t, F, \hat{u}) \quad (3.179)$$

$$\dot{N} = f(\underline{z}, F) \quad (3.180)$$

and

$$P = \frac{\eta P_0 D(N)}{R_S^2(t)} \cos[\phi(\underline{z}, \hat{u})] \quad (3.181)$$

For a particular orbit  $P$  is assumed to be zero for eccentric longitudes between  $F_2$  and  $F_1$  where  $F_2$  is the eccentric longitude at entry into the earth's shadow and  $F_1$  is the eccentric longitude either at exit from the shadow or after a turn-on delay time after leaving the shadow.

The unaveraged Hamiltonian is

$$H = \underline{\lambda}^T \dot{\underline{x}} = H_z + H_m + H_N \quad (3.182)$$

where

$$H_z = \underline{\lambda}_z^T \dot{\underline{z}} \quad (3.183)$$

$$H_m = \lambda_m \dot{m} \quad (3.184)$$

$$H_N = \lambda_N \dot{N} \quad (3.185)$$

The averaged Hamiltonian is

$$\begin{aligned} \tilde{H} = \int_{-\pi}^{\pi} H(\underline{x}, \underline{\lambda}, \bar{t}, F, \hat{u}) s(\bar{h}, \bar{k}, F) dF &= \int_{-\pi}^{\pi} \underline{\lambda}_z^T \dot{\underline{z}}(\underline{x}, \bar{t}, F, \hat{u}) \\ &+ \bar{\lambda}_m \dot{m}(\underline{x}, \bar{t}, F, \hat{u}) s(\bar{h}, \bar{k}, F) dF + \int_{-\pi}^{\pi} \bar{\lambda}_N \dot{N}(\underline{z}, F) s(\bar{h}, \bar{k}, F) dF \end{aligned} \quad (3.186)$$

The state equations are

$$\dot{\underline{z}} = \frac{\partial \tilde{H}^T}{\partial \underline{\lambda}_z} = \int_{F_1}^{F_2} 2 \dot{\underline{z}}(\underline{x}, \bar{t}, F, \hat{u}) s(\bar{h}, \bar{k}, F) dF = \frac{2}{mc} \int_{F_1}^{F_2} P(\underline{x}, \bar{t}, F, \hat{u}) M(\underline{z}, F) s(\bar{h}, \bar{k}, F) dF \quad (3.187)$$

$$\dot{\underline{m}} = \frac{\partial \tilde{H}}{\partial \underline{\lambda}_m} = \int_{F_1}^{F_2} \dot{m}(\underline{x}, \underline{t}, F, \hat{\underline{u}}) s(\bar{h}, \bar{k}, F) dF = - \frac{1}{c^2} \int_{F_1}^{F_2} P(\underline{x}, \underline{t}, F, \hat{\underline{u}}) s(\bar{h}, \bar{k}, F) dF \quad (3.188)$$

$$\dot{N} = \frac{\partial \tilde{H}}{\partial \underline{\lambda}_N} = \int_{-\pi}^{\pi} \dot{N}(\underline{z}, F) s(\bar{h}, \bar{k}, F) dF \quad (3.189)$$

The averaged Hamiltonian can be broken up into three parts

$$\tilde{H} = \tilde{H}_z + \tilde{H}_m + \tilde{H}_N \quad (3.190)$$

where

$$\tilde{H}_z = \underline{\lambda}_z^T \dot{\underline{z}} \quad (3.191)$$

$$\tilde{H}_m = \underline{\lambda}_m \dot{\underline{m}} \quad (3.192)$$

$$\tilde{H}_N = \underline{\lambda}_N \dot{N} \quad (3.193)$$

The costate derivatives are

$$\begin{aligned} \dot{\underline{\lambda}}_z^T &= - \frac{\partial \tilde{H}}{\partial \underline{z}} = - \int_{F_1}^{F_2} \left\{ \underline{\lambda}_z^T \frac{\partial \dot{\underline{z}}}{\partial \underline{z}}(\underline{x}, \underline{t}, F, \hat{\underline{u}}) \cdot s(\bar{h}, \bar{k}, F) \right. \\ &+ \left. \left( \underline{\lambda}_z^T \dot{\underline{z}}(\underline{x}, \underline{t}, F, \hat{\underline{u}}) + \underline{\lambda}_m \dot{m}(\underline{x}, \underline{t}, F, \hat{\underline{u}}) \frac{\partial s}{\partial \underline{z}}(\bar{h}, \bar{k}, F) \right) \right\} dF \\ &- \frac{dF}{d\underline{z}} \Big|_{F_2} \left[ \underline{\lambda}_z^T \dot{\underline{z}}(\underline{x}, \underline{t}, F_2, \hat{\underline{u}}) + \underline{\lambda}_m \dot{m}(\underline{x}, \underline{t}, F_2, \hat{\underline{u}}) \right] s(\bar{h}, \bar{k}, F_2) \\ &+ \frac{dF}{d\underline{z}} \Big|_{F_1} \left[ \underline{\lambda}_z^T \dot{\underline{z}}(\underline{x}, \underline{t}, F_1, \hat{\underline{u}}) + \underline{\lambda}_m \dot{m}(\underline{x}, \underline{t}, F_1, \hat{\underline{u}}) \right] s(\bar{h}, \bar{k}, F_1) \\ &- \int_{-\pi}^{\pi} \left\{ \underline{\lambda}_N \frac{\partial \dot{N}}{\partial \underline{z}}(\underline{z}, F) s(\bar{h}, \bar{k}, F) + \underline{\lambda}_N \dot{N}(\underline{z}, F) \frac{\partial s}{\partial \underline{z}}(\bar{h}, \bar{k}, F) \right\} dF \quad (3.194) \end{aligned}$$

This can also be written

$$\begin{aligned}
\dot{\bar{\lambda}}_z^T &= - \int_{F_1}^{F_2} \left\{ \bar{\lambda}_z^T \frac{\partial \dot{z}}{\partial \bar{z}} (\bar{x}, \bar{t}, F, \hat{u}) s(\bar{h}, \bar{k}, F) + \left[ H_z (\bar{x}, \bar{\lambda}_z, \bar{t}, F, \hat{u}) \right. \right. \\
&\quad \left. \left. + H_m (\bar{x}, \bar{\lambda}_m, \bar{t}, F, \hat{u}) \right] \frac{\partial s(\bar{h}, \bar{k}, F) dF}{d\bar{z}} \right. \\
&\quad \left. - \frac{dF}{d\bar{z}} \Big|_{F_2} \left( H_z (\bar{x}, \bar{\lambda}_z, \bar{t}, F_2, \hat{u}) + H_m (\bar{x}, \bar{\lambda}_m, \bar{t}, F_2, \hat{u}) s(\bar{h}, \bar{k}, F_2) \right) \right. \\
&\quad \left. + \frac{dF}{d\bar{z}} \Big|_{F_1} \left( H_z (\bar{x}, \bar{\lambda}_z, \bar{t}, F_1, \hat{u}) + H_m (\bar{x}, \bar{\lambda}_m, \bar{t}, F_1, \hat{u}) s(\bar{h}, \bar{k}, F_1) \right) \right. \\
&\quad \left. - \int_{-\pi}^{\pi} \bar{\lambda}_N \left\{ \frac{\partial \dot{N}(\bar{z}, F)}{\partial \bar{z}} s(\bar{h}, \bar{k}, F) + \dot{N}(\bar{z}, F) \frac{\partial s(\bar{h}, \bar{k}, F)}{\partial \bar{z}} \right\} dF \right. \quad (3.195)
\end{aligned}$$

Next

$$\dot{\bar{\lambda}}_m = - \frac{\partial \tilde{H}}{\partial \bar{m}} = \frac{2}{\bar{m}^2 c} \int_{F_1}^{F_2} \bar{\lambda}_z^T P(\bar{x}, \bar{t}, F, \hat{u}) M(\bar{z}, F) s(\bar{h}, \bar{k}, F) dF \quad (3.196)$$

but this just yields

$$\dot{\bar{\lambda}}_m = \frac{\tilde{H}_z}{\bar{m}} \quad (3.197)$$

Finally

$$\dot{\bar{\lambda}}_N = - \frac{\partial \tilde{H}}{\partial \bar{N}} = - \frac{2}{c} \int_{F_1}^{F_2} \frac{\partial P(\bar{x}, \bar{t}, F, \hat{u})}{\partial \bar{N}} \left\{ \frac{\bar{\lambda}_z^T M(\bar{z}, F) \hat{u}}{\bar{m}} - \frac{\bar{\lambda}_m}{c} \right\} s(\bar{h}, \bar{k}, F) dF \quad (3.198)$$

The dependence of P on N comes from the D(N) factor, the damage function. Thus simplifying

$$\dot{\bar{\lambda}}_N = - \frac{\partial D(N)}{\partial N} \frac{(\tilde{H}_z + \tilde{H}_m)}{D(N)} \quad (3.199)$$

### 3.13 Spacecraft Parameter Output

It was desired to have the option of printing various spacecraft parameters at various points on an orbit. These parameters and the method of calculating them are discussed in this section. The parameters include: in-plane and out-of-plane thrust angles, yaw, pitch, and roll angles, the panel orientation angle, the sun incidence angles on the panel and the three contiguous sides of the center body.

A nominal x-y-z body centered coordinate system was defined earlier and illustrated in Fig. 1-1. The yaw axis,  $\hat{e}_z$ , is pointed along the radius vector toward the earth, the pitch axis,  $\hat{e}_y$  is normal to the orbit plane in a "downward" direction, the roll axis,  $\hat{e}_x$  is in the orbit plane perpendicular to the radius vector in the forward hemisphere. In terms of the equinoctial orbital frame  $\hat{f}$ ,  $\hat{g}$ ,  $\hat{w}$ ,

$$\hat{e}_x = -\frac{Y_1}{r} \hat{f} + \frac{X_1}{r} \hat{g} \quad (3.200)$$

$$\hat{e}_y = -\hat{w} \quad (3.201)$$

$$\hat{e}_z = -\frac{X_1}{r} \hat{f} - \frac{Y_1}{r} \hat{g} \quad (3.202)$$

The thrust acceleration direction is available in the equinoctial coordinate system. Using the above transformation it can be obtained in the  $\hat{e}_x$ ,  $\hat{e}_y$ ,  $\hat{e}_z$  system. The in-plane angle,  $\theta_i$ , and the out-of-plane angle,  $\theta_o$ , are related to the unit thrust acceleration direction by

$$\hat{u} = \cos \theta_o \cos \theta_i \hat{e}_x - \sin \theta_o \hat{e}_y - \cos \theta_o \sin \theta_i \hat{e}_z \quad (3.203)$$

which is illustrated in Fig. 3-7, where  $\hat{e}_r = -\hat{e}_z$  and  $\hat{e}_h = -\hat{e}_y$ .

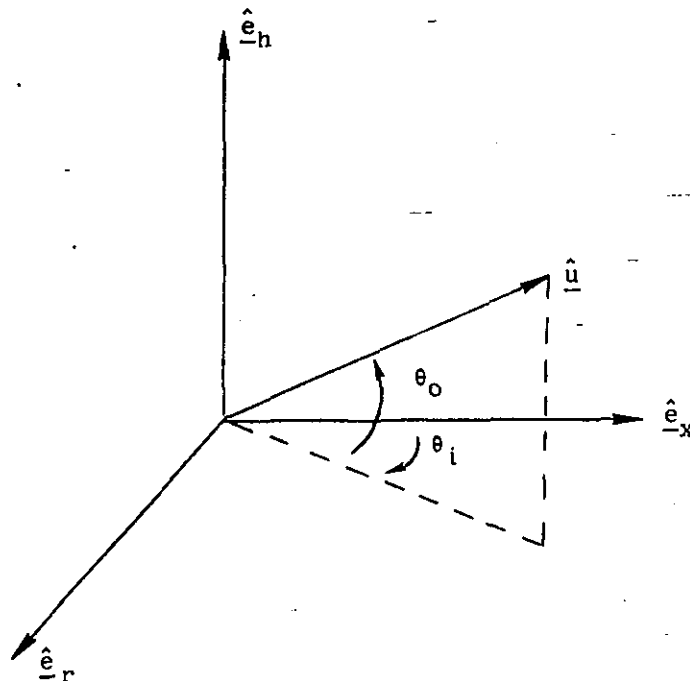


Fig. 3-7 In-plane and Out-of-plane Angles

Then  $\theta_o$  and  $\theta_i$  can be calculated from

$$\sin \theta_o = -u_y, \quad |\theta_o| \leq \frac{\pi}{2} \quad (3.204)$$

$$\cos \theta_i = \frac{u_x}{\cos \theta_o} \quad (3.205)$$

$$\sin \theta_i = -\frac{u_z}{\cos \theta_o} \quad (3.206)$$

If pitch and roll are constrained to be zero then  $\theta_i = 0$ .

The Euler angle order is yaw, pitch, and roll. The thrust acceleration direction as given in terms of yaw,  $\psi_y$ , and pitch,  $\theta$ , by

$$\hat{u} = \cos \theta \cos \psi_y \hat{e}_{-x} + \cos \theta \sin \psi_y \hat{e}_{-y} - \sin \theta \hat{e}_{-z} \quad (3.207)$$

which is illustrated in Fig. 3-8. Note that the axes are not the same as in Fig. 3-7.

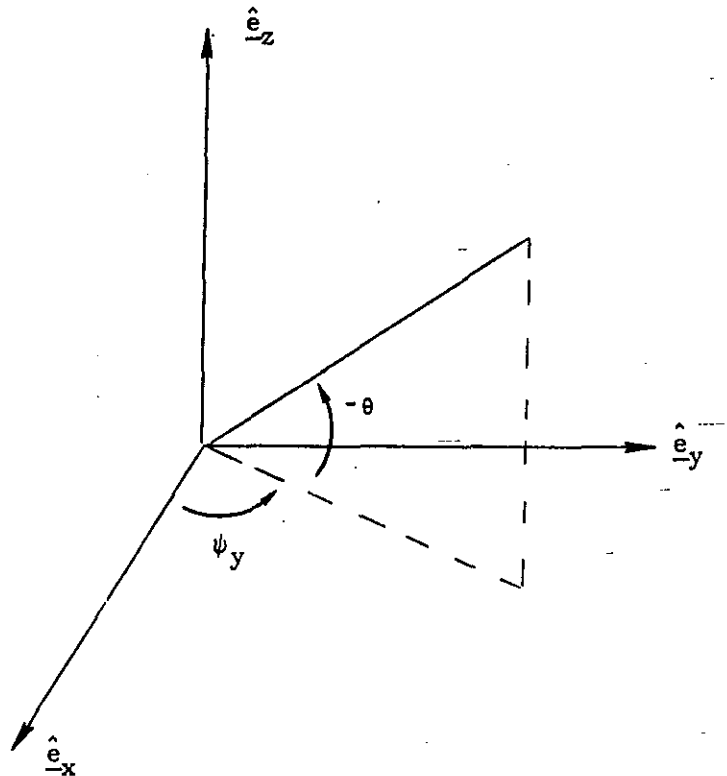


Fig. 3-8 Yaw and Pitch Angles

Since  $\hat{u}$  is known  $\psi_y$  and  $\theta$  can be calculated from

$$\sin \theta = -u_z \quad |\theta| \leq \frac{\pi}{2} \quad (3.208)$$

$$\cos \psi_y = \frac{u_x}{\cos \theta} \quad (3.209)$$

$$\sin \psi_y = \frac{u_y}{\cos \theta} \quad (3.210)$$

For the pitch constrained case  $\theta = 0$  and  $\psi_y = \theta_0$ .

For the constrained case roll is assumed to be zero. If there is no roll constraint, then by a roll rotation and by a panel rotation about their longitudinal axis the panels can be faced directly at the sun to produce maximum power. If the roll is accomplished before the panel rotation, then the roll angle should be such that the panel axis is perpendicular to the sun line. The vector along the panel axis (also the pitch axis) after the yaw, pitch, and roll rotations should have an inner product with the vector pointing toward the sun of zero. Thus

$$(R_s^{xyz})^T [\psi_y]^T [\theta]^T [\sigma]^T \begin{bmatrix} 0 \\ 1 \\ 0 \end{bmatrix} = 0 \quad (3.211)$$

where the yaw rotation matrix is

$$[\psi_y] = \begin{bmatrix} \cos \psi & \sin \psi & 0 \\ -\sin \psi & \cos \psi & 0 \\ 0 & 0 & 1 \end{bmatrix} \quad (3.212)$$

The pitch rotation matrix is

$$[\theta] = \begin{bmatrix} \cos \theta & 0 & -\sin \theta \\ 0 & 1 & 0 \\ \sin \theta & 0 & \cos \theta \end{bmatrix} \quad (3.213)$$

and the roll rotation matrix is

$$[\sigma] = \begin{bmatrix} 1 & 0 & 0 \\ 0 & \cos \sigma & \sin \sigma \\ 0 & -\sin \sigma & \cos \sigma \end{bmatrix} \quad (3.214)$$

Since  $\psi_y$  and  $\theta$  are already known let

$$\begin{bmatrix} R'_x \\ R'_y \\ R'_z \end{bmatrix} = [\theta] [\psi_y] R_s^{xyz} \quad (3.215)$$

and then

$$R'_y \cos \sigma + R'_z \sin \sigma = 0 \quad (3.216)$$

Let

$$\tan \sigma = \frac{-R'_y}{R'_z} \quad (3.217)$$

with a  $360^\circ$  range.

We assume the panel orientation angle is zero when the normal to the panel is pointed in the z direction. Since for the roll free case the panel axis is perpendicular to the sun direction after roll, the panel can be faced directly at the sun. If roll is constrained to be zero, the panel will be rotated to minimize the angle between the normal to the panels and the direction to the sun. Let

$$\begin{bmatrix} R''_x \\ R''_y \\ R''_z \end{bmatrix} = [\phi] [\theta] [\psi] R_s^{xyz} \quad (3.218)$$

which is the sun direction in the rotated coordinate frame. Since the normal to the panel is nominally along the z direction it must be rotated by an angle given by

$$\cos \zeta = R''_z \quad (3.219)$$

for the unconstrained case. The sun incidence angle will then be zero. For the constrained case, we want to maximize the cosine of the incidence angle. This is given by

$$\cos i_p = \cos \zeta R''_z + \sin \zeta R''_x \quad (3.220)$$

which is maximized by setting

$$\cos \zeta = \frac{R''_z}{\sqrt{R''_x^2 + R''_z^2}} \quad (3.221)$$

$$\sin \zeta = \frac{R_x''}{\sqrt{R_x''^2 + R_z''^2}} \quad (3.222)$$

and then

$$i_p = \cos^{-1} \sqrt{R_x''^2 + R_z''^2} \quad (3.223)$$

The above three formulas are valid for the unconstrained case also since then  $R_y'' = 0$  and  $i_p = 0^\circ$ .

After the three Euler rotations the direction of the sun in the rotated system is just  $(R_x'', R_y'', R_z'')$ . These are the cosines of the angle between the normal to the sides of the spacecraft and the spacecraft sun vector and thus yield the incidence angles on the spacecraft surfaces.

Some additional quantities are also calculated such as the sun angle in x-y, i.e., the angle which the projection of the sun vector on the  $\hat{e}_x, \hat{e}_y$  plane makes with the  $\hat{e}_x$  axis and the thrust angle  $\psi$  defined as  $\psi = \psi_y - \text{sun angle}$ . This is the control angle used in Section 3.6.

## SECTION 4

### RADIATION AND POWER LOSS MODEL

#### 4.1 Introduction

Solar cell degradation models are an integral part of low thrust solar electric spacecraft trajectory calculations. For these missions the thrust magnitude decays as the solar cell power is degraded by exposure of the cell to energetic trapped particles. Solar electric spacecraft trajectory computer programs include both codes that accurately simulate a mission and codes that optimize trajectories. An example of the former is the program SEOR<sup>(5)</sup> which uses a detailed radiation degradation calculation based upon the models of Obenschain<sup>(30)</sup>. The code described in this report and its predecessor in Ref. 2 are examples of trajectory optimization codes. These two types of codes place different requirements on the model used for radiation degradation calculations. For simulations the computational goal is maximum realism so that an accurate assessment of the mission requirements can be made. For optimization codes the goal of maximum realism is maintained, but the constraint of maintaining tractable run times imposes severe limitations on the degradation calculations.

There are two basic types of degradation models which have been constructed: Those that recall basic NSSDC (National Space Science Data Center) subroutines for the magnetic field and spectral flux and determine the degradation integral at each trajectory sample point; and those which establish a data file of orbital average degradation. An example of the former is the highly accurate and comprehensive degradation calculation used in SEOR<sup>(5)</sup>. The SEOR type procedure whereby the fluence is calculated during the trajectory integration via the calling of several NSSDC subroutines would be excessively time consuming when used in an optimization program. For an orbit of 18 sample points, and for 15 energy bands, the NSSDC subroutines INVARA and MODEL combined with a simple energy integration code require a computation time of 0.2 seconds/orbit on an IBM 360. A typical trajectory optimization run with SECKSPOT may comprise some 50 separate trajectories and iterate the solar cell degradation calculation 50,000 times. Therefore several hours of machine time would be required if these calculations were made by the standard codes. Thus efficiency demands an approach for the degradation model used in optimization codes different than that frequently used in simulations

To achieve this efficiency most degradation models used in optimization programs are of the data file type. The model in the GEOTOP<sup>(31)</sup> program is of this type and is based on a table look up approach allowing only limited values of orbit parameters between which interpolation is used. Entries in the table are total 1MEV equivalent fluence for one orbit, and the table arguments are apogee, perigee, and inclination. The maximum orbital inclination of the GEOTOP model is 30°. A simpler model than the GEOTOP model has been used in optimization codes such as MOLTOP<sup>(4)</sup>. This model is restricted to a single inclination and has no provision for changing cell characteristics.

The degradation model presented in this paper extends the latitude range, provides a continuous and smooth representation of the flux field, and provides for changing the cell characteristics. And the deficiencies of the above data file models have been avoided without sacrificing computational speed; a typical trajectory fluence calculation requires only a fraction of a minute for thousands of sample points. Further, the model is extremely simple to code, with all required information presented in this section. It is based upon two analytic expressions:  $D(N, BR, TH)$  which describes solar cell power degradation as a function 1MEV equivalent fluence ( $N$ ), cell base resistivity ( $BR$ ) and thickness ( $TH$ ), and  $f(R, L, SH)$  which describes a spatial field of 1MEV equivalent electron flux. The parameter  $R$  is distance from the earth's centroid,  $L$  is latitude, and  $SH$  is cell shield thickness. When the flux  $f$  is time integrated over a sequence of trajectory time steps the result is a fluence value  $N$  which is entered into the degradation equation  $D(N, BR, TH)$  to obtain the fractional power loss. By constructing the model in an analytic format it is possible to make computation time minimal, and also to allow analytic differentiation of the flux and power loss for computation of adjoint variables for optimization studies in codes like SECKSPOT. The analytical expressions for  $D$  and  $f$  contain a number of coefficients derived externally from the trajectory optimization code using the NSSDC codes. A major advantage of this approach is that the coefficients can be altered to reflect new cell damage data or radiation belt data with minimal effort. 1MEV flux values are averaged over one day in the model. Although this is not a requirement for the construction of this type of model it eliminates the requirement for integration time steps that are a small fraction of a day. The flux field is defined in geocentric coordinates to eliminate the need for a series of transformations from geomagnetic to geocentric coordinates. A model dividing the problem into the same two sub-models was previously constructed by Ives<sup>(32)</sup>, however, the Ives model was tabular in format, limited to equatorial orbits, and did not contain cell characteristics as parameters.

#### 4.2 1MEV Equivalent Electron Flux Field Model

Construction of the 1MEV flux analytical model is a two step procedure. In the first step a space of discrete values of 1MEV flux is generated from particle spectral flux data, and from data concerning the conversion of spectral flux to 1MEV flux. The second step consists of fitting the array of discrete points with analytic expressions by means of a multivariate regression analysis.

Generation of the 1MEV equivalent electron field points is accomplished by a series of integrations. The complete procedure is illustrated in Fig. 4-1. A symbolic guide to the flow diagram is given below in Table 4-1. The process begins by calling the NSSDC code INVARA<sup>(33)</sup> which converts a set of geocentric coordinates to the magnetic coordinates B and L. B is the magnetic field intensity, and L is the magnetic invariant associated with particle momentum along the magnetic field lines. Seven choices of a model for the magnetic field are available within the code INVARA. For the work here the IGRF (International Geophysical Reference Field) option has been selected. This option was recommended by E. G. Stassinopoulos (in a private communication) of NSSDC as an often used reference model. The time selected for the field was 1978.

Flow Diagram for SEP Degradation Calculation

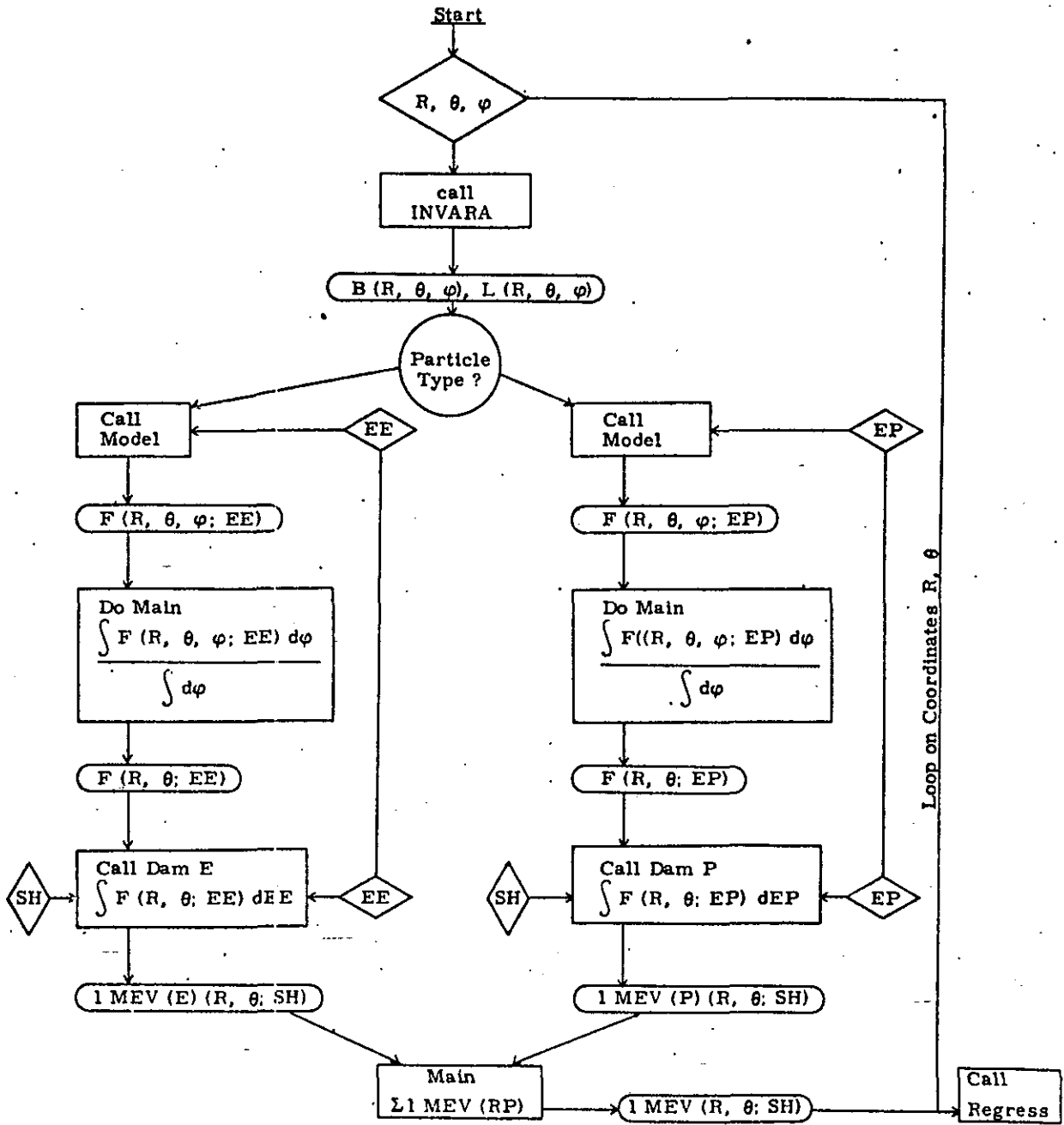


Fig. 4-1 Flow Diagrams for Flux Field Calculations

Table 4-1 Legend for Figure 4-1

Key:	Do X, Y	Indicates code, activity
	A, B	Input Function
	?	Branch point
	Σ I, r <sub>1</sub>	Results
Definitions:	R	= Radius, i. e., dist. from center of earth
	θ	= Latitude
	φ	= Longitude
	B	= Magnetic field intensity
	L	= Magnetic invariant
	EE, FP	= Electron and proton energy array
	F	= Particle flux (spectral)
	SH	= Shield thickness
	1 MEV	= Equivalent 1 MEV particle flux
Codes:	INVARA	= From NSSDC, magnetic field code
	MODEL	= From NSSDC, flux code
	MAIN	= Calling code, input output, etc.
	DAM E	= Electron damage subroutine
	DAM P	= Proton damage subroutine
	REGRESS	= IBM code for multivariate regression

The magnetic coordinates B and L are entered into the subroutine MODEL which computes proton and electron flux within a selected energy interval. This is done for the entire range of important energies. MODEL<sup>(34)</sup> is a standard particle flux code produced by NSSDC, and the fluxes it produces are based upon smoothed satellite data. The data in MODEL is in block form, and interpolation is used between defined points. MODEL data is based upon satellite measurements made in the period 1964-1967. It represents a solar cycle maximum. The energy intervals selected for flux evaluation are dictated in part by the MODEL code. The code allows energy increments which vary over the total energy range. Practical upper limits on energy are set by flux values which are less than unity. Lower energy limits are set both by MODEL and by shielding considerations. For protons, the lower energy cut-off is related to shield thickness (SH) by the relationship

$$EP \text{ (MEV)} = 1.53 \text{ (SH)}^{.66}$$

which was obtained by a fit to the data of Rasmussen<sup>(35)</sup>. For both electrons and protons fifteen energy steps have been used. The proton energy range is 0 to 40 MEV with the lower end adjusted by the above formula. For electrons the range used was 0.2 to 4.8 MEV.

Spectral flux values produced by subroutine MODEL are averaged over longitude to give a one day mean flux. The aim of this averaging is to avoid keeping time of day in the trajectory optimization code. Retaining time would require additional coordinate transformations and would add another dimension of complexity to the field fitting problem. Variation of the flux field with longitude is considerable. An example of the range of flux values is shown below in Table 4-2 for protons in the energy range 4-5 MEV.

Table 4-2 Longitudinal Variation of Proton Flux  
(particles/cm<sup>2</sup>/sec)

Longitude	0°	60°	120°
Flux	.135E06	.540E06	.871E06
Longitude	180°	240°	300°
Flux	.393E06	.794E04	.449E03

These values have been obtained near the proton peak at 2.2 earth radii, and at a North latitude of 21.5°. The average value is .330E06. Variations with longitude are caused by two effects, namely the non-dipole asymmetry in the magnetic field, and the non-alignment of the magnetic pole with the geodetic pole. Generally asymmetry effects dominate.

These values have been obtained near the proton peak at 2.2 earth radii, and at a North latitude of 21.5°. The average value is .330E06. Variations with longitude are caused by two effects, namely the non-dipole asymmetry in the magnetic field, and the non-alignment of the magnetic pole with the geodetic pole. Generally asymmetry effects dominate.

Orbital fluence calculations are little affected by the longitudinal averaging since the rotation of the earth and the consequent rotation of the radiation belts does effectively average the fluence.

The next step in the field model construction is an integration which converts the azimuth-averaged spectral flux data to an equivalent 1MEV electron flux. This is accomplished with a weighting function in a Fredholm integral. Using the Figure 4-1 notation, the integral (for electrons) is

$$F'(SH) = \int F(EE) DAME(EE, SH) dEE$$

where EE is the electron energy and SH is the shield thickness, DAME is the electron weight function and F' is the spectral, longitude averaged flux. The function DAME was constructed from data taken from the curves of Rasmussen<sup>(35)</sup> however because of the inaccuracy of this type of data transfer the data had to be restructured. It can be argued by analogy with optical extinction processes that the relationship between shield thickness and the weight function should be exponential, i. e.,

$$\log_{10} DAME = -m(EE)SH + \log_{10} DAME \Big|_{SH=0}$$

This function was found to fit the data very closely and thus was used for the restructuring. The functional form for m(EE) was found to be

$$\log_{10} m(EE) = m' \cdot EE + C$$

where m' and C were obtained by regression. In terms of energy and shield thickness, the function DAME can thus be written

$$DAME = B(EE) 10^{-(10^{m' \cdot EE + C})SH}$$

The coefficient B(EE) is the appropriate DAME function for SH=0. Again, by a regression analysis, B(EE) was found to be (to ± 3%)

$$B(EE) = 10^{(1/2.30)(1.84 + 13.169/\sqrt{EE} + 6.92/EE - 22.6/EE^2)}$$

The equivalent 1MEV flux for protons is computed by the Fredholm integral

$$F'(SH) = \int \text{DAMP}(EP, SH) F(EP) dEP$$

where EP is proton energy. The weighting function for protons (DAMP) was also obtained from the curves of Rasmussen<sup>(35)</sup>. In addition to the cut-off energy described above, the function DAMP is defined by

$$\text{DAMP} = \begin{cases} 10^{-0.72 \log_{10} EP + 4.13} & EP_0 \leq EP < 11 \text{ MEV} \\ 2200 & 11 < EP < 46 \text{ MEV} \\ 10^{-1.1 \log_{10} EP + 5.26} & 46 < EP \text{ MEV} \end{cases}$$

Computation of the weight integrals completes the process of generating raw data for the field model. The raw data is a collection of 1MEV equivalent electron values defined at discrete spatial points with solar cell shield thickness as a parameter. Graphical examples of the flux field data are shown in Figures 4-2 and 4-3. Points are generated at 10° latitude increments for the radii listed in Table 4-3. 1MEV flux was computed for four values of shield thickness, namely 3, 10, 20, 30 mils. The various combinations of latitude, radii, and shield thickness yield approximately 2500 flux values.

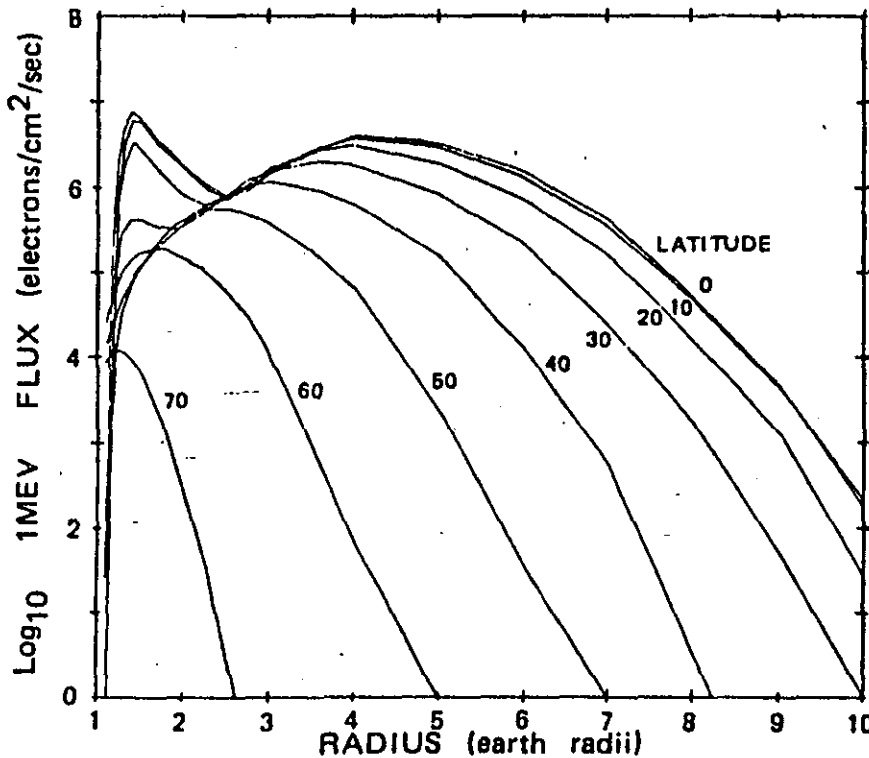


Fig. 4-2 Electron Contribution to Total Flux vs. Radius, SH=10 mils

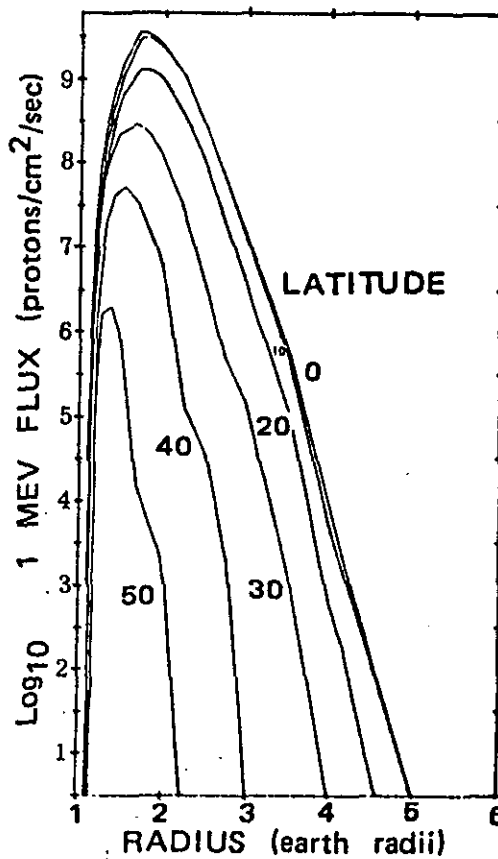


Fig. 4-3 Proton Contribution to Total Flux vs. Radius, SH=10 mils

Table 4-3 Defined Radial Points for Flux Field (in earth radii with R=1.0 at earth's surface)

For Protons		For Electrons		
1.10	1.80	1.10	1.70	3.50
1.15	1.90	1.15	1.80	4.00
1.18	2.00	1.18	1.90	5.00
1.20	2.25	1.20	2.00	6.00
1.25	2.50	1.25	2.25	7.00
1.30	3.00	1.30	2.50	8.00
1.40	4.00	1.40	2.75	9.00
1.50	5.00	1.50	3.00	10.00

1-

The second part of the flux generating process consists of fitting these discrete points with analytic functions. A multivariate regression (subroutine STEPR)<sup>(27)</sup> was used as the vehicle for the data fitting, and a two step process was used for protons and electrons separately. In the first step the radial flux points were fit for each latitude and shield thickness. Since the electron data has two peaks at the inner and outer Van Allen belts, quartic functions of radius were used. To reduce the dynamic range of the flux,  $\ln(\text{flux})$  was used as the dependent variable. Finally to force the flux to zero as radius approaches unity, the radial variable  $S = \ln(R-1)$  was used. Thus the radial functions are of the form

$$\ln(F) = \sum_{i=0}^4 A_i S^i \quad (4.1)$$

where the coefficients  $A_i$  are functions of latitude and shield thickness. These coefficients were then fit with a function of latitude and shield thickness, vis.,

$$A_i = \sum_{k=0}^4 \sum_{j=0}^2 (B_{ij} SH^j) C_{ik} LAT^k. \quad (4.2)$$

b.

Substituting (4.2) in (4.1) for  $A_i$  and taking the exponent thus yields a single analytic expression for the 1MEV equivalent electron flux as a function of latitude, radial distance and shield thickness. There are four separate Eq. 4.1's, one for protons and one for electrons for both the front and the back shielding, and the fluxes from these are added to obtain the complete flux. The coefficients used are tabulated in Tables 4-4 and 4-5, however the regression analysis yields directly products of B and C, and therefore the products are listed instead of B and C. We redefine  $A_i$  as follows:

$$A_i = \sum_{j=1}^5 \sum_{m=0}^2 K_{i,j+5m} LAT^{j-1} SH^m \quad (4.3)$$

This field model is not completely general. In the latitude region 50° to 60° it is valid only for  $R > 1.5$  earth radii. In the region 60° to 75° A is restricted to  $R > 2.5$ . The restrictions stem from function fitting problems and not from the data. Hopefully they can be removed with improved function choices. Above a latitude of 75° the field is set to zero in accord with the zero flux output from subroutine MODEL.

Over the defined region of R, LAT, SH space the field accuracy is as follows: For protons the mean deviation of the value predicted by Eq. (4-3) from the MODEL value at the defined R,LAT points is 5.6%. The average of the absolute value of the deviations is 28%. For electrons the mean deviation is 1.2% and the average absolute deviation is 25%.

#### 4.3 Power Loss Model

The second part of the two-part analytical model is an expression relating 1MEV fluence to fractional power loss. The data for this expression is provided by the curves of Carter and Tada<sup>(36)</sup>, and it can be fit closely by an expression of the form

$$\ln D = C_1 + C_2[\log_{10}\Sigma N]^{12} \quad (4.4)$$

Here D is the fractional power loss after the cells have been subjected to fluence  $\Sigma N$  ( $\Sigma N$  in units of 1MEV equivalent electrons/cm<sup>2</sup>/sec and is summed over front and back shielding and electrons and protons). Constants  $C_1$  and  $C_2$  are functions of cell thickness, and a simple quadratic has been found to adequately represent this variable. Although variations in cell base resistivity have a relatively small effect on the degradation function, the effect is represented in the Carter and Tada<sup>(36)</sup> data. Two sets of degradation curves are presented, one for base resistivity 1 to 3 $\Omega$  cm, the other for 7 to 13 $\Omega$  cm. We therefore provide two sets of functions for  $C_1$  and  $C_2$ . TH is the cell thickness in mils.

$$\begin{aligned} C_1 &= [0.22647 + 0.05217 TH - 0.00443 (TH)^2] 0.1 \\ C_2 &= [+0.05151 + 0.03641 TH - 0.00144 (TH)^2] (-10^{-14}) \end{aligned} \quad (4.5)$$

$$\begin{aligned} C_1 &= [0.04914 + 0.07056 TH - 0.00435 (TH)^2] 0.1 \\ C_2 &= [-0.05118 + 0.04517 TH - 0.00156 (TH)^2] (-10^{-14}) \end{aligned} \quad (4.6)$$

The C values are defined for cell thickness in the range 4 to 14 mil, and D is valid for fluence values above  $10^{11}$  (> 0.1% degradation).

#### 4.4 Conclusions

Since trajectory optimization normally involves the evaluation of several quantities which are functions of spatial coordinates at a sequence of time steps, it is a simple matter to apply the analytic degradation model described here. At each sample point in the trajectory the flux function (4.3) is evaluated. Multiplication of the resultant flux by the sample time step yields an incremental fluence, and these are simply summed up to a given sample time to provide a total fluence which is used in (4.4) to find the power loss. Since this process involves the evaluation of only two analytic expressions it requires very little computation time. Modeling of the 1MEV flux field as a separate entity allows simple consideration of both front and back shielding. The various coefficients in the analytic expressions relate to specific cell damage data, however having established the general analytical characteristics of the model, it is a simple matter to update the coefficients using the latest cell damage data.

## SECTION 5

### NUMERICAL RESULTS

Two sets of cases will be discussed in this section. The first, which assumes an inverse square gravity field and thrusting with no oblateness, degradation, or shadowing was also reported previously<sup>(25)</sup>. This set includes both attitude constrained and unconstrained examples. The second set includes the new degradation model reported in Section 4 as well as other perturbations. All examples in this set include attitude constraints. All cases were run on an IBM 360/75 computer. The code is in Fortran IV using double precision.

#### 5.1 Examples Without Power Degradation

Several SERT-C type cases were run. All of these assume only the inverse square gravitational field with or without attitude constraints. No oblateness, shadowing or power degradation due to radiation are assumed. Comparisons are made between the unconstrained case and attitude constrained cases while varying launch date and time. A particular constrained example is looked at in greater detail.

Table 5-1 summarizes the characteristics of the SERT-C type cases. The final orbit is geosynchronous. These cases were run with a 10 day time step and averaged around an orbit using either two 4 point or two 8 point quadratures. The variation in resulting flight times and  $\Delta V$ 's from using sets of 4 or 8 point quadratures was less than .5%.

Table 5-1 SERT-C Example Data

Initial a	=	9528.16 km
Initial e	=	0.
Initial i	=	28.3°
Initial mass	=	849.6 kg
Maximum power	=	4.828 kw
Specific Impulse	=	2900 sec
Final a	=	42164.km
Final e	=	0
Final i	=	0°

The effect of varying the time of launch during a day for the constrained case can be shown by varying the initial longitude of the ascending node. Changing the launch time affects the sun-spacecraft geometry and therefore the resulting trajectory. This effect is illustrated in Fig. 5-1 for a launch date of March 21, 1988. The flight time ( $t_f$ ) and  $\Delta V$  are plotted versus initial longitude of ascending node. The dotted line indicates the unconstrained value. The flight time varies by about 18 days with a minimum of 130 days around  $\Omega = 135^\circ$  compared to the unconstrained value of 124 days. The range of increased flight time over the unconstrained case is from about 5 to 20%. The unconstrained  $\Delta V$  is 4.65 km/sec and the constrained cases vary from less than 1% to about 12% greater. In the minimum case about 15% of the initial mass was consumed. This was only about .6 kg more than the unconstrained case.

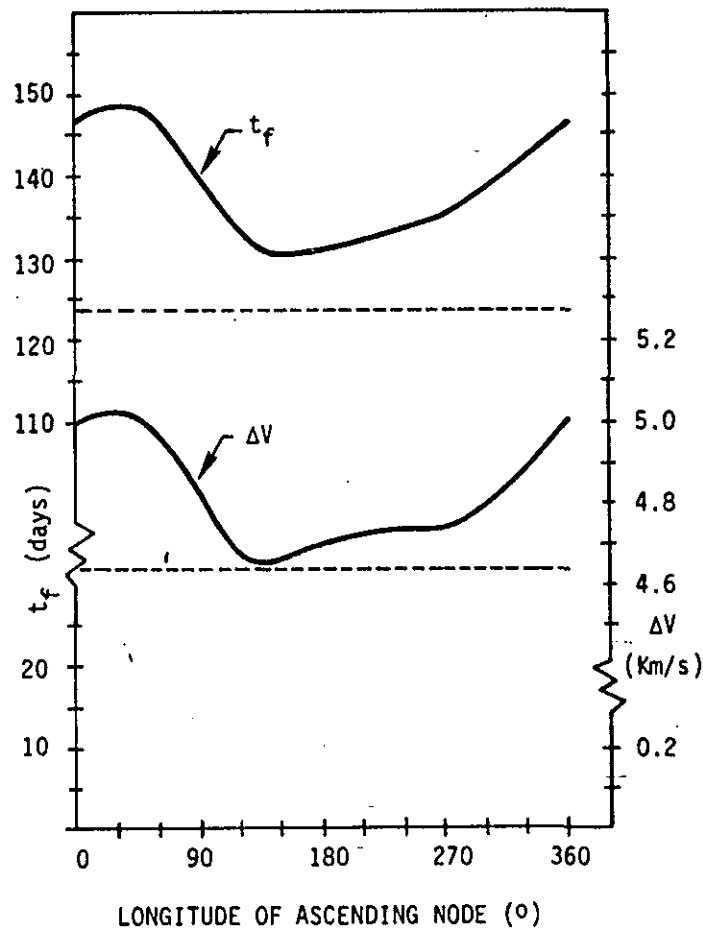


Fig. 5-1 Flight Time and  $\Delta V$  Versus Nodal Angle

Four cases of the attitude constrained example were run varying the date of launch. The initial longitude of ascending node was  $0^\circ$ . The percent increase in flight time and  $\Delta V$  over the unconstrained case is shown in Fig. 5-2. For any date of launch a curve such as shown in Fig. 5-1 would result. Although an absolute minimum time would occur on a particular day, it is expected that by varying the time of launch during the day that a nearly minimum flight time would be found. In summary, for this example, for appropriate selection of launch date and time the attitude constrained case results in as little as a 1% increase in  $\Delta V$  and a 5% increase in flight time over the nonconstrained case.

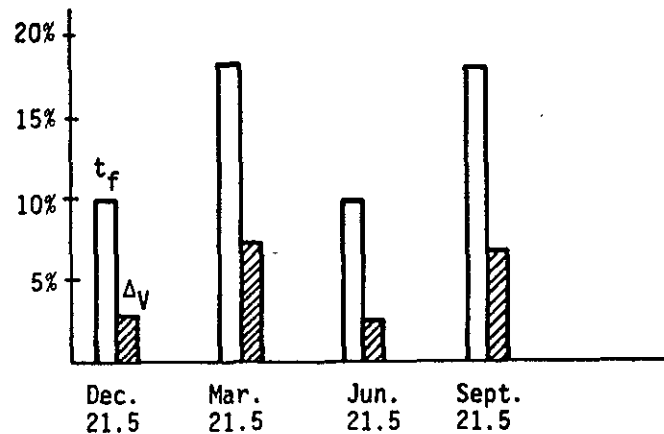


Fig. 5-2 Flight Time and  $\Delta V$  for Various Launch Dates

The  $\Omega = 135^\circ$  case which results in the lowest flight time and  $\Delta V$  will be looked at in greater detail, including further comparisons with the unconstrained case. The semimajor axis and inclination histories for these two cases are plotted in Fig. 5-3. The maximum yaw angle is plotted in Fig. 5-4 for the two cases. The yaw deviates from zero by plus and minus approximately this same amount over one orbit. For the unconstrained case the maximum yaw occurs when the spacecraft is at the line of nodes. As the spacecraft nears geosynchronous orbit the maximum yaw increases to over  $90^\circ$  for the constrained case, but to somewhat less,  $73^\circ$ , for the unconstrained case. Since only discrete points every  $15^\circ$  were printed out, the actual maximum may have been slightly higher than plotted. For this circle to circle transfer the pitch angle for the unconstrained case is always zero.

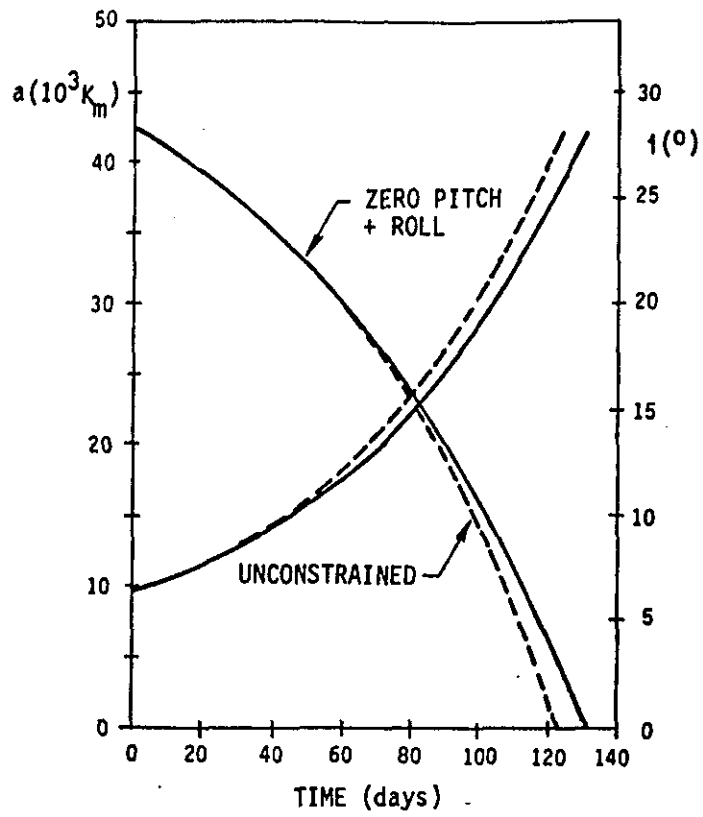


Fig. 5-3 Semimajor Axis and Inclination Histories

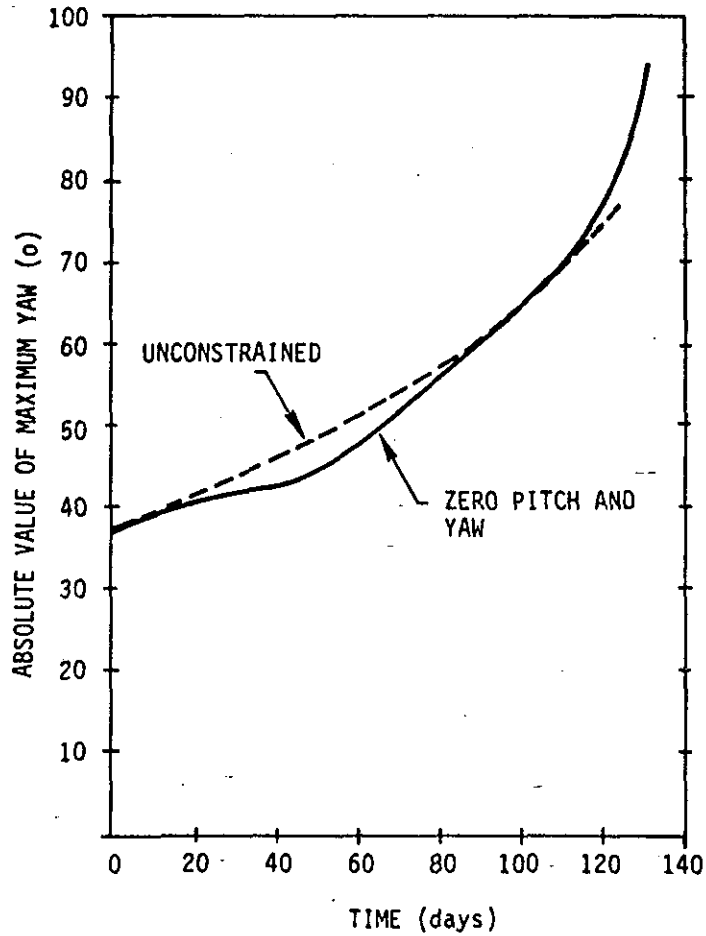


Fig. 5-4 Maximum Yaw Histories

Fig. 5-5 shows yaw plotted as a function of eccentric longitude for the initial and the final orbits. Because of the coupling with power, the maximum does not occur at exactly the line of nodes (which would be  $135^\circ$  and  $315^\circ$ ) as in the unconstrained case. There are two jumps in yaw of about  $60^\circ$  for the final orbit. This will be discussed further.

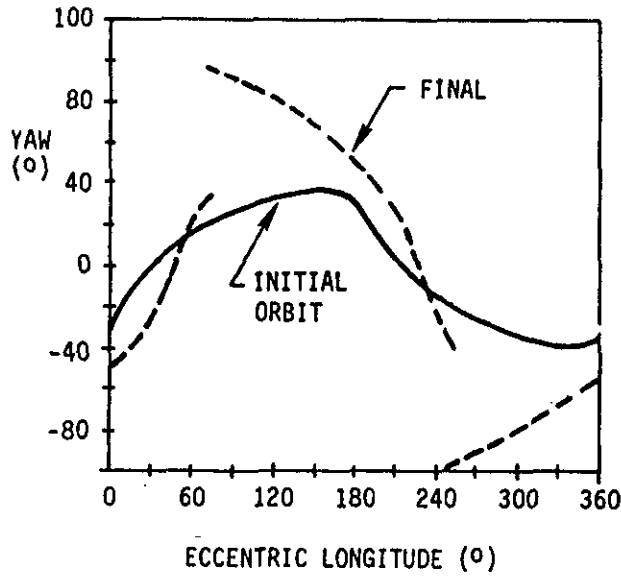


Fig. 5-5 Yaw for Initial and Final Orbits

Fig. 5-6 shows a plot of the ratio of power to maximum power versus eccentric longitude for the initial and final orbits. For the initial orbit the power is near maximum for nearly the entire orbit, dropping to a minimum of .91 but with an average of .98. For the final orbit the minimum reaches .707 which is the absolute minimum possible and which occurs at a jump point of the control. Even so, the average power ratio is over .9. The two other relative minimums for each orbit occur near to the minimum and maximum of the primer vector angle ( $\alpha$ ) (and also the thrust angle,  $\psi$ ).

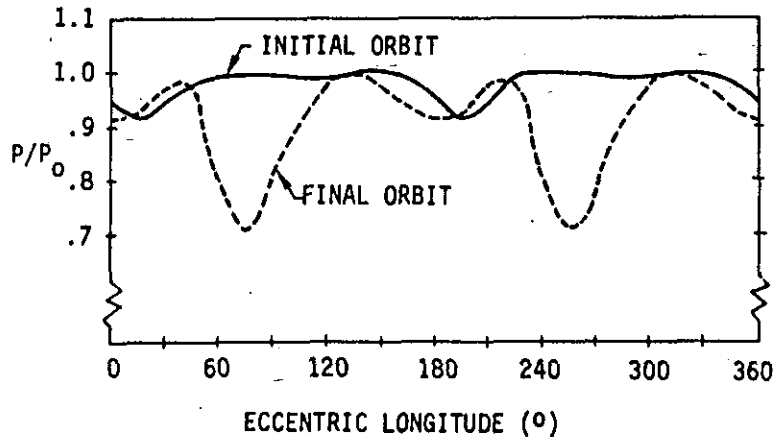


Fig. 5-6 Ratio of Power to Maximum Power for Initial and Final Orbits

In Fig. 5-7 are plotted the primer vector angle ( $\alpha$ ), the thrust angle ( $\psi$ ), and the sun angle ( $\beta$ ) for the initial orbit. These angles are defined in the  $\hat{e}_1 - \hat{e}_2 - \hat{e}_3$  system defined in Section 3.5 and were illustrated in Fig. 3-2 and Fig. 3-4. The sun angle is the angle between the radius vector and the line to the sun, and can vary by at most  $180^\circ$  depending on the orientation of the orbit. For the initial orbit the variation is approximately  $140^\circ$ . The thrust angle is a function of  $\alpha$  and  $\beta$  and is equal to  $\alpha$  at  $\alpha = 0^\circ$  and  $180^\circ$ . For this orbit  $\psi = 90^\circ$  when  $\alpha = 90^\circ$ . Since  $\beta \approx 157^\circ$  and  $23^\circ$  for the two positions at which  $\alpha = 90^\circ$  there is no jump in  $\psi$  (for a jump  $45^\circ < \beta < 135^\circ$ ).

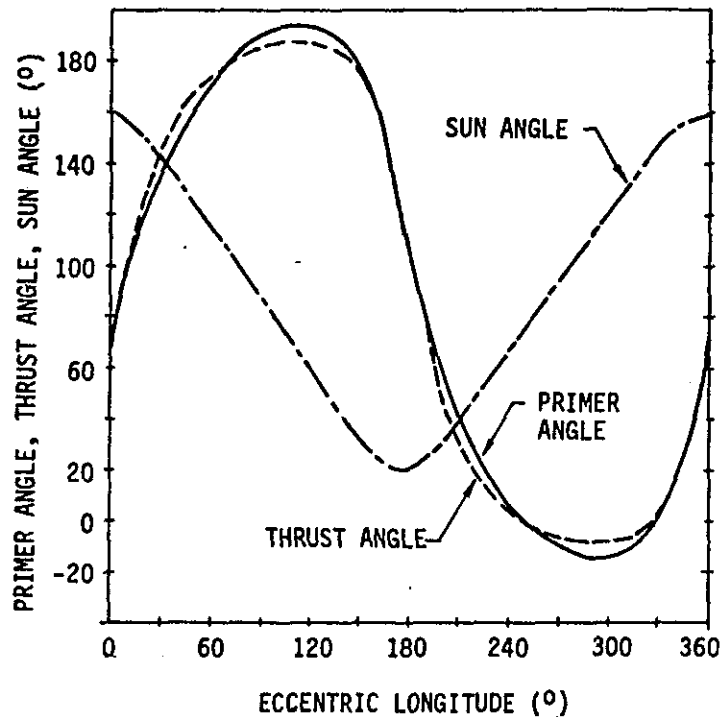


Fig. 5-7 Primer Angle ( $\alpha$ ), Thrust Angle ( $\psi$ ) and Sun Angle ( $\beta$ ) for Initial Orbit

The primer vector angle ( $\alpha$ ), thrust angle ( $\psi$ ), and sun angle ( $\beta$ ) are plotted for the final orbit in Fig. 5-8. Obviously for this orbit there is a jump in  $\psi$  when  $\alpha = 90^\circ$ . Note that at this point  $\beta \approx 124^\circ$  for the first jump and  $\beta \approx 56^\circ$  for the second. For these values of  $\beta$  the jump in  $\psi$  is approximately  $60^\circ$ . It is interesting to note that after the first jump  $\psi$  decreases slightly even as  $\alpha$  increases ( $\psi$  increasing as  $\alpha$  decreases after the second jump) as the changing  $\beta$  allows a closer alignment with the primer vector at less power loss penalty. Jumps in  $\psi$  occur during about the last 20 days of the trajectory.

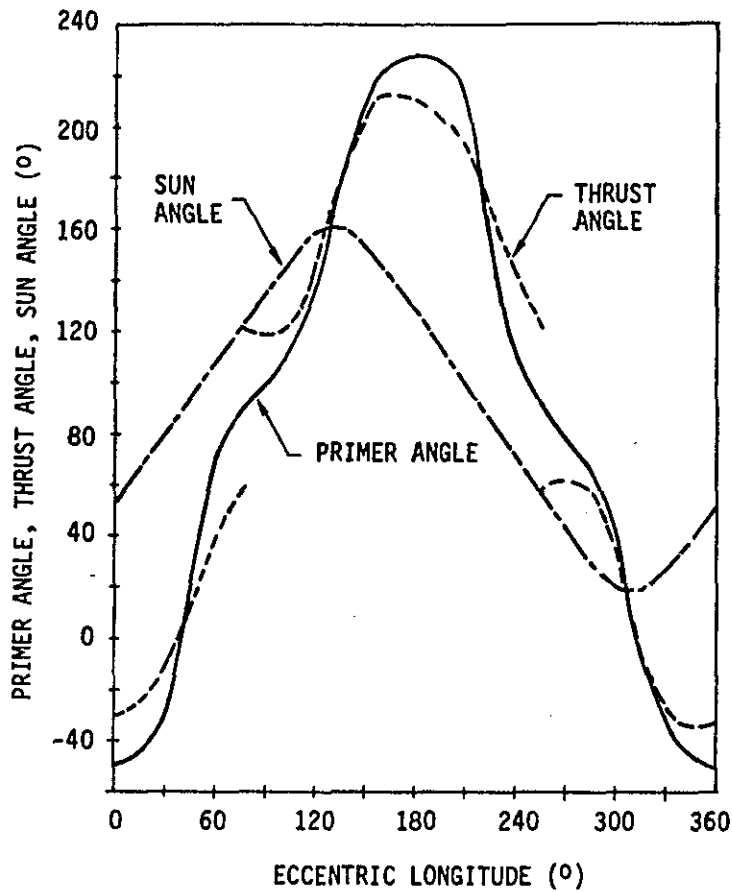


Fig. 5-8 Primer Angle ( $\alpha$ ), Thrust Angle ( $\psi$ ) and Sun Angle ( $\beta$ ) for Final Orbit

The panel orientation angle (defined in Eq. (3.85)) is plotted in Fig. 5-9 for the initial and final orbits. In both cases there is a rotation through a full  $360^\circ$ . For the final orbit there are discontinuities at the point where there are discontinuous changes in the thrust direction. Both jumps are about  $80^\circ$  (note panel angles of  $180^\circ$  and  $-180^\circ$  are equivalent).

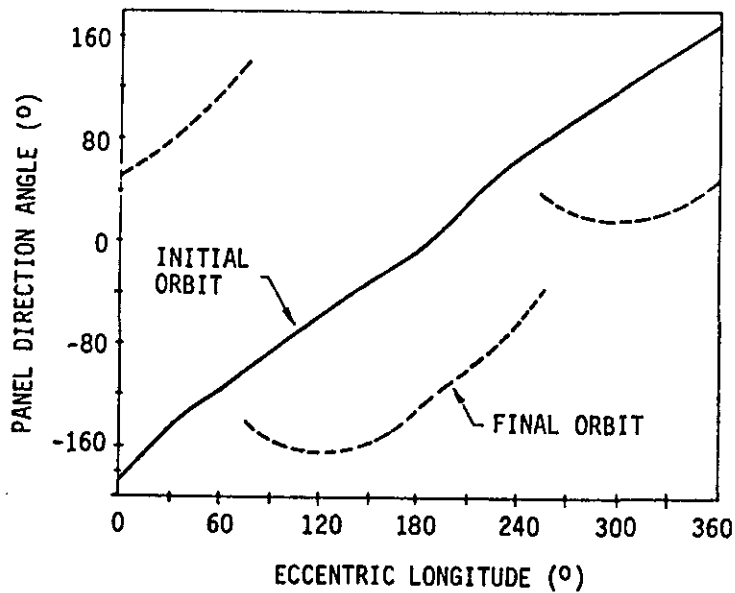


Fig. 5-9 Panel Orientation Angle for Initial and Final Orbits

In summary, for the attitude constrained and unconstrained cases compared here, flight time and trajectory histories differed only somewhat. The main differences are the discontinuities in thrust direction and in solar panel orientation which occur during the last 20 days of the constrained case. Average power levels were at most 10% less than the unconstrained case. Since these were circle to circle transfers the effect of a zero pitch constraint is not illustrated.

## 5.2 Examples With Power Degradation

Several cases were run to illustrate the use of the final version of the code. Most of the cases were of a SERT-C type, although some GEOSEPS-type missions and some cases which originated in an elliptical orbit were run. All of these cases included oblateness and the new power degradation model. Unless otherwise noted, all assumed that pitch and roll were constrained to be zero. The constants in the coefficients of the power loss function for these runs were slightly different than those given in Eqs. 4.5 and 4.6. --

The SERT C cases are discussed first. Table 5-2 lists conditions on the initial and final orbits and the spacecraft.

Table 5-2 SERT-C Example Data

Initial a	=	9528 km
Initial e	=	0
Initial i	=	28.3°
Mass	=	850 kg
Maximum initial jet power	=	4.828 kw
Specific Impulse	=	2900 sec
Final a	=	42104 km
Final e	=	0
Final i	=	0°

Cases with other final orbits were also run.

For the cases discussed in this section a four-point quadrature was used between the points where the primer vector angle,  $\alpha$ , crossed  $\pm 90^\circ$  (see Section 3.5). For the initially circular cases there were two intervals per orbit. A ten day time step was generally used, although some cases had a 15 day time step. A Newton-Raphson iterator and a four step Runge-Kutta integrator without accuracy controls were used.

The characteristics of one set of runs are listed in Table 5-3. Launch date, launch time (determined by the initial longitude of ascending node,  $\rho$ ) and solar array parameters were varied. Shadowing was not included. A 10 ohm-cm solar cell base resistivity was assumed. If additional values for launch date and time were run then a curve such as in Fig. 5-1 could be drawn. For the limited number of runs shown in Table 5-3, the variations in transfer time and  $\Delta V$  are small. The power degradation which is near 56% increases transfer time significantly compared to the constant power case discussed previously. Without infinite back shielding transfer time is increased by 14% as the degradation factor decreases an additional .08. Increasing the cell thickness changes the shape of the degradation versus flux curve. The increase from 6 to 10 mils caused a final damage factor decrease from .56 to .41 and a 30% increase in transfer time.

The case shown in the first column will be illustrated in more detail. Fig. 5-10 is a time history plot of semimajor axis, inclination, and the longitude of the ascending node. The change in the latter is largely due to oblateness which is strongest at lower altitudes and high inclinations. The semimajor axis actually overshoots the final value somewhat. This overshoot comes about because initially greater effort is put into reaching higher altitudes at higher inclinations where the flux is less. As the higher altitudes are reached, effort is expended to reduce inclination.

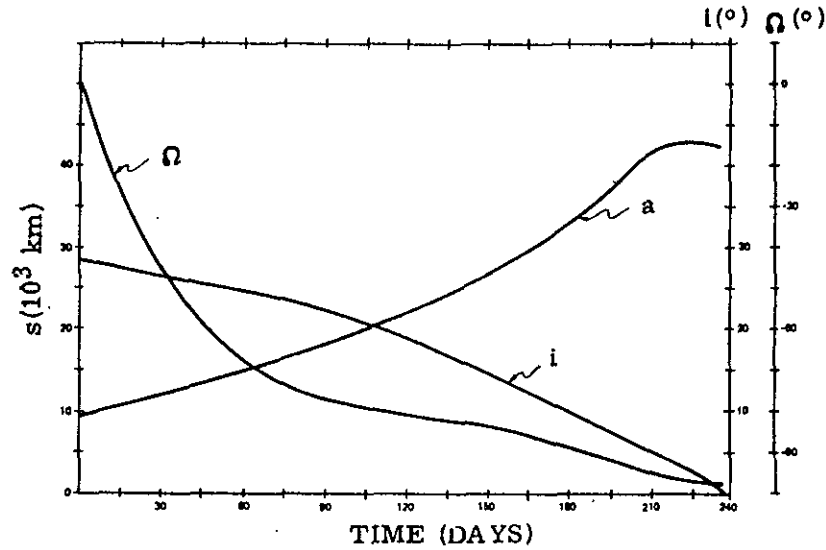


Fig. 5-10 Semimajor Axis, Inclination, and Longitude of Node Histories

Table 5-3 SERT C Example Results  
(10 ohm-cm base resistivity)

Launch date	Mar 21.5	Mar 21.5	Dec 21.5	Dec 21.5	Mar 21.5	Mar 21
Longitude of node	0°	45°	0°	45°	0°	0°
Cell Thickness (mils)	6	6	6	6	6	10
Front Shield Thickness (mils)	6	6	6	6	6	6
Back Shield Thickness (mils)	infinite	infinite	infinite	infinite	6	infinite
$\Delta V$ (km/sec)	4.89	4.92	4.82	4.91	4.85	4.83
Transfer Time (days)	236.	236.	231.	237.	269.	308.
$m_f/m_o$	.842	.841	.844	.841	.843	.844
Damage factor	.563	.571	.564	.569	.482	.412
Initial Costate	3657.3	8366.5	4331.1	4797.6	2545.9	6074.5
	121.6	286.5	97.6	350.0	170.7	238.6
	298.0	86.6	263.7	71.7	441.1	615.6
	-6072.8	-25714.	-6300.6	-26335.	-8327.	-8408.9
	-35259.	-24085.	-33507.	-19704.	-31798.	-29438.
	-33428.	-37246.	-31866.	-31619.	-35878.	-46571
	-106.87	-121.89	-87.53	-89.73	-52.31	-174.53

Fig. 5-11 shows the yaw angle for the initial and final orbits. For the initial orbit the variation is fairly smooth, with a range of about  $60^\circ$  either side of the orbit plane. The final orbit contains two jumps in the yaw angle; one at  $1.3^\circ$  and one at  $180.3^\circ$ . On each orbit of this trajectory there were two points at which the primer vector angle was  $\pm 90^\circ$  (see Section 3.5), but the sun angle was between  $45^\circ$  and  $135^\circ$  (thus causing a jump in yaw) for the first time at about 105 days. The final yaw angle has a range of  $125^\circ$  either side of the orbit plane. The thrusting at yaw magnitudes greater than  $90^\circ$  causes a decrease in semimajor axis near the end of the trajectory as illustrated in Fig. 5-10.

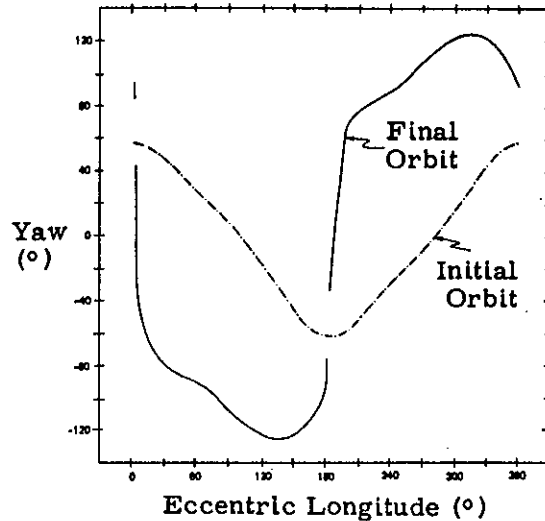


Fig. 5-11 Yaw for the Initial and Final Orbits

Fig. 5-12 shows the power variations caused by the inability of the panels to directly face the sun at all times on the initial and final orbits, where the maximum is unity. For the initial orbit power decreases to .90 of its maximum, and the average is .954. For the final orbit power decreases to .707 of the maximum at the jump points and the average is 0.88.

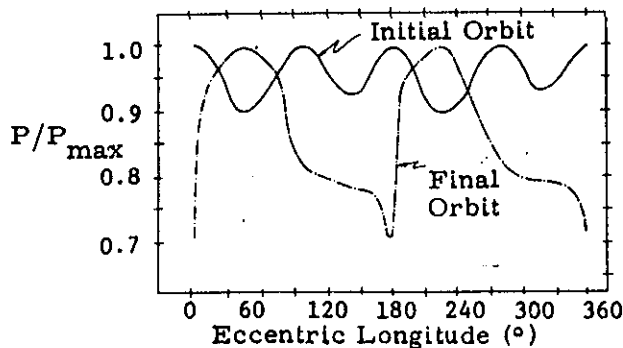


Fig. 5-12 Power Variation for the Initial and Final Orbits

In Fig. 5-13 are plotted the primer vector angle,  $\alpha$ , the sun angle,  $\beta$ , and the thrust angle  $\psi$  for the final orbit (see Section 3.5, especially Fig. 3-3 and 3-4). The primer vector angle and thrust angle coincide at  $0^\circ$  or  $180^\circ$ . When  $\alpha$  crosses  $-90^\circ$  there are jumps of about  $36^\circ$  when  $\beta = 48^\circ$  and  $\beta = 132^\circ$ .

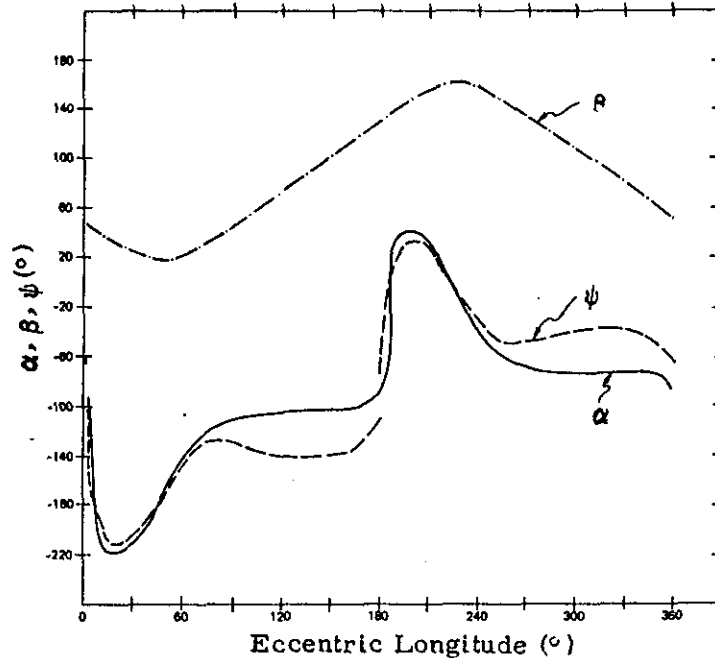


Fig. 5-13 Primer Vector Angle ( $\alpha$ ), Sun Angle ( $\beta$ ), and Thrust Angle ( $\psi$ ) for the Final Orbit

The equivalent of 1 MEV fluence is plotted in Fig. 5-14 for three cases. Power versus time is shown for the same cases in Fig. 5-15. The case with infinite back shielding and a cell thickness of 6 mils (first column of Table 5-3) has the lowest accumulated fluence and the least degradation (to .56) and the lowest transfer time. With a six mil back shield the total fluence is doubled and power degrades to .48. With infinite back shielding and a cell thickness of 10 mils (6th column of Table 5-3) the fluence curve coincides with the 6 mil case through 60 days, then increases somewhat more since at that time in the flight it is at lower altitudes and thus in a stronger radiation field. Its power curve in Fig. 5-15 falls the fastest to a final value of .41. Note that most of the fluence is encountered during the first 80 days or so and that power drops off sharply initially and reaches an essentially constant value after 80 or 100 days.

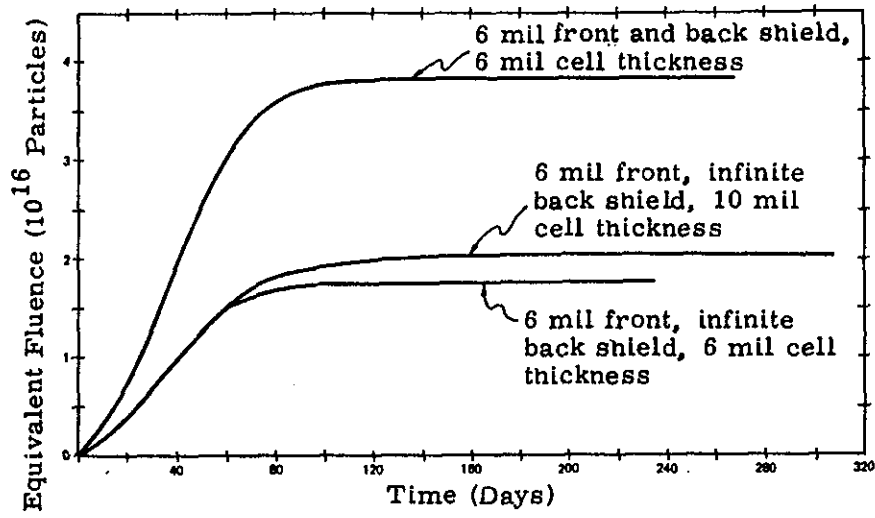


Fig. 5-14 Fluence versus Time

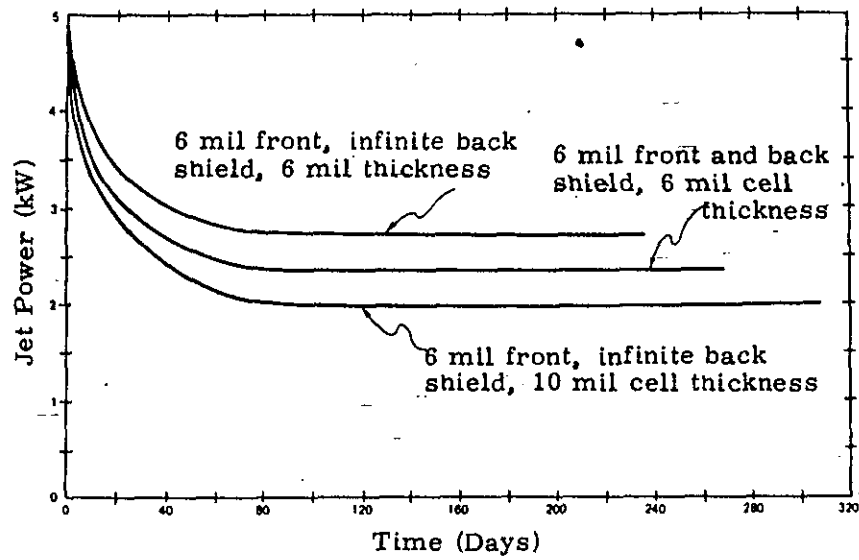


Fig. 5-15 Power Degradation Histories

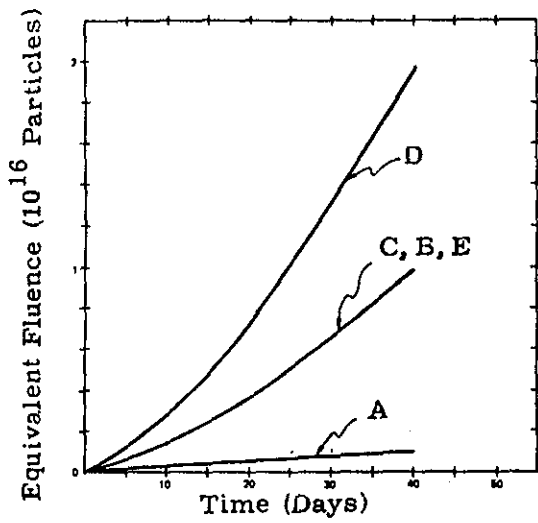
In order to further illustrate the effect of various array parameters, several cases of considerably shorter transfer time are listed in Table 5-4. These have the same initial data as shown in Table 5-3, but terminate at  $a = 12800$  km,  $i = 25^\circ$ . The third, fourth, and fifth columns correspond to shorter versions of the cases shown in the first, fifth, and sixth columns of Table 5-3.

Table 5-4 Short SERT-C Example Results

Launch Date	Mar 21.5				
Longitude of node	0°	0°	0°	0°	0°
Cell Thickness (mils)	6	6	6	6	10
Front Shield Thickness (mils)	20	6	6	6	6
Back Shield Thickness (mils)	infinite	infinite	infinite	6	6
Base Resistivity (ohm-cm)	10	2	10	10	10
$\Delta V$	1.03	1.03	1.03	1.03	1.03
Transfer Time	35.4	46.5	41.9	46.1	50.6
$M_f/M_o$	.965	.964	.964	.904	.964
Damage factor	.797	.516	.611	.533	.462

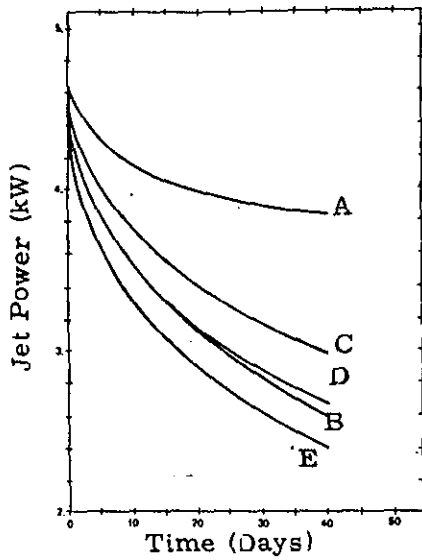
The case shown in the first column has a very thick front array shield of 20 mils. The degradation is about one half of that for the 6 mil shield listed in the third column. The  $\Delta V$ 's are the same but flight time decreases by 15%. The case in the second column assumes a base resistivity of 2 ohm-cm rather than 10 ohm-cm which was used for all other cases. This assumption affects the power versus fluence curve resulting in a greater degradation (an extra 10%) when compared to column 3.

To further illustrate these five cases fluence is plotted in Fig. 5-16 and power in Fig. 5-17. The accumulated fluence does not vary with changes in cell thickness or base resistivity on the scale shown by the plot. After 40 days, the case with infinite back shielding and 20 mil front shielding has about 10% as much fluence as the case with 6 mil front shielding and 5% as much fluence as the 6 mil front and 6 mil back shielded case. Power variations diverge for the five cases, some of which reach near-steady state values in 40 days. However, the 20 mil shielded case is at a much higher power level. The 10 mil cell thickness case results in the greatest degradation.



- A. 20 mil front, infinite back shield, 6 mil cell thickness, 10 ohm-cm base resistivity
- B. 6 mil front, infinite back shield, 6 mil cell thickness, 2 ohm-cm base resistivity
- C. 6 mil front, infinite back shield, 6 mil cell thickness, 10 ohm-cm base resistivity

Fig. 5-16 Fluence versus Time



- D. 6 mil front and back shield, 6 mil cell thickness, 10 ohm-cm base resistivity
- E. 6 mil front and back shield, 10 mil cell thickness, 10 ohm-cm base resistivity

Fig. 5-17 Power Degradation Histories

No complete SERT-C cases with shadowing were run, although some shorter cases were. A case similar to that listed in the third column of Table 5-4, but with the final  $a = 13200$  km (rather than 12800) and  $i = 25.3^\circ$  (rather than  $25^\circ$ ), took 83 days with shadowing and delay (compared to 42 without shadowing). The initial orbit has a period of 2.6 hours. The time in shadow is 36 minutes and the delay time is 14 minutes. Together they are almost one third of the orbital period. Thus for lower orbits, shadowing and delay in thruster turn-on can considerably lengthen the flight time, at higher altitudes proportionally much less time is spent in shadow. Since the spacecraft spends more time at lower altitudes, the power degradation is more severe, also lengthening flight time.

Four GEOSEPS-type cases were run. Table 5-5 lists conditions for these cases.

Table 5-5 GEOSEPS Example Data

Initial a	=	29378 km
Initial e	=	0
Initial i	=	$7^\circ$
Initial mass	=	2796 kg
Maximum initial jet power	=	13 kw
Specific impulse	=	2900 sec
Final a	=	42164 km
Final e	=	0
Final i	=	$0^\circ$

These cases assumed attitude constraints, power degradation, oblateness, and shadowing. A five day time step and a 4-point quadrature between jumps points and shadow entrance and thruster turn-on points. Jump points were calculated. The launch date was March 21, 5, and two initial nodal angles were considered. For each, cases with and without delay were run. Table 5-6 summarizes the results. A change in the line of nodes of  $45^\circ$  results in a 6% decrease in transfer time, the addition of a delay in thruster turn-on time causes only about a 2% increase in flight time. Not all orbits of these transfers enter the shadow and because of the high altitude the time in shadow and the delay time is small compared to the orbital period (unlike the early orbits of a SERT-C mission). There is little variation in  $\Delta V$  for these cases. Because of the initially high orbit, power degradation is less than 6%, more than half of which occurs during the first orbit.

Table 5-6 GEOSEPS Example Results

Longitude of the node	0	0	45°	45°
Delay	yes	no	yes	no
$\Delta V$ (km/sec)	.887	.885	.876	.874
Transfer time (days)	37.9	37.3	35.4	34.9
$m_f/m_o$	.969	.969	.970	.970
Damage factor	.946	.947	.947	.947
Initial costate	1179.1	1161.2	1033.3	1023.0
	-184.7	15.9	-101.1	-23.0
	-882.2	-661.4	-464.6	-345.4
	12643.	13003.	-23487.	-23858.
	-44386.	-44125.	-27212.	-26826.
	-1512.8	-1510.7	-1292.1	-1290.1
	-1517.2	-1533.8	-1304.3	-1318.4

The semimajor axis and inclination history are plotted in Fig. 5-18. Their changes are monotonic. Fig. 5-19 shows the yaw for the initial and final orbits. The yaw for the initial orbit varies fairly smoothly 60° either side of the orbit plane. The spacecraft thrusters are off for eccentric longitudes between 168 and 201° because of the shadow. The yaw for the final orbit varies 90° either side of the orbit plane and there are two jumps in the yaw angle, one at 151.6° and one at 317.4°.

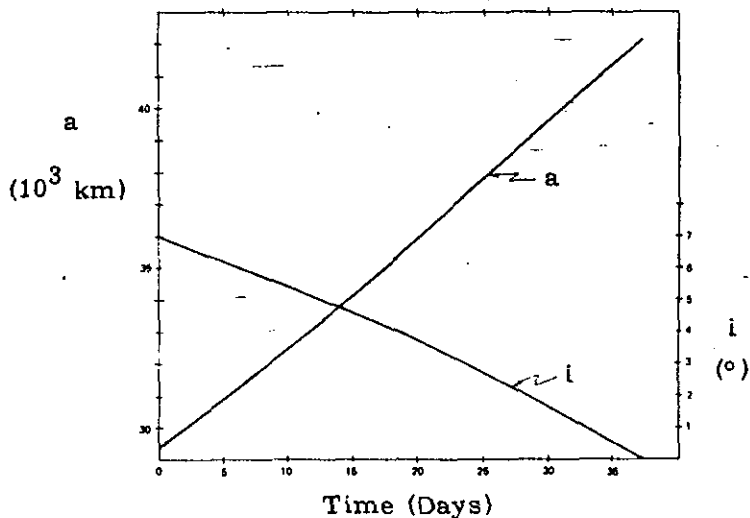


Fig. 5-18 Semimajor Axis and Inclination Histories

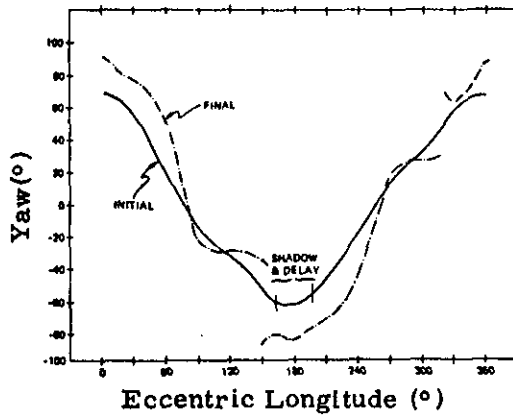


Fig. 5-19 Yaw for the Initial and Final Orbits

The power variation over the initial and final orbits is shown in Fig. 5-20. For the initial orbit power reaches .855 of the maximum with an average of .938. For the final orbit the minimum of .707 is reached at the jump points. The average is .853.

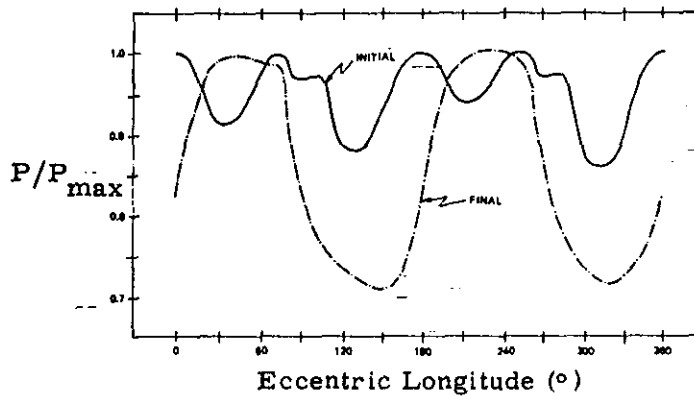


Fig. 5-20 Power Variation for the Initial and Final Orbits

The primer vector angle,  $\alpha$ , sun angle,  $\beta$ , and thrust angle,  $\psi$  are plotted for the final orbit in Fig. 5-21. The sun angle varies between 13 and 167°. The thrust angle and primer vector angle coincide at 180°. When  $\alpha$  passes through 90° there is a jump in  $\psi$  of 78° when  $\beta = 64^\circ$  (at  $F = 151.67^\circ$  and a jump of 87° when  $\beta = 101^\circ$  (at  $F = 317.4^\circ$ ).

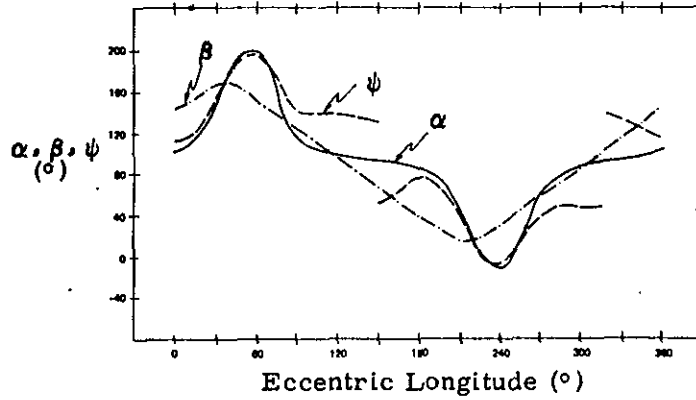


Fig. 5-21 Primer Vector Angle ( $\alpha$ ), Sun Angle ( $\beta$ ), and Thrust Angle ( $\psi$ ) for the Final Orbit

Fig. 5-22 plots the time in shadow and the corresponding delay time (added to shadow time) versus the flight time. Time in shadow reaches a maximum of about 59 minutes. Delay is always at least 12 minutes when thrusters shut down.

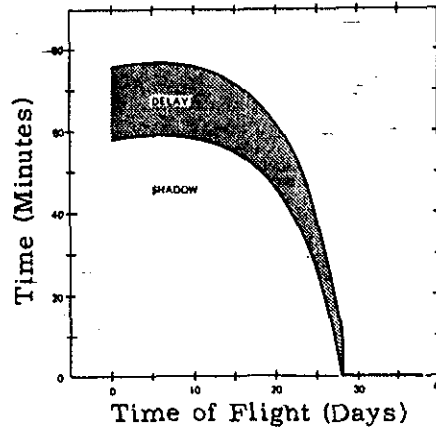


Fig. 5-22 Shadow and Delay Times

Two other cases were considered that had initial elliptical orbits. One case assumed zero pitch but free roll and terminated at an equatorial geosynchronous orbit. The other had both roll and pitch constrained, but was a shorter transfer. The spacecraft parameters were the same as for the SERT C cases without shadowing discussed previously. Table 5-7 summarizes the initial and final orbits and transfer characteristics.

Table 5-7 Elliptical Orbit Examples

Roll	free	constrained
Initial a	10400 km	10400
Initial e	.378	.378
Initial i	28.3°	28.3
Initial $\Omega$	0°	0
Initial $\omega$	90°	90
Final a	42164 km	18100
Final e	0	.3
Final i	0°	22.2
Final $\Delta V$	4.46 km/sec	1.72
Final $t_f$	181.3 days	72.0
Final $m_f/m_o$	.855	.941
Final damage factor	.627	.638
Initial costate	9947.3	9612.4
	4365.8	7945.8
	-767.1	-470.9
	-718.2	-1162.5
	-16925.	-19673.
	-26014	-10090.
	-112.22	-77.15

Fig. 5-23 shows the semimajor axis, eccentricity, and inclination histories for the free roll example. There was also a rotation of  $\Omega$  from 0° to -70° and a rotation of  $\omega$  from 90° to 217°, primarily caused by earth oblateness, although some pericenter rotation may have been caused by an effect to avoid intense radiation, thus lowering power and increasing transfer time. Power dropped from 4.828 kw to 3.03 kw; most of the drop occurred during the first 70 days as in previous examples.

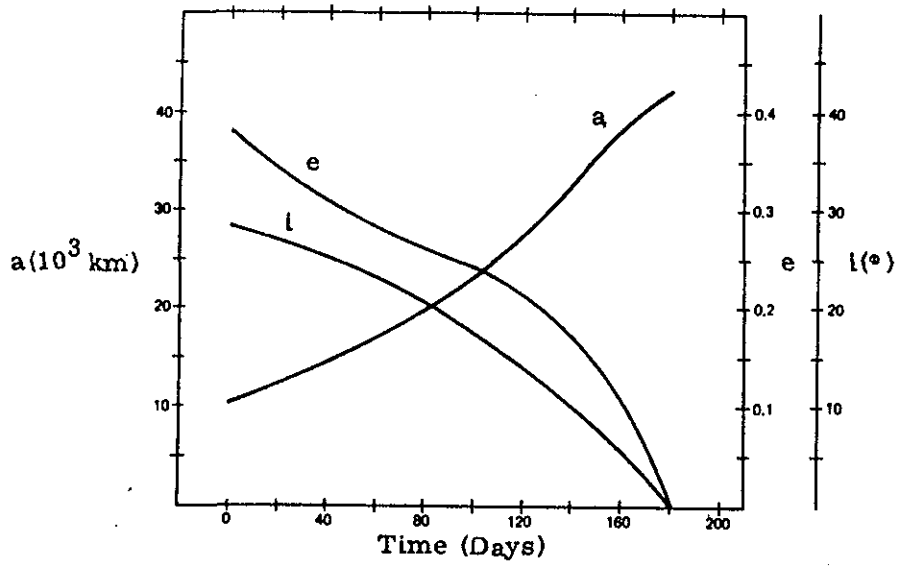


Fig. 5-23 Semimajor Axis, Eccentricity, and Inclination Histories

Fig. 5-24 shows the yaw for the initial and final orbits.

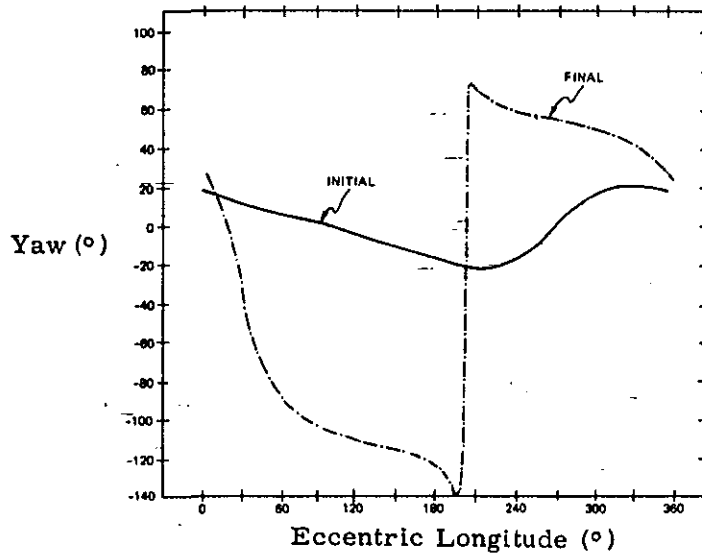


Fig. 5-24 Yaw for the Initial and Final Orbits

One of the interesting characteristics of the pitch and roll constrained example was that there were two points per orbit at which the primer vector projection was perpendicular to the sun vector ( $\alpha = \pm 90^\circ$ ) except very close to the end of the trajectory where there were four such points. There were no jumps in the thrust direction for the orbits with only two such points since the sun angle,  $\beta$ , was not between  $45^\circ$  and  $135^\circ$ . The yaw angle is plotted in Fig. 5-25 for the initial and final orbits and for a segment of an orbit at 66 days. There are two jumps during the final orbit but none for the orbit at 66 days or for earlier orbits. Fig. 5-26 shows the primer vector angle,  $\alpha$ , the sun angle,  $\beta$ , and the thrust angle,  $\psi$ , for the final orbit. The primer vector angle crosses the  $90^\circ$  point four times, but for the first two,  $\beta$  is not in the  $45$  to  $135^\circ$  range. Then the primer vector angle briefly goes above the  $90^\circ$  line between  $F = 286^\circ$  and  $F = 336^\circ$ . At  $F = 226^\circ$ ,  $\beta = 48^\circ$ , and there is a  $30^\circ$  jump in  $\psi$ . At  $F = 336^\circ$ ,  $\beta = 85^\circ$  and there is nearly a  $90^\circ$  jump in  $\psi$ . For the 66 day orbit the primer vector curve looks very similar but it does not quite reach the  $90^\circ$  line in this orbit segment and these two jumps do not occur.

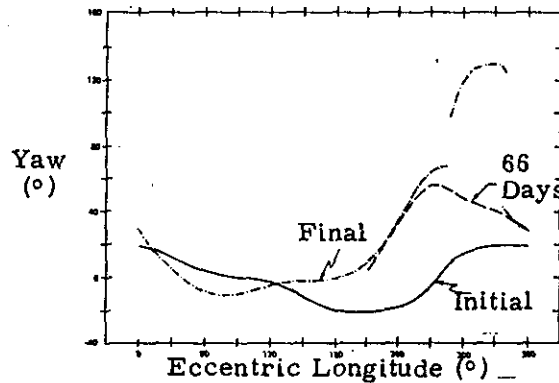


Fig. 5-25 Yaw for the Initial, 66 Day, and Final Orbits

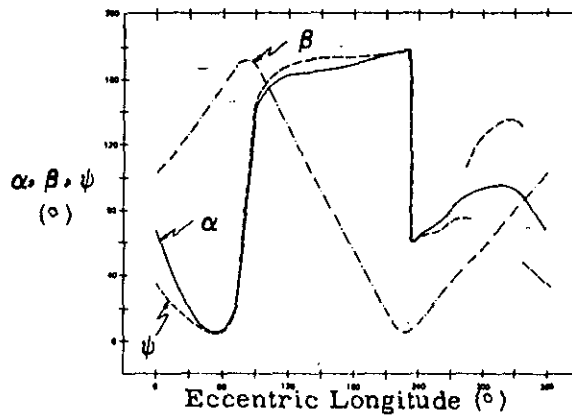


Fig. 5-26 Primer Vector Angle ( $\alpha$ ), Sun Angle ( $\beta$ ), and Thrust Angle ( $\psi$ ) for the Final Orbit

### 5.3 Run Time and Accuracy

Some of the additions to the new version of the program have contributed to greater run time, although averaging and the analytic radiation model cause the run time to be orders of magnitude shorter than a precision trajectory calculation. Many trajectories are run for one optimization, however. Shadow calculations cause an increase in run time and the resulting trajectory often requires a shorter integration time step to maintain the accuracy needed to obtain convergence. The new thruster turn-on delay calculation requires additional time. The constrained thrust direction calculation requires additional calculations which must be performed at every quadrature point of every orbit for every trajectory. Calculation of possible jumps points in the control greatly increase run time. For accuracy a separate quadrature may be used between jump points and shadow entrance and exit points. With no shadowing and two jump points there will be two quadrature intervals. With shadowing, and if there are two jump points not in the shadow, then there are three intervals. There may be up to 6 jump points (for non-circular orbits). (Jump points refers to points where  $\alpha = \pm 90$ . There may or may not be an actual jump in  $\psi$  depending on the value of  $\beta$ .) Some cases were run without calculating jump points and just arbitrarily dividing up the orbit into two quadrature intervals. The loss of accuracy adversely affects convergence and the increase in the number of trajectories calculated may increase total run time. For the results in this section a four-point quadrature was used. For higher order quadratures run time is greater. A smaller time step increases the run time of a trajectory.

The results in this section were generated on an IBM 360/75 computer. The program is coded in Fortran IV on the H compiler. These runs took several minutes each. To get a rough idea of the time needed, the approximate CPU time per "time step" was calculated. With oblateness, degradation and attitude constraints, two 4-point quadratures per orbit and jump points calculated the value was .025 min. Thus for a trajectory 250 days long with a 10 day time step there were 25 steps or .625 minutes per trajectory. Four iterations of the Newton-Raphson iterator generate at least 26 trajectories (4 nominals, 3 sensitivity matrices and one time history), requiring 16.25 minutes. Without calculating the jump points the CPU/time step was approximately .018 so the same case would take 11.7 minutes. The shadow cases in this section had similar CPU/time step, often one of the jump points was inside the shadow, and so not calculated precisely, reducing computation time.

Experience indicates that using higher order quadratures and smaller time steps than used for the results in this section change  $\Delta V$  and transfer time very little, perhaps 1 or 2%. However, the initial costate may be changed on the order of 10 or 20%. For mission comparisons and to obtain approximate trajectory

characteristics less accuracy may be acceptable. If costate histories are to be used for guidance, increased accuracy and therefore smaller time steps and additional points per orbit must be used.

More complex and longer cases required better initial guesses to obtain convergence. Such cases usually required an iterative procedure involving converging to successive points along a reference trajectory.

## SECTION 6

### CONCLUDING REMARKS

The program discussed in this report is a generalization of a previously developed code which calculated time optimal geocentric trajectories for solar electric propelled spacecraft with an optional high thrust stage. The new code continues the use of the method of averaging and an analytic radiation and degradation model in order to reduce computation time. A nonsingular set of orbital elements is utilized. Oblateness, shadowing and solar motion may be included. For the new code, attitude constraints may be included, a delay in thruster turn-on upon leaving the shadow is modeled, and the radiation and power loss model is revised and generalized to various solar array parameters.

A suboptimal control for the attitude constrained case of zero roll and pitch which is nearly time optimal without wasting fuel has been developed. Because of the constraints the panels may not always directly face the sun, and power becomes a function of spacecraft orientation. The resulting control strategy may call for discontinuous jumps in the yaw and panel orientation angles. The minimum possible power during an orbit which occurs at a jump point is .707 of the maximum, although the average is usually .9 or higher.

The code is computationally fast due to averaging and the analytic radiation model compared to precision code (although unlike most precision codes, many individual trajectories are run in order to converge to the desired final conditions). The code is applicable to general orbits, spacecraft and solar array characteristics.

The radiation and power loss model represents a close approximation to actual data. The analytic format is easy to code and computes rapidly. Partial derivatives, necessary for the costate equations, are easy to obtain. The coefficients in the mathematical models can easily be altered for new data. Shield thickness, solar cell thickness, and cell base resistivity may be varied.

The time step for the integrator and the number of points calculated per orbit for the averaging quadrature affect accuracy and computation time. Experience with a limited number of examples indicates that using 8 points per orbit or 16, or halving the time step from 10 to 5 days in an over 100 day trajectory may change  $\Delta V$  and flight time by 1 or 2%, but the initial values for the costate may change

on the order of 10% or more. In order to obtain convergence for complex cases better initial guesses and more accuracy is required. It may be necessary to obtain a nominal trajectory from a more simple case and then to converge to various points along that nominal, at each stage using the initial values from the previous stage as initial guesses for the later stage.

Comparisons were made for a SERT-C type mission between constrained and unconstrained cases for an inverse square gravity field. Flight time and  $\Delta V$  vary for the constrained cases as a function of launch date and time of day. A launch time can be found for which the constrained  $\Delta V$  is less than 1%, and the transfer time less than 5% more than the unconstrained case. Jumps in the control did occur during the last 20 days of a 130 day mission. For the examples considered most orbits had at most two jumps in the thrust direction. Noncircular orbits can have up to six jump points.

The time in shadow and the delay in thruster turn-on can be a significant proportion of the orbital period at lower altitudes. As a result the spacecraft spends greater amounts of time in the more intense lower radiation zones, thus power degrades faster which contributes to longer transfer times.

The inclusion of power degradation can nearly double transfer time for a SERT-C type mission. The intense radiation at lower altitudes causes the power to drop to about 50% of its initial value, the exact amount depending on solar cell characteristics and the particular trajectory. Most of the degradation is in the early portion of the trajectory.

Further refinements of the code could include extending the valid region of the radiation model to those low altitudes between latitudes  $50^\circ$  and  $75^\circ$ , and effects to make the program more efficient in terms of individual trajectory calculations and convergence characteristics in order to reduce run time further.

The program offers a tool for mission performance evaluation and comparisons. The costate histories generated are first order approximations to precision costate histories and with sufficient accuracy control the code can form the basis of a guidance scheme.

## APPENDIX A

### HIGH THRUST EQUATIONS

#### A.1 Introduction

In this appendix the details of the high thrust phase are discussed, including a brief description of Huntington Small's technique and code<sup>(12, 13)</sup> which were used for the initial high thrust phase. Since this code uses a special set of variables, the transformation to the equinoctial state and costate, used in the following low thrust phase, is presented. This appendix is a condensed version of Section 4 of Ref. 2.

#### A.2 The High Thrust Code

The initial high thrust phase of the program utilizes code developed by H. Small. This code calculates time-open minimum  $\Delta V$  trajectories in an inverse square field. This subsection discusses the method of Small and presents certain equations some of which will be used in Section 4.3 which considers the interface between the high and low thrust code.

The following is taken mainly from References 12 and 13. Taking the orbital elements as state variables and the characteristic velocity as independent variable, the rates of change of the state variables can be written

$$\dot{x}_j = \frac{d_j(\underline{x}, u)}{dt} \underline{g} \quad j = 1, \dots, 5 \quad (\text{A.1})$$

in which  $\underline{g}$ , the unit vector in the direction of thrust, and  $u$ , an angular variable in the instantaneous orbital plane are controls and the problem is to generate extremals which minimize the independent variable between end states. The Hamiltonian is  $H = \sum_{j=1}^5 \lambda_j \frac{d_j}{dt} \underline{g}$  and is constant and can be taken equal to unity. The optimal  $\underline{g} = \sum \lambda_j \frac{d_j}{dt} = \underline{\lambda}_v^*$  and the optimal  $u$  maximizes  $H(u)^2 = [\underline{\lambda}_v^*(u)]^2$ .

Using any set of orbital elements

$$\begin{aligned} \underline{\lambda}_v^* &= \Lambda_1 \sin(u+\Lambda_2) \hat{e}_R \\ &+ \left[ \Lambda_3 + (1+\psi)\Lambda_1 \cos(u+\Lambda_2) \right] / \psi \hat{e}_L \\ &+ \Lambda_4 \sin(u+\Lambda_5) / \psi \hat{e}_h \end{aligned} \quad (\text{A. 2})$$

in which  $\hat{e}_R$ ,  $\hat{e}_L$  and  $\hat{e}_h$  are unit vectors in the radial, circumferential and out-of-plane directions; and  $\psi = 1 + e \cos f$  where  $e$  is the eccentricity and  $f = u - \omega$ , the true anomaly. The  $\Lambda$ 's are functions of  $\underline{x}$  and  $\underline{\lambda}$  and will be defined later for our elements.

The Hamiltonian will be maximized at some  $u$  if  $[\lambda_v^*(u+\Delta u)]^2 \geq 0 \forall \Delta u$  with equality only at  $\Delta u = 2\pi, 4\pi, \dots$ . Defining  $t = \tan(\Delta u/2)$  this inequality becomes the ratio of two sixth-degree polynomials in  $t$ . Small then reduces the maximizing test to the form

$$t^2(\alpha_0 + \alpha_1 t + \alpha_2 t^2 + \alpha_3 t^3 + \alpha_4 t^4) \geq 0 \forall t \quad (\text{A. 3})$$

He then develops a general test for the positive definite quartic. The requirements are (Eq. 4 of Ref. 13)

$$\alpha_0 > 0 \quad (\text{A. 4a})$$

$$16\alpha_0^2(\alpha_2^2 + 3z_1) \geq (3\alpha_1^2 - 8\alpha_0\alpha_2)^2 \text{ if } 3\alpha_1^2 > 8\alpha_0\alpha_2 \quad (\text{A. 4b})$$

$$z_1 \left[ (\alpha_2^2 - z_1)^2 + 9\alpha_2 z_2 \right] - \alpha_2^3 z_2 - 27z_2^2/4 > 0 \quad (\text{A. 4c})$$

where

$$z_1 = 4\alpha_0\alpha_4 - \alpha_1\alpha_3$$

$$z_2 = \alpha_1^2\alpha_4 + \alpha_0\alpha_3^2 - \alpha_1\alpha_2\alpha_3 \quad (\text{A. 5})$$

There are other simple conditions that the  $\alpha_i$  must meet such as  $\alpha_4 > 0$  but they are all contained in Eq. (A. 4). Eq. (A. 4) will be violated first as the coefficients change during a firing requiring a switch through an angle described by

$$t_s = \frac{2(\alpha_1^2 - 4\alpha_0\alpha_2)(\alpha_2^2 + 3z_1) - 4\alpha_0(9z_2 - 8\alpha_2 z_1)}{4\alpha_0\alpha_3(\alpha_2^2 + 3z_1) + \alpha_1(9z_1 - 8\alpha_2 z_1)} \quad (\text{A. 6})$$

The  $\alpha_0 > 0$  case generates an impulse.

The  $H_u = 0$  condition (Eq. A. 3) and the  $\alpha_i$  are explicit functions of eight variables in Eq. (A. 2) but because  $(\lambda_v^*)^2$  can be scaled to 1 and  $u$  just depends on an arbitrary reference axis, it turns out that they can be written as functions of six independent parameters. Small chooses  $e \sin f$ ,  $\psi$ ,  $\phi$ ,  $\tau$  where

$$\lambda_v^* = \sin \phi \underline{e}_R + \cos \phi \cos T \underline{e}_L + \cos \phi \sin T \underline{e}_h \quad (\text{A. 7})$$

(illustrated in Fig. A-1,  $\cos \phi \geq 0$ ) and two others defined by

$$k \equiv [\Lambda_3 + \Lambda_1 \cos(u + \Lambda_2)] / (\psi \cos \phi) \quad (\text{A. 8})$$

$$\begin{aligned} j &\equiv \{ \Lambda_4 \sin(u + \Lambda_5) \sin \phi + \Lambda_4 \cos(u + \Lambda_5) \cos \phi \cos T \\ &\quad + [\Lambda_1 \cos(u + \Lambda_2) e \sin f \\ &\quad - \Lambda_1 \sin(u + \Lambda_2) e \cos f] \cos \phi \sin T \} / \cos^2 \phi \\ &= [\Lambda_4 \cos(u + \Lambda_5) / \cos \phi + e \sin f \sin T] \cos T \\ &\quad + [\tan \phi - k e \sin f] \sin T \end{aligned} \quad (\text{A. 9})$$

Further manipulations yield

$$\tan \phi = \frac{(j \sin T + k e \sin f)}{1 + k \psi \cos T} \quad (\text{A. 10})$$

and expressions for the  $\alpha_i$

$$\begin{aligned} \alpha_0 &= \psi [1 - \psi k^2 - (2 + \psi k^2) \tan^2 \phi] - j^2 \\ \alpha_1 &= 4\psi \tan \phi (2k - \cos T) - 2e \sin f (1 - 2 \tan^2 \phi) \\ \alpha_2 &= \alpha_0 + \alpha_4 + 8e \sin f \tan \phi (\cos T - k) \\ &\quad - 4(\psi - 1) [\cos T - k]^2 - \tan^2 \phi \\ \alpha_3 &= \alpha_1 + 8(\psi - 1) \tan \phi (\cos T - k) \\ &\quad + 4e \sin f [\cos T - k]^2 - \tan^2 \phi \\ \alpha_4 &= [(3 - \psi) \cos T - 2k] [2k - \cos T] - (\psi - 1) \sin^2 T \end{aligned} \quad (\text{A. 11})$$

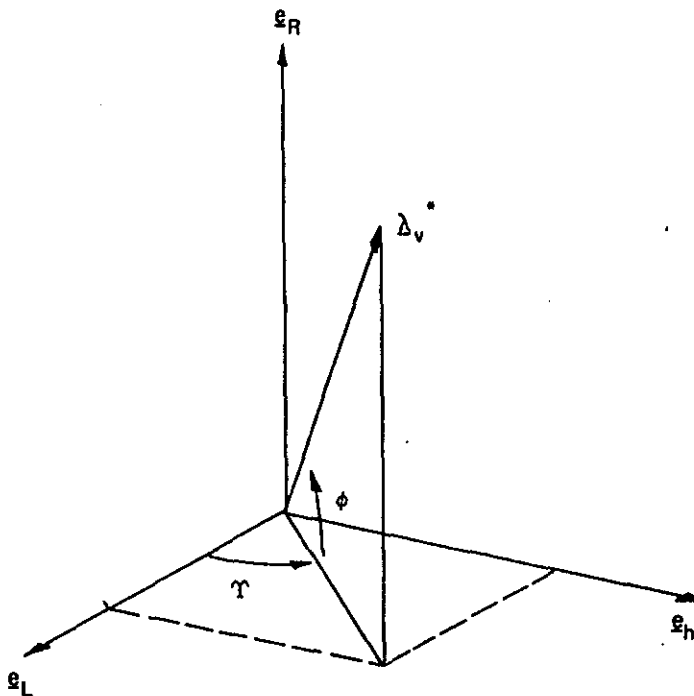


Figure A-1. Firing angles  $\tau$  and  $\phi$ .

The  $k$  and  $j$  variables can also be written in terms of the radius and velocity vectors and their adjoints.

$$k = h(\underline{\lambda}_R^* \cdot \underline{R})/h^* \psi \cos \phi \quad (\text{A. 12})$$

$$j = \frac{\mu h \lambda_v^*}{h^{*2} \cos^2 \phi} \underline{K} \quad (\text{A. 13})$$

where  $h$  is the angular momentum magnitude and  $h^*$  is the angular momentum magnitude at some reference orbit,  $\mu$  is the gravitation constant, and

$$\underline{K} = \underline{R} \times \underline{\lambda}_R^* + \underline{V} \times \underline{\lambda}_V^* \quad (\text{A. 14})$$

which is a constant of motion.

Small notes some special cases. If  $e = 0$ ,  $\alpha_1 = \alpha_3$  and  $\alpha_2 = \alpha_0 + \alpha_4$  so that  $z_2 = 0$  and Eq. (A.4c) reduces to  $z_1 > 0$ . Eq. (A.4a) is automatically satisfied. The double maximum occurs when  $\dot{z}_1 = 0$  at  $t_s = -2\alpha_0/\alpha_3$ . A second case is the Generalized Hohmann Transfer for which  $e \sin f = j = 0$  implies  $\tan \phi = \alpha_1 = \alpha_3 = z_2 = 0$  so Eq. (A.4c) reduces to  $\alpha_4 > 0$  and Eq. (4.4b) to  $4\alpha_0\alpha_4 \geq \alpha_2^2$  if  $\alpha_2 < 0$ . This equation turns out not to be restrictive and the double maximum occurs when  $\alpha_4 = 0$  at  $\Delta u = 180^\circ$ .

Small's code works in the following manner. An initial set of parameters ( $e, f, \tau, j\psi^{-1/2}, k\psi^{1/2}$ ) which satisfy Eq. (A.4) is input (for our program  $e = 0, f = 0, \psi = 1$  so the input is  $(0, 0, \tau, j, k)$ ). The initial  $h$  is arbitrary, just scaling  $\tau = h\Delta v/\mu$  which is the independent variable within the code. We have set  $h^* = h_0 = 1$ . Then  $\tau$  is incremented by a succession of  $\Delta\tau$ . The corresponding values of  $\alpha_1, \psi$  and Eq. (A.4c) are computed until Eq. (A.4c) is zero at some  $\tau_s$ . The values of  $\Lambda_1 \sin(u + \Lambda_2), \Lambda_1 \cos(u + \Lambda_2), \Lambda_3, \Lambda_4 \sin(u + \Lambda_5)$  and  $\Lambda_4 \cos(u + \Lambda_5)$  are computed from the known values of  $e, f, \tau, j, k$  at  $\tau_s$  and all variables are switched to a new peak by adding  $\Delta u_s$  computed from Eq. (A.6); then the next impulse continues by incrementing  $\tau$  again. The result is a series of known impulses and coasting arcs. Since for our case the initial orbit was circular, the location of the first impulse was arbitrary (as far as the high thrust code is concerned) and so the initial  $f = 0$ . We limited the number of impulses to two and specified the total  $\Delta V$ . In this case only the remaining available  $\Delta V$  was used on the final impulse. The location was optimal although the  $\Delta V$  might be less (or more) than called for by Small's program.

### A.3 Coupling of High and Low Thrust Code

In the combined high and low thrust program the output of Small's code must be interfaced with the beginning of the low thrust code. In addition we have constrained Small's code by 1) requiring the initial (high thrust) orbit to be circular, 2) specifying the maximum number of initial impulses and the corresponding total  $\Delta V$ . The first constraint allows us to calculate the limits on the permissible input to Small's code, i.e., the requirement that the input satisfy Eq. (A.4)

The requirement that the initial high thrust orbit be circular and the assumption that the first impulse is in the  $-\underline{e}_L$  direction in order to raise the orbit, combined with the inequalities of Eq. (A.4) yield the following requirements on  $\tau, k$  and  $j$ .

$$|\tau| \leq \frac{\pi}{2} \quad (\text{A.15})$$

$$\frac{\cos T}{2} < k < \cos T \quad (\text{A. 16})$$

$$|j| < (1 + k \cos T) \sqrt{\frac{\cos T - k}{\cos T + k}} \quad (\text{A. 17})$$

These constraints guarantee that values picked for  $T$ ,  $k$ ,  $j$  will yield an optimal impulse.

For a given total  $\Delta V$  and a given set of initial conditions, a one, two, three or more impulses optimal transfer may result. We are limiting the number of impulses to two. If the specified total  $\Delta V$  is less than the maximum for the first impulse calculated by the code, that impulse is still optimal under the constraint. If the total  $\Delta V$  is greater than the maximum for the first impulse, then all of the remaining  $\Delta V$  will be used at the second impulse. If the remainder is less than or equal to the maximum for the second impulse calculated by Small's code, then the transfer is still optimal under the constraint. If the remainder is greater, then the transfer is not optimal. A three or more impulse transfer could have reached the same orbit with less  $\Delta V$ . Usually for transfers of interest, one or two impulses will be optimal.

For the calculations in Small's code a "first orbit" coordinate frame was assumed. In this frame the initial orbit has zero inclination and the initial impulse is assumed to occur at  $f = 0$ . Also  $\omega = \Omega = 0$  initially. The orbital elements and their adjoints which are contained in Small's  $S(I, J, K)$  array are with respect to this coordinate system. The elements of the  $S$  array are made up of orbital elements and other of Small's variables. This array is calculated by Small's code and it is from this array that we must obtain the equinoctial orbital elements and their adjoints and other information for input to the low thrust code. In Small's code the  $I$  in  $S(I, J, K)$  varies over different trajectories (he calculated neighboring trajectories along with a nominal trajectory for a purely high thrust Newton iteration). For our program  $I$  was set to 1.  $J$  varies over different orbits. For our case  $J$  varies from 1 to 3 for a two impulse trajectory.  $K$  varies from 1 to 20 and these quantities are listed in Table A. 1. In what follows, for brevity,  $S_K$  will be used for  $S(I, J, K)$ .

Table A-1†

K	S(I, J, K)	11	$\psi^{1/2}(\cos T - k)$
1	$\tau$	12	$\cos(u + \Omega)$
2*	$D\tau$	13	$\sin(u + \Omega)$
3*	$\psi^{-1/2} \tan(\Delta u/2)$	14*	$\cos \Delta u$
4	$(h/h^*) \psi^{-1/2} \cos \phi$	15*	$\sin \Delta u$
5	$\psi^{-1/2} e \sin f$	16	$\cos i$
6	$k \psi^{1/2}$	17	$\sin i \cos u$
7	$\tan \phi$	18	$\sin i \sin u$
8	$\Lambda_4 \cos(u + \Lambda_5) / \cos \phi$	19	$\sin i \cos \Omega$
9	$\psi^{1/2} \sin T$	20	$\sin i \sin \Omega$
10	$\psi$		

\*Information for  $J^{\text{th}}$  impulse is stored in S(I, J+1, K).

†This is essentially Table D. 1 of Reference 12.

In our program,  $h^*$  was set to one and the initial orbit is assumed circular. Thus for each orbit ( $J=1, 2, 3$ )

$$h = S_4 \sqrt{S_{10}} / \cos \phi \quad (\text{A. 18})$$

$$a = a_0 h^2 / (1 - e^2) \quad (\text{A. 19})$$

$$e = [(S_{10} - 1)^2 + S_{10} \cdot S_5^2]^{1/2} \quad (\text{A. 20})$$

In the "first orbit" coordinate frame,

$$\cos i = S_{16} \quad (\text{A. 21})$$

$$\sin i = (S_{19}^2 + S_{20}^2)^{1/2} \quad (\text{A. 22})$$

$$\tan \Omega = \frac{S_{20}}{S_{19}} \quad (\text{A. 23})$$

In addition

$$\tan u = S_{18} / S_{17} \quad (\text{A. 24})$$

$$\tan f = \frac{S_5 \sqrt{S_{10}}}{S_{10} - 1} \quad (\text{A. 25})$$

$$\omega = u - f \quad (\text{A. 26})$$

$$\tan \phi = S_7 \quad (\text{A. 27})$$

$$\tan T = \frac{S_9}{S_{11} + S_6} \quad (\text{A. 28})$$

Now the orbital elements of the first orbit are known with respect to the inertial reference coordinate frame,  $a$ ,  $e$ ,  $i_1$ ,  $\Omega_1$ ,  $\omega_1$  (obtaining  $\omega_1$  is discussed later). In the "first orbit" frame,  $i_1 = 0$ ,  $\Omega_1 = 0$ ,  $\omega_1 = 0$ . A vector in the first orbit frame is related to a vector in the reference frame by the transformation

$$T_I = \begin{bmatrix} \cos \omega_I \cos \Omega_I & \cos \omega_I \sin \Omega_I & \sin \omega_I \cos i_I \\ -\sin \omega_I \cos i_I \sin \Omega_I & +\sin \omega_I \cos i_I \cos \Omega_I & \\ -\sin \Omega_I \cos \Omega_I & -\sin \omega_I \sin \Omega_I & \cos \omega_I \sin i_I \\ -\cos \omega_I \cos i_I \sin \Omega_I & +\cos \omega_I \cos i_I \cos \Omega_I & \\ \sin i_I \sin \Omega_I & -\sin i_I \cos \Omega_I & \cos i_I \end{bmatrix} \quad (\text{A. 29})$$

The coordinate frame dependent orbital elements of the second or third orbit are obtained in the "first orbit" frame by using the S array; call these  $i_2$ ,  $\Omega_2$ ,  $\omega_2$ . The orbital elements in the reference frame,  $i_3$ ,  $\Omega_3$ ,  $\omega_3$ , can be obtained from

$$T_3 = T_2 T_I \quad (\text{A. 30})$$

where  $T_2$  is given by Eq. (A. 29) with the subscript I replaced by 2. The elements of  $T_3$  are defined similarly.  $T_3$  can then be solved for  $i_3$ ,  $\Omega_3$ ,  $\omega_3$ . Let  $t_{ij}$  be the  $i$ - $j$ <sup>th</sup> element of  $T_3$ . Then

$$\sin i_3 = \sqrt{t_{31}^2 + t_{32}^2} \quad (\text{A. 31})$$

$$\cos i_3 = t_{33} \quad (\text{A. 32})$$

$$\sin \omega_3 = \iota_{13} / \sin i_3 \quad (\text{A. 33})$$

$$\cos \omega_3 = \iota_{23} / \sin i_3 \quad (\text{A. 34})$$

$$\sin \Omega_3 = \iota_{31} / \sin i_3 \quad (\text{A. 35})$$

$$\cos \Omega_3 = -\iota_{32} / \sin i_3 \quad (\text{A. 36})$$

If  $i_3 = 0$  then  $\omega_3 + \Omega_3$  can be found from

$$\cos(\omega_3 + \Omega_3) = \iota_{11} \quad (\text{A. 37})$$

$$\sin(\omega_3 + \Omega_3) = \iota_{12} \quad (\text{A. 38})$$

The equinoctial elements, h, k are given by

$$h = e \sin(\omega_3 + \Omega_3) \quad (\text{A. 39})$$

$$k = e \cos(\omega_3 + \Omega_3) \quad (\text{A. 40})$$

It is possible to get p, q directly from  $T_3$ .

$$p = \frac{\iota_{31}}{1 + \iota_{33}} \quad (\text{A. 41})$$

$$q = \frac{-\iota_{32}}{1 + \iota_{33}} \quad (\text{A. 42})$$

The  $\Lambda_i$ 's are given in terms of the classical state and costate by Eq. A-8 of Ref. 12. This can be inverted to give the costate in terms of the  $\Lambda_i$ .

$$\lambda_a = \frac{1}{2} \sqrt{\frac{\mu}{a^3(1-e^2)}} \left[ \Lambda_3 - e \Lambda_1 \cos(\Lambda_2 + \omega) \right] \quad (\text{A. 43})$$

$$\lambda_e = \sqrt{\frac{\mu}{a(1-e^2)^3}} \left[ \Lambda_1 \cos(\Lambda_2 + \omega) - e \Lambda_3 \right] \quad (\text{A. 44})$$

$$\lambda_i = \sqrt{\frac{\mu}{a(1-e^2)}} \Lambda_4 \sin \Lambda_5 \quad (\text{A. 45})$$

$$\lambda_{\omega} = -e \sqrt{\frac{\mu}{a(1-e^2)}} \Lambda_1 \sin(\Lambda_2 + \omega) \quad (\text{A.46})$$

$$\lambda_{\Omega} = \sqrt{\frac{\mu}{a(1-e^2)}} \Lambda_4 \cos \Lambda_5 \sin i + \lambda_{\omega} \cos i \quad (\text{A.47})$$

However, this costate is given in terms of the "first orbit" coordinate frame. Since in this frame  $i = 0$  and  $e = 0$  initially, then initially  $\lambda_{\omega} = \lambda_{\Omega} = 0$ . In the equatorial reference frame if  $\Omega$  and  $\omega$  are free, then  $\lambda_{\Omega} = 0$  and  $\lambda_{\omega} = 0$  initially. The  $\lambda_a$  and  $\lambda_e$  will be the same in the equatorial reference frame as in the "first orbit frame". The form of  $\lambda_i$  at the initial time follows from the requirement that  $\lambda_{\Omega} = 0$ . This condition also yields the location of the first impulse. If in the reference frame  $\Omega$  is fixed initially then  $\lambda_{\Omega}$  is free though  $\lambda_{\omega}$  is still zero.

In the reference frame the first impulse occurs at  $\omega_I$ . The adjoints to  $\Omega$  and  $i$  in the reference frame can be related to  $\omega_I$  by the following equations derived from results listed in Appendix B of Reference 2.

$$\lambda'_i = \sqrt{\frac{\mu}{a_0}} \Lambda_4 \sin(\Lambda_5 - \omega_I) \quad (\text{A.48})$$

$$\lambda'_{\Omega} = \sqrt{\frac{\mu}{a_0}} \Lambda_4 \sin i_I \cos(\Lambda_5 - \omega_I) \quad (\text{A.49})$$

If in the reference frame, we require that  $\lambda'_{\Omega} = 0$ , then for  $\Lambda_4 \sin i \neq 0$

$$\Lambda_5 - \omega_I = \pm \frac{\pi}{2}$$

or

$$\omega_I = \Lambda_5 \pm \frac{\pi}{2}$$

Taking the convention that  $\lambda_i'$  and  $\Lambda_4$  have the same sign determines that

$$\omega_I = \Lambda_5 - \frac{\pi}{2} \quad (\text{A. 50})$$

Then

$$\lambda_i' = \sqrt{\frac{\mu}{a_0}} \Lambda_{40} \quad (\text{A. 51})$$

If the initial  $\Omega$  is fixed then  $\lambda_\Omega$  is free and not necessarily zero although  $\lambda_\omega$  is still zero. For this case it is no longer necessarily true that  $\omega_I = \Lambda_5 - \frac{\pi}{2}$ ; rather  $\omega_I$  is arbitrary but then determines  $\lambda_\Omega'$  and  $\lambda_i'$  through Eqs. (A. 48) and (A. 49).

The formulas for  $\lambda_a$  and  $\lambda_e$  are valid at any time during the initial high thrust phase. During the high thrust phase  $\lambda_\Omega$  remains constant, but  $\lambda_i$  and  $\lambda_\omega$  may change. Initially, there are some  $i_I, \Omega_I, \omega_I$ , then using results from Appendix B of Ref. 2 and the fact that  $\lambda_\omega' = 0$ , let

$$\begin{aligned} c_1 &= \lambda_i' \cos \Omega_I - \lambda_\Omega' \cot i_I \sin \Omega_I \\ c_2 &= \lambda_i' \sin \Omega_I + \lambda_\Omega' \cot i_I \cos \Omega_I \\ c_3 &= \lambda_\Omega' \end{aligned} \quad (\text{A. 52})$$

For any set of  $i, \Omega, \omega$  in the reference frame

$$\lambda_i = c_1 \cos \Omega + c_2 \sin \Omega \quad (\text{A. 53})$$

$$\lambda_\Omega = c_3 \quad (\text{A. 54})$$

$$\lambda_\omega = \sin i (c_1 \sin \Omega - c_2 \cos \Omega) + c_3 \cos i \quad (\text{A. 55})$$

For SEP and high thrust in an axially symmetric field, the fixed  $\Omega$  option should be used (in which case the initial  $\omega$  should be driven to  $\Lambda_5 - \frac{\pi}{2}$  so as to make  $\lambda_\Omega = 0$ ). If this option is not used and  $\Omega$  is allowed to be free initially, then varying  $\Omega$  initially will have no effect on the final conditions, and the partial derivative matrix will be singular.

We need  $\Lambda_1, \Lambda_2, \Lambda_3$  and  $\Lambda_4$  in terms of S array. From Eq. (4.2), (4.7), (4.8) and from Table B-1 the following quantities are obtained.

$$\Lambda_3 = \cos \phi [(1+\psi)k - \cos T] \quad (\text{A. 56})$$

$$\Lambda_1 \cos \Lambda_2 = \cos \phi [\cos T - k] \cos u + \sin \phi \sin u \quad (\text{A. 57})$$

$$\Lambda_1 \sin \Lambda_2 = -\cos \phi [\cos T - k] \sin u + \sin \phi \cos u \quad (\text{A. 58})$$

$$\Lambda_4 \cos \Lambda_5 = \cos \phi (S_8 \cos u + \psi \sin T \sin u) \quad (\text{A. 59})$$

$$\Lambda_4 \sin \Lambda_5 = \cos \phi (-S_8 \sin u + \psi \sin T \cos u) \quad (\text{A. 60})$$

In order to calculate  $\lambda_a$  and  $\lambda_e$  we need the combination

$$\Lambda_1 \cos \Lambda_2 \cos \omega - \Lambda_1 \sin \Lambda_2 \sin \omega = \sin f \sin \phi + \cos f \cos \phi \left( \frac{S_{11}}{\sqrt{S_{10}}} \right) \quad (\text{A. 61})$$

where we have used  $u = \omega + f$ , and where  $\phi$  and  $f$  were derived in terms of the S array previously. Obtaining  $\Lambda_3$  in terms of the S array,

$$\Lambda_3 = \frac{h^*}{h} S_4 (S_{10} \cdot S_6 - S_{11}) \quad (\text{A. 62})$$

$\Lambda_4$  is needed only on the first orbit where  $u = f = \omega = 0$ ; on the first orbit

$$\Lambda_4 \cos \Lambda_5 = S_8 \cos \phi \quad (\text{A. 63})$$

$$\Lambda_4 \sin \Lambda_5 = S_9 \sqrt{S_{10}} \cos \phi \quad (\text{A. 64})$$

$\Lambda_4$  can be obtained by taking the square root of the sum of the squares of the above two quantities. There is an ambiguity of sign, however. The computer code picks the sign by the criterion that if the inclination is desired to be reduced,  $\Lambda_4$  (and thus  $\lambda_i$ ) should be negative; similarly if it is desired to increase inclination,  $\lambda_i$  and  $\Lambda_4$  should be positive. This choice can be overridden by an input to the program. Once the sign of  $\Lambda_4$  is picked,  $\Lambda_5$  can be found unambiguously (as long as  $\Lambda_4 \neq 0$ ).  $\lambda_a$ ,  $\lambda_e$ ,  $\lambda_i$  and  $\lambda_\Omega$  can now be calculated.

Finally the equinoctial costate is given, at each orbit using Eq. (3.25),

$$\lambda_a = \lambda_a \quad (\text{A.65})$$

$$\lambda_h = \sin(\omega_3 + \Omega_3) \lambda_e + \cos(\omega_3 + \Omega_3) \frac{\lambda_\omega}{e} \quad (\text{A.66})$$

$$\lambda_k = \cos(\omega_3 + \Omega_3) \lambda_e - \sin(\omega_3 + \Omega_3) \frac{\lambda_\omega}{e} \quad (\text{A.67})$$

$$\lambda_p = 2 \sin \Omega_3 \cos^2 \frac{i_3}{2} \lambda_i + \frac{\cos \Omega_3}{\tan(i_3/2)} (\lambda_\Omega - \lambda_\omega) \quad (\text{A.68})$$

$$\lambda_q = 2 \cos \Omega_3 \cos^2 \frac{i_3}{2} \lambda_i - \frac{\sin \Omega_3}{\tan i_3/2} (\lambda_\Omega - \lambda_\omega) \quad (\text{A.69})$$

A multiplicative scale factor may also be needed before input to the low thrust code.

Since  $\Lambda_5$  and therefore  $\omega_3$  cannot be calculated unambiguously if  $\Lambda_4 = 0$ , this case can lead to difficulties in running the program.  $\Lambda_4 = 0$  if  $j = \Gamma = 0$ . This implies a zero inclination change during the initial high thrust phase. Because of the radiation and shadowing effects, which for SEP will generally cause an optimal trajectory to contain some inclination variation even if the initial and final inclinations are the same, this case will generally not arise for SEP. It could arise for constant power and zero inclinations change and so the program may not work for this case. The initial guesses for  $T$  and  $j$  should not both be zero.

APPENDIX B

THE MATRIX M AND ITS PARTIALS

Table B-1 Elements of M

$$M_{11} = \frac{2\dot{X}_1}{n^2 a}, M_{12} = \frac{2\dot{Y}_1}{n^2 a}, M_{13} = 0$$

$$M_{21} = \frac{\sqrt{1-h^2-k^2}}{na^2} \left[ \frac{\partial X_1}{\partial k} + \frac{\dot{X}_1}{n} (\sin F - h\beta) \right]$$

$$M_{22} = \frac{\sqrt{1-h^2-k^2}}{na^2} \left[ \frac{\partial Y_1}{\partial k} + \frac{\dot{Y}_1}{n} (\sin F - h\beta) \right]$$

$$M_{23} = \frac{k(qY_1 - pX_1)}{na^2 \sqrt{1-h^2-k^2}}$$

$$M_{31} = \frac{\sqrt{1-h^2-k^2}}{na^2} \left[ \frac{\partial X_1}{\partial h} - \frac{\dot{X}_1}{n} (\cos F - k\beta) \right]$$

$$M_{32} = \frac{\sqrt{1-h^2-k^2}}{na^2} \left[ \frac{\partial Y_1}{\partial h} - \frac{\dot{Y}_1}{n} (\cos F - k\beta) \right]$$

$$M_{33} = \frac{-h(qY_1 - pX_1)}{na^2 \sqrt{1-h^2-k^2}}$$

$$M_{41} = 0, M_{42} = 0, M_{43} = \frac{(1+p^2+q^2)Y_1}{2na^2 \sqrt{1-h^2-k^2}}$$

$$M_{51} = 0, M_{52} = 0, M_{53} = \frac{(1+p^2+q^2)X_1}{2na^2 \sqrt{1-h^2-k^2}}$$

Table B-2 Partial of  $X_1$  and  $Y_1$  with  
Respect to  $h$  and  $k$

$$\begin{aligned} \frac{\partial X_1}{\partial h} &= a \left[ \frac{-h\beta \cos F - (\beta + h^2 \beta^3)}{1-\beta} (h \cos F - k \sin F) \right] \\ \frac{\partial Y_1}{\partial h} &= a \left[ \frac{k\beta \cos F - 1 + hk\beta^3}{1-\beta} (h \cos F - k \sin F) \right] \\ \frac{\partial X_1}{\partial k} &= a \left[ \frac{h\beta \sin F - 1 - hk\beta^3}{1-\beta} (h \cos F - k \sin F) \right] \\ \frac{\partial Y_1}{\partial k} &= a \left[ \frac{-k\beta \sin F + (\beta + k^2 \beta^3)}{1-\beta} (h \cos F - k \sin F) \right] \end{aligned}$$

Table B-3 Partial of  $M$  with Respect to  $a$

$$\frac{\partial M}{\partial a} = \frac{1}{2a} \begin{bmatrix} 3 & 0 & 0 & 0 & 0 \\ 0 & 1 & 0 & 0 & 0 \\ 0 & 0 & 1 & 0 & 0 \\ 0 & 0 & 0 & 1 & 0 \\ 0 & 0 & 0 & 0 & 1 \end{bmatrix} M$$

Table B-4 Partial of M with Respect to h

$$\frac{\partial M_{11}}{\partial h} = \frac{2}{n^2 a} \frac{\partial \dot{X}_1}{\partial h}, \quad \frac{\partial M_{12}}{\partial h} = \frac{2}{n^2 a} \frac{\partial \dot{Y}_1}{\partial h}, \quad \frac{\partial M_{13}}{\partial h} = 0$$

$$\frac{\partial M_{21}}{\partial h} = \frac{-hM_{21}}{1-h^2-k^2} + \frac{\sqrt{1-h^2-k^2}}{na^2} \left[ \frac{\partial^2 X_1}{\partial h \partial k} + \frac{\partial \dot{X}_1}{\partial h} \frac{(\sin F - h\beta)}{n} - \frac{\dot{X}_1}{n} \frac{(\beta + h^2 \beta^3)}{1-\beta} \right]$$

$$\frac{\partial M_{22}}{\partial h} = \frac{-hM_{22}}{1-h^2-k^2} + \frac{\sqrt{1-h^2-k^2}}{na^2} \left[ \frac{\partial^2 Y_1}{\partial h \partial k} + \frac{\partial \dot{Y}_1}{\partial h} \frac{(\sin F - h\beta)}{n} - \frac{\dot{Y}_1}{n} \frac{(\beta + h^2 \beta^3)}{1-\beta} \right]$$

$$\frac{\partial M_{23}}{\partial h} = \frac{hM_{23}}{1-h^2-k^2} + \frac{k}{na^2 \sqrt{1-h^2-k^2}} \left( q \frac{\partial Y_1}{\partial h} - p \frac{\partial X_1}{\partial h} \right)$$

$$\frac{\partial M_{31}}{\partial h} = \frac{-hM_{31}}{1-h^2-k^2} - \frac{\sqrt{1-h^2-k^2}}{na^2} \left[ \frac{\partial^2 X_1}{\partial h^2} - \frac{\partial \dot{X}_1}{\partial h} \frac{(\cos F - k\beta)}{n} + \frac{\dot{X}_1}{n} \frac{hk\beta^3}{1-\beta} \right]$$

$$\frac{\partial M_{32}}{\partial h} = \frac{-hM_{32}}{1-h^2-k^2} - \frac{\sqrt{1-h^2-k^2}}{na^2} \left[ \frac{\partial^2 Y_1}{\partial h^2} - \frac{\partial \dot{Y}_1}{\partial h} \frac{(\cos F - k\beta)}{n} + \frac{\dot{Y}_1}{n} \frac{hk\beta^3}{1-\beta} \right]$$

$$\frac{\partial M_{33}}{\partial h} = \frac{hM_{33}}{1-h^2-k^2} + \frac{M_{33}}{h} - \frac{h}{na^2 \sqrt{1-h^2-k^2}} \left( q \frac{\partial Y_1}{\partial h} - p \frac{\partial X_1}{\partial h} \right)$$

$$\frac{\partial M_{41}}{\partial h} = 0, \quad \frac{\partial M_{42}}{\partial h} = 0, \quad \frac{\partial M_{43}}{\partial h} = \frac{hM_{43}}{1-h^2-k^2} + \frac{M_{43}}{Y_1} \frac{\partial Y_1}{\partial h}$$

$$\frac{\partial M_{51}}{\partial h} = 0, \quad \frac{\partial M_{52}}{\partial h} = 0, \quad \frac{\partial M_{53}}{\partial h} = \frac{hM_{53}}{1-h^2-k^2} + \frac{M_{53}}{X_1} \frac{\partial X_1}{\partial h}$$

Table B-5 Partial of M with Respect to k

$$\frac{\partial M_{11}}{\partial k} = \frac{2}{n^2 a} \frac{\partial \dot{X}_1}{\partial k}, \quad \frac{\partial M_{12}}{\partial k} = \frac{2}{n^2 a} \frac{\partial \dot{Y}_1}{\partial k}, \quad \frac{\partial M_{13}}{\partial k} = 0$$

$$\frac{\partial M_{21}}{\partial k} = \frac{-kM_{21}}{1-h^2-k^2} + \frac{\sqrt{1-h^2-k^2}}{na^2} \left[ \frac{\partial^2 X_1}{\partial k^2} + \frac{\partial \dot{X}_1}{\partial k} \frac{(\sin F - h\beta)}{n} - \frac{\dot{X}_1}{n} \frac{hk\beta^3}{1-\beta} \right]$$

$$\frac{\partial M_{22}}{\partial k} = \frac{-kM_{22}}{1-h^2-k^2} + \frac{\sqrt{1-h^2-k^2}}{na^2} \left[ \frac{\partial^2 Y_1}{\partial k^2} + \frac{\partial \dot{Y}_1}{\partial k} \frac{(\sin F - h\beta)}{n} - \frac{\dot{Y}_1}{n} \frac{hk\beta^3}{1-\beta} \right]$$

$$\frac{\partial M_{23}}{\partial k} = \frac{M_{23}}{k} + \frac{kM_{23}}{1-h^2-k^2} + \frac{k}{na^2 \sqrt{1-h^2-k^2}} \left( q \frac{\partial Y_1}{\partial k} - p \frac{\partial X_1}{\partial k} \right)$$

$$\frac{\partial M_{31}}{\partial k} = -\frac{kM_{31}}{1-h^2-k^2} - \frac{\sqrt{1-h^2-k^2}}{na^2} \left[ \frac{\partial^2 X_1}{\partial k \partial h} - \frac{\partial \dot{X}_1}{\partial k} \left( \frac{\cos F - k\beta}{n} \right) + \frac{\dot{X}_1}{n} \frac{(\beta + k^2 \beta^3)}{1-\beta} \right]$$

$$\frac{\partial M_{32}}{\partial k} = \frac{-kM_{32}}{1-h^2-k^2} - \frac{\sqrt{1-h^2-k^2}}{na^2} \left[ \frac{\partial^2 Y_1}{\partial k \partial h} - \frac{\partial \dot{Y}_1}{\partial k} \left( \frac{\cos F - k\beta}{n} \right) + \frac{\dot{Y}_1}{n} \frac{(\beta + k^2 \beta^3)}{1-\beta} \right]$$

$$\frac{\partial M_{33}}{\partial k} = \frac{kM_{33}}{1-h^2-k^2} - \frac{h}{na^2 \sqrt{1-h^2-k^2}} \left( q \frac{\partial Y_1}{\partial k} - p \frac{\partial X_1}{\partial k} \right)$$

$$\frac{\partial M_{41}}{\partial k} = 0, \quad \frac{\partial M_{42}}{\partial k} = 0, \quad \frac{\partial M_{43}}{\partial k} = \frac{kM_{43}}{1-h^2-k^2} + \frac{M_{43}}{Y_1} \frac{\partial Y_1}{\partial k}$$

$$\frac{\partial M_{51}}{\partial k} = 0, \quad \frac{\partial M_{52}}{\partial k} = 0, \quad \frac{\partial M_{53}}{\partial k} = \frac{kM_{53}}{1-h^2-k^2} + \frac{M_{53}}{X_1} \frac{\partial X_1}{\partial k}$$

Table B-6 Non-zero Partialials of M with Respect to p

$$\frac{\partial M_{23}}{\partial p} = \frac{-kX_1}{\sqrt{1-h^2-k^2} na^2}$$

$$\frac{\partial M_{33}}{\partial p} = \frac{hX_1}{\sqrt{1-h^2-k^2} na^2}$$

$$\frac{\partial M_{43}}{\partial p} = \frac{pY_1}{\sqrt{1-h^2-k^2} na^2}$$

$$\frac{\partial M_{53}}{\partial p} = \frac{pX_1}{\sqrt{1-h^2-k^2} na^2}$$

Table B-7 Non-zero Partialials of M with Respect to q

$$\frac{\partial M_{23}}{\partial q} = \frac{kY_1}{\sqrt{1-h^2-k^2} na^2}$$

$$\frac{\partial M_{33}}{\partial q} = \frac{-hY_1}{\sqrt{1-h^2-k^2} na^2}$$

$$\frac{\partial M_{43}}{\partial q} = \frac{qY_1}{\sqrt{1-h^2-k^2} na^2}$$

$$\frac{\partial M_{53}}{\partial q} = \frac{qX_1}{\sqrt{1-h^2-k^2} na^2}$$

Table B-8 Partial of  $\dot{X}_1$  and  $\dot{Y}_1$  with Respect to h and k

$$\begin{aligned} \frac{\partial \dot{X}_1}{\partial h} &= \frac{a}{r} \frac{\dot{X}_1 \sin F + na^2}{r} \left[ \frac{(h \sin F + k \cos F) (\beta + h^2 \beta^3) + h \beta \sin F}{1 - \beta} \right] \\ \frac{\partial \dot{Y}_1}{\partial h} &= \frac{a}{r} \frac{\dot{Y}_1 \sin F + na^2}{r} \left[ \frac{-k \beta \sin F - h k \beta^3 (h \sin F + k \cos F)}{1 - \beta} \right] \\ \frac{\partial \dot{X}_1}{\partial k} &= \frac{a}{r} \frac{\dot{X}_1 \cos F + na^2}{r} \left[ \frac{h \beta \cos F + h k \beta^3 (h \sin F + k \cos F)}{1 - \beta} \right] \\ \frac{\partial \dot{Y}_1}{\partial k} &= \frac{a}{r} \frac{\dot{Y}_1 \cos F + na^2}{r} \left[ \frac{-(h \sin F + k \cos F) (\beta + k^2 \beta^3) - k \beta \cos F}{1 - \beta} \right] \end{aligned}$$

Table B-9 Second Partial of  $X_1$  and  $Y_1$  with Respect to h and k

$$\begin{aligned} \frac{\partial^2 X_1}{\partial h^2} &= a \left[ \frac{h \beta^3}{1 - \beta} (-h \cos F + k \sin F) \left( \frac{3 + h^2 \beta^2 (3 - 2\beta)}{(1 - \beta)^2} \right) - \frac{2 \cos F (\beta + h^2 \beta^3)}{1 - \beta} \right] \\ \frac{\partial^2 Y_1}{\partial h^2} &= a \left[ \frac{k \beta^3}{1 - \beta} (h \cos F - k \sin F) \left( \frac{1 + h^2 (3\beta^2 - 2\beta^3)}{(1 - \beta)^2} \right) + \frac{2 h k \beta^3}{1 - \beta} \cos F \right] \\ \frac{\partial^2 X_1}{\partial k^2} &= a \left[ \frac{h \beta^3}{1 - \beta} (-h \cos F + k \sin F) \left( \frac{1 + k^2 (3\beta^2 - 2\beta^3)}{(1 - \beta)^2} \right) + \frac{2 h k \beta^3}{1 - \beta} \sin F \right] \\ \frac{\partial^2 Y_1}{\partial k^2} &= a \left[ \frac{k \beta^3}{1 - \beta} (h \cos F - k \sin F) \left( \frac{3 + k^2 (3\beta^2 - 2\beta^3)}{(1 - \beta)^2} \right) - \frac{2 \sin F (\beta + k^2 \beta^3)}{1 - \beta} \right] \\ \frac{\partial^2 X_1}{\partial h \partial k} &= \frac{\partial^2 \dot{X}_1}{\partial k \partial h} = a \left[ \frac{k \beta^3}{1 - \beta} (-h \cos F + k \sin F) \left( \frac{1 + h^2 (3\beta^2 - 2\beta^3)}{(1 - \beta)^2} \right) - \frac{h k \beta^3}{1 - \beta} \cos F + \frac{\sin F (\beta + h^2 \beta^3)}{1 - \beta} \right] \\ \frac{\partial^2 Y_1}{\partial k \partial h} &= \frac{\partial^2 \dot{Y}_1}{\partial h \partial k} = a \left[ \frac{h \beta^3}{1 - \beta} (h \cos F - k \sin F) \left( \frac{1 + k^2 (3\beta^2 - 2\beta^3)}{(1 - \beta)^2} \right) - \frac{h k \beta^3}{1 - \beta} \sin F + \frac{\cos F (\beta + k^2 \beta^3)}{1 - \beta} \right] \end{aligned}$$

APPENDIX C

AN ALTERNATE FORM OF THE M-MATRIX

In Reference 28, page 30, a new form of the M or  $\frac{\partial Z}{\partial \dot{r}}$  equation was written with respect to the equinoctial orbit frame. The partials of a, h, k, p and q are repeated here. The "M-matrix" is just made up of the coefficients of the basis vectors in the following expressions.

$$\begin{aligned}\frac{\partial a}{\partial \dot{r}} &= \frac{2(\dot{X}_1 \hat{f} + \dot{Y}_1 \hat{g})}{n^2 a} \\ \frac{\partial h}{\partial \dot{r}} &= \frac{1}{u} [G \hat{f} + r \dot{X}_1 \hat{y}] + \frac{k}{G} [q Y_1 - p X_1] \hat{w} \\ \frac{\partial k}{\partial \dot{r}} &= \frac{1}{\mu} [G \hat{g} + r \dot{Y}_1 \hat{y}] - \frac{h}{G} [q Y_1 - p X_1] \hat{w} \\ \frac{\partial p}{\partial \dot{r}} &= \frac{(1+p^2+q^2)}{2G} Y_1 \hat{w} \\ \frac{\partial q}{\partial \dot{r}} &= \frac{(1+p^2+q^2)}{2G} X_1 \hat{w}\end{aligned}\tag{C.1}$$

where  $\hat{f}$ ,  $\hat{g}$ ,  $\hat{w}$  are the equinoctial basis vectors defined in Section 3.2 and  $X_1$  and  $Y_1$  are the  $\hat{f}$  and  $\hat{g}$  components of position respectively. Also

$$G = na^2 \sqrt{1-h^2-k^2} = \dot{Y}_1 X_1 - \dot{X}_1 Y_1\tag{C.2}$$

$$\hat{y} = \hat{w} \times \underline{r}/r = (X_1 \hat{g} - Y_1 \hat{f})/r\tag{C.3}$$

$$r = \sqrt{X_1^2 + Y_1^2}\tag{C.4}$$

$$n = \sqrt{\frac{\mu}{a^3}}\tag{C.5}$$

A useful form of  $\frac{\partial z}{\partial \underline{r}}$  for the constrained case when thrust must be orthogonal to the radial direction is to write it with respect to the  $\hat{\underline{e}}_r, \hat{\underline{e}}_s, \hat{\underline{e}}_w$  frame where  $\hat{\underline{e}}_r$  is parallel to the radius vector,  $\hat{\underline{e}}_w$  is normal to the orbit frame and  $\hat{\underline{e}}_s$  completes the orthogonal triad. In terms of the equinoctial basis vectors

$$\hat{\underline{e}}_r = (X_1 \hat{\underline{f}} + Y_1 \hat{\underline{g}})/r \quad (C. 6)$$

$$\hat{\underline{e}}_s = (-Y_1 \hat{\underline{f}} + X_1 \hat{\underline{g}})/r \quad (C. 7)$$

$$\hat{\underline{e}}_w = \hat{\underline{w}} \quad (C. 8)$$

Applying the inverse of this transformation to the previous  $\frac{\partial z}{\partial \underline{r}}$  equations yields

$$\begin{aligned} \frac{\partial a}{\partial \underline{r}} &= \frac{2}{na} (\dot{X}_1 + \dot{Y}_1 Y_1) \hat{\underline{e}}_r + \frac{2G}{n^2 a r} \hat{\underline{e}}_s \\ \frac{\partial h}{\partial \underline{r}} &= \frac{1}{\mu} \left[ \frac{GX_1}{r} \hat{\underline{e}}_r + \left( r\dot{X}_1 - \frac{GY_1}{r} \right) \hat{\underline{e}}_s \right] + \frac{k}{G} (qY_1 - pX_1) \hat{\underline{e}}_w \\ \frac{\partial k}{\partial \underline{r}} &= \frac{1}{\mu} \left[ \frac{GY_1}{r} \hat{\underline{e}}_r + \left( r\dot{Y}_1 + \frac{GX_1}{r} \right) \hat{\underline{e}}_s \right] - \frac{h}{G} (qY_1 - pX_1) \hat{\underline{e}}_w \\ \frac{\partial p}{\partial \underline{r}} &= \frac{1+p^2+q^2}{2G} Y_1 \hat{\underline{e}}_w \\ \frac{\partial q}{\partial \underline{r}} &= \frac{1+p^2+q^2}{2G} X_1 \hat{\underline{e}}_w \end{aligned} \quad (C. 9)$$

When thrust is constrained to be orthogonal to the radius vector, the  $\hat{\underline{e}}_r$  terms drop out. If this form is used in evaluating state equations there would be fewer calculations. The partials needed for the costate equations would also be simpler. The unconstrained case would still involve calculating all the terms.

## APPENDIX D

### SUN-EARTH RELATION

For the solar electric program, the sun's location in equinoctial coordinates is needed. The distance from earth to sun varies due to the ellipticity of earth's orbit. The following is taken from Reference 2.

The sun's location in earth equatorial coordinates is given by

$$\hat{\underline{R}}'_S = \begin{bmatrix} -\cos(\omega+v) \\ -\cos O \sin(\omega+v) \\ -\sin O \sin(\omega+v) \end{bmatrix} \quad (D.1)$$

where

$O$  is the obliquity of the ecliptic,

$\omega$  is the argument of perihelion,

$v$  is the true anomaly of the earth at the time of interest.

The true anomaly can be approximated by (see Ref. 37, p. 55)

$$v = M + (2e - \frac{e^3}{4})\sin M + \frac{5}{4}e^2\sin 2M + \frac{13}{12}e^3\sin 3M \quad (D.2)$$

and  $M = nt + M_0$ .

The orbital elements of the earth are taken from Ref. 37, p. 378, for an epoch of Julian Date 2436935.0 (1960 Jan. 1.5.E.T.). In particular,

$$\omega = 102^\circ 25' 25.3''$$

$$M_0 = -1^\circ 9' 05.62''$$

$$e = .016726$$

$$n = .985609^\circ/\text{day}$$

The distance to the sun (in A. U.) is just

$$|\underline{R}_s| = \frac{1 - e^2}{1 + e \cos v} \quad (D. 3)$$

The difference between the sun-spacecraft distance and the earth-sun distance is assumed negligible.

In equinoctial coordinates

$$\underline{\hat{R}}_s = [\underline{\hat{f}} \ \underline{\hat{g}} \ \underline{\hat{w}}]^T \underline{\hat{R}}'_s \quad (D. 4)$$

where the equinoctial basis vectors were given in Eq. (3.4). In the analysis, it is necessary to have the partials of the  $\underline{\hat{f}}$  and  $\underline{\hat{g}}$  components of  $\underline{\hat{R}}_s$  with respect to the equinoctial orbital elements. These two components are  $X_s = \underline{\hat{R}}_s \cdot \underline{\hat{f}}$  and  $Y_s = \underline{\hat{R}}_s \cdot \underline{\hat{g}}$ . Since  $\underline{\hat{f}}$  and  $\underline{\hat{g}}$  are functions only of  $p$  and  $q$ , we need

$$\begin{aligned} \frac{\partial X_s}{\partial p} &= \underline{\hat{R}}_s \cdot \frac{\partial \underline{\hat{f}}}{\partial p} = -\frac{2}{1+p^2+q^2} (qY_s + Z_s) \\ \frac{\partial X_s}{\partial q} &= \underline{\hat{R}}_s \cdot \frac{\partial \underline{\hat{f}}}{\partial q} = \frac{2pY_s}{1+p^2+q^2} \\ \frac{\partial Y_s}{\partial p} &= \underline{\hat{R}}_s \cdot \frac{\partial \underline{\hat{g}}}{\partial p} = \frac{2qX_s}{1+p^2+q^2} \\ \frac{\partial Y_s}{\partial q} &= \underline{\hat{R}}_s \cdot \frac{\partial \underline{\hat{g}}}{\partial q} = \frac{2(-pX_s + Z_s)}{1+p^2+q^2} \end{aligned} \quad (D. 5)$$

which utilize the formulas

$$\begin{aligned} \frac{\partial \underline{\hat{f}}}{\partial p} &= -\frac{2}{1+p^2+q^2} (q \underline{\hat{g}} + \underline{\hat{w}}) \\ \frac{\partial \underline{\hat{f}}}{\partial q} &= \frac{2p}{1+p^2+q^2} \underline{\hat{g}} \\ \frac{\partial \underline{\hat{g}}}{\partial p} &= \frac{2q}{1+p^2+q^2} \underline{\hat{f}} \\ \frac{\partial \underline{\hat{g}}}{\partial q} &= \frac{2}{1+p^2+q^2} (-p \underline{\hat{f}} + \underline{\hat{w}}) \end{aligned} \quad (D. 6)$$

## APPENDIX E

### WORST CASE EVALUATION OF SUBOPTIMAL APPROXIMATION

In Section 3.6 two reasons were given for utilizing a suboptimal approximation where only part of the Hamiltonian is maximized with respect to the thrust direction. The first reason is that it reduces the optimality condition from the root of a 6th to a 3rd order polynomial. The latter can be solved in closed form with consequent savings in machine time. The second reason is that it is aesthetically unsatisfying to bias the control so that the desired acceleration component is decreased while the thrust is increased. This result is mathematically time optimal because it increases the mass flow rate and reduces the mass. While time optimal solutions are of more practical interest than fuel optimal solution, it does not seem desirable to simply throw fuel away.

This appendix is intended to show that the suboptimal approximation is negligibly different from the time optimal case for practical missions by analyzing the worst possible case. This case occurs when the radius vector to the spacecraft is always at right angles to the Earth-sun line and the primer vector is orthogonal to the Earth-sun line. A simple example of such a case is the coplanar enlargement of a circular orbit normal to the earth sun line. Such a case will be characterized by a 41% increase in  $\Delta V$  and a 100% increase in flight time as compared to the unconstrained case. For the more practical examples treated in the body of this report, the fuel and time penalties due to attitude constraints are much smaller than this. For these practical cases, the difference between the suboptimal and minimum time solutions will be smaller than for the extreme case treated herein.

This case may be characterized by only two state variables, the mean orbital speed  $v$  and the mass  $m$ . The rates of change of these two variables are given in Eqs. E. 1 and E. 2.

$$\dot{v} = - \frac{2P_o}{mc} \cos\psi \sin\psi \quad (\text{E. 1})$$

$$\dot{m} = -\frac{2P_0}{c^2} \cos \psi \quad (\text{E. 2})$$

The Hamiltonian of this problem is given by Eq. E. 3.

$$H = -\lambda_v \frac{2P_0}{mc} \cos \psi \sin \psi - \lambda_m \frac{2P_0}{c^2} \cos \psi \quad (\text{E. 3})$$

The value of the yaw angle  $\psi$  that maximizes H is given by Eq. E. 4.

$$\sin \psi^* = \sqrt{\left(\frac{\lambda_m m}{4\lambda_v c}\right)^2} + \frac{1}{2} - \frac{\lambda_m m}{4\lambda_v c} \quad (\text{E. 4})$$

The rates of change of the Lagrange multipliers are given by the canonical Eqs. E. 5 and E. 6.

$$\dot{\lambda}_v = 0 \quad (\text{E. 5})$$

$$\dot{\lambda}_m = -\lambda_v \frac{2P_0}{m^2 c} \sin \psi \cos \psi \quad (\text{E. 6})$$

Three first integrals result from equations E. 5, E. 7 and E. 8. Equation E. 7 follows from the autonomous nature of the problem while Eq. E. 8 follows from Eq. E. 3.

$$\dot{H} = 0 \quad (\text{E. 7})$$

$$\frac{d\lambda_m m}{dt} = m\dot{\lambda}_m + \dot{m}\lambda_m = H \quad (\text{E. 8})$$

The three first integrals resulting from these equations are given by E. 9, E. 10 and E. 11. The values of the integrals follow from the transversality conditions for a minimum time problem.

$$H = -1 \quad (\text{E. 9})$$

$$\lambda_m m = -(t-t_f) \quad (\text{E. 10})$$

$$\lambda_v = \frac{m_f c}{P_0} \quad (\text{E. 11})$$

Substituting into Eq. E. 4 yields E. 11

$$\sin \psi^* = \sqrt{\left(\frac{t-t_f}{4m_f c} P_o\right) + \frac{1}{2}} + \frac{t-t_f}{4m_f c^2} P_o \quad (\text{E. 12})$$

The problem can now be solved by quadrature to yield Eqs. E. 13, E. 14 and E. 15.

$$\frac{m}{m_f} = 2 \cos^2 \psi \cot \psi \quad (\text{E. 13})$$

$$v_f - v = c \left[ \sqrt{2} - 2 \sin \psi + 3 \ln \frac{\sec \psi + \tan \psi}{1 + \sqrt{2}} \right] \quad (\text{E. 14})$$

$$t_f - t = \frac{m_f c^2}{2P_o} [4 \sin \psi - 2 \csc \psi] \quad (\text{E. 15})$$

The corresponding results for the suboptimal approximation used in the paper are given by Eqs. E. 16 and E. 17.

$$v_f - v = \frac{c}{\sqrt{2}} \ln \frac{m}{m_f} \quad (\text{E. 16})$$

$$t_f - t = \frac{c^2}{\sqrt{2} P_o} (m - m_f) \quad (\text{E. 17})$$

The optimal and suboptimal cases are compared in Fig. E-1, which plots the normalized time and mass against the normalized velocity change. The plot shows that the difference between the two cases is negligible for mass ratios characteristic of SERT-C ( $> .84$ ). For smaller mass ratios the suboptimal approximation will take longer but use less fuel than the minimum time case. For practical missions the differences should be indistinguishable.

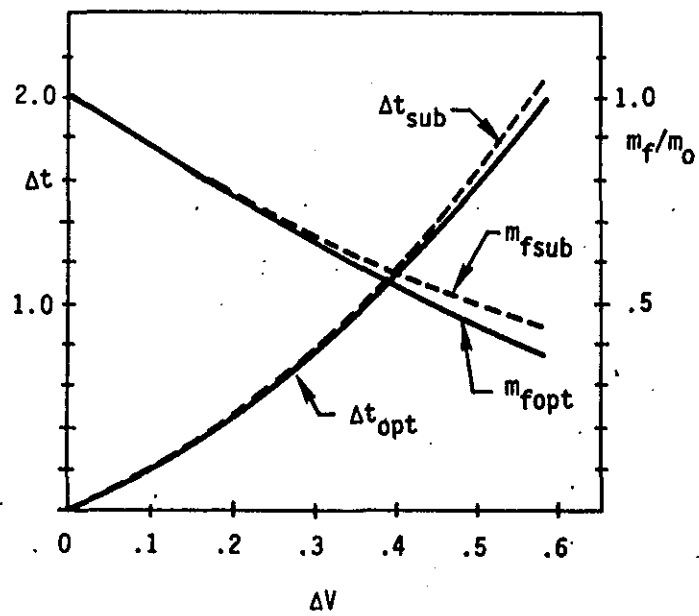


Fig. E-1 Normalized Time and Mass Change Versus Normalized Velocity Change

APPENDIX F

SINGLE AVERAGED OBLATENESS EQUATIONS

In these equations  $R_e$  is the earth's radius,  $\mu$  is the gravitational constant,  $n$  is the orbital angular speed,  $J_2$  the oblateness coefficient and  $a, h, k, p, q$  the equinoctial orbital elements.

Table F-1  $J_2$  Variation of Parameters Equations

$$\dot{h}_{J_2} = \frac{3\mu R_e^2 J_2 k [1 - 6(1^2 + q^2) + 3(p^2 + q^2)^2]}{2na^5 (1 - h^2 - k^2) (1 + p^2 + q^2)^2}$$

$$\dot{k}_{J_2} = \frac{3\mu R_e^2 J_2 h [1 - 6(p^2 + q^2) + 3(p^2 + q^2)^2]}{2na^5 (1 - h^2 - k^2)^2 (1 + p^2 + q^2)^2}$$

$$\dot{p}_{J_2} = \frac{3\mu R_e^2 J_2 q (1 - p^2 - q^2)}{2na^5 (1 - h^2 - k^2)^2 (1 + p^2 + q^2)}$$

$$\dot{q}_{J_2} = \frac{3\mu R_e^2 J_2 p (1 - p^2 - q^2)}{2na^5 (1 - h^2 - k^2)^2 (1 + p^2 + q^2)}$$

Table F-2 Partial of  $J_2$  Equations with Respect to  $a$

$$\frac{\partial \dot{h}}{\partial a} = -\frac{7}{2} \frac{\dot{h}}{a}$$

$$\frac{\partial \dot{k}}{\partial a} = -\frac{7}{2} \frac{\dot{k}}{a}$$

$$\frac{\partial \dot{p}}{\partial a} = -\frac{7}{2} \frac{\dot{p}}{a}$$

$$\frac{\partial \dot{q}}{\partial a} = -\frac{7}{2} \frac{\dot{q}}{a}$$

Table F-3 Partial of  $J_2$  Equations with Respect to  $h$

$$\frac{\partial \dot{h}}{\partial h} = \frac{4h\dot{h}}{1-h^2-k^2}$$

$$\frac{\partial \dot{k}}{\partial h} = \frac{\dot{k}}{h} + \frac{4hk}{1-h^2-k^2}$$

$$\frac{\partial \dot{p}}{\partial h} = \frac{4h\dot{p}}{1-h^2-k^2}$$

$$\frac{\partial \dot{q}}{\partial h} = \frac{4h\dot{q}}{1-h^2-k^2}$$

Table F-4 Partial of  $J_2$  Equations with Respect to  $k$

$$\frac{\partial \dot{h}}{\partial k} = \frac{\dot{h}}{k} + \frac{4k\dot{h}}{1-h^2-k^2}$$

$$\frac{\partial \dot{k}}{\partial k} = \frac{4k\dot{k}}{1-h^2-k^2}$$

$$\frac{\partial \dot{p}}{\partial k} = \frac{4k\dot{p}}{1-h^2-k^2}$$

$$\frac{\partial \dot{q}}{\partial k} = \frac{4k\dot{q}}{1-h^2-k^2}$$

Table F-5 Partial of  $J_2$  Equations with Respect to  $p$

$$\frac{\partial \dot{h}}{\partial p} = \left( \frac{12\mu R_e^2 J_2}{na^5} \right) \frac{kp(3(p^2+q^2)-2)}{(1-h^2-k^2)^2 (1+p^2+q^2)^3}$$

$$\frac{\partial \dot{k}}{\partial p} = \left( \frac{12\mu R_e^2 J_2}{na^5} \right) \frac{hp(3(p^2+q^2)-2)}{(1-h^2-k^2)^2 (1+p^2+q^2)^3}$$

$$\frac{\partial \dot{p}}{\partial p} = \frac{-2\dot{p}}{1-(p^2+q^2)^2}$$

$$\frac{\partial \dot{q}}{\partial p} = \frac{-\dot{q}}{p} \left[ \frac{1+(p^2+q^2)^2}{1-(p^2+q^2)^2} \right]$$

Table F-6 Partial of  $J_2$  Equations with Respect to  $q$

$$\frac{\partial \dot{h}}{\partial q} = \left( \frac{12\mu R_e^2 J_2}{na^5} \right) \frac{kq(3(p^2+q^2)-2)}{(1-h^2-k^2)^2 (1+p^2+q^2)^3}$$

$$\frac{\partial \dot{k}}{\partial q} = \left( \frac{12\mu R_e^2 J_2}{na^5} \right) \frac{hq(3(p^2+q^2)-2)}{(1-h^2-k^2)^2 (1+p^2+q^2)^3}$$

$$\frac{\partial \dot{p}}{\partial q} = \frac{-\dot{p}}{q} \left[ \frac{1+(p^2+q^2)^2}{1-(p^2+q^2)^2} \right]$$

$$\frac{\partial \dot{q}}{\partial q} = \frac{-2\dot{q}}{1-(p^2+q^2)^2}$$

## APPENDIX G

### SHADOW CALCULATIONS

This appendix contains a summary of results from Ref. 2 for shadowing. From geometrical considerations an equation can be derived which the entry and exit angles must satisfy. Such an equation is given in Reference 38 and the equation given in this section is essentially the same, except that it is given in terms of equinoctial orbital elements.

The spacecraft position is given by

$$\underline{r} = X_1 \underline{\hat{f}} + Y_1 \underline{\hat{g}} \quad (G.1)$$

where  $X_1$  and  $Y_1$  were given in Eq. (3.19) and (3.20). Let the unit vector from the earth to the sun be given by

$$\underline{\hat{R}}_s = X_s \underline{\hat{f}} + Y_s \underline{\hat{g}} + Z_s \underline{\hat{w}}$$

This is in terms of the equinoctial coordinate frame and thus depends on the equinoctial orbital elements  $p$  and  $q$ . The calculation of the sun's direction in the equinoctial coordinate system is discussed in Appendix D. If  $a_e$  designates the earth's radius, the cosine of the angle between  $\underline{r}$  and  $\underline{\hat{R}}_s$  is given by

$$\frac{\underline{\hat{R}}_s \cdot \underline{r}}{|\underline{r}|} = - \frac{(|\underline{r}|^2 - a_e^2)^{1/2}}{|\underline{r}|} \quad (G.2)$$

or,

$$X_1 X_s + Y_1 Y_s = - (|\underline{r}|^2 - a_e^2)^{1/2} \quad (G.3)$$

Squaring and rearranging

$$S \equiv (1 - X_s^2) X_1^2 + (1 - Y_s^2) Y_1^2 - 2 X_s Y_s X_1 Y_1 - a_e^2 = 0 \quad (G.4)$$

This is the shadow equation which must be satisfied by the entry and exit angles.  $X_1$  and  $Y_1$  are functions of  $\cos F$ ,  $\sin F$ ,  $a$ ,  $h$ , and  $k$  (see Eq. (3.19) and (3.20)). By further manipulations one can derive a quartic equation in  $\cos F$ . The coefficients

of this quartic equation are given in Table G-1. Spurious roots can be eliminated by the criteria that  $S = 0$  and that  $\underline{R} \cdot \underline{r} < 0$ . In addition, for the entry angle  $\partial S/\partial F < 0$  and for the exit angle  $\partial S/\partial F > 0$ .

Table G-1 The Shadow Quartic Equation

$$b_1 = 1 - h^2 \beta$$

$$b_2 = hk\beta$$

$$b_3 = 1 - k^2 \beta$$

$$d_1 = 1 - X_s^2$$

$$d_2 = 1 - Y_s^2$$

$$d_3 = 2Y_s X_s$$

$$h_1 = d_1(b_1^2 - b_2^2) + d_2(b_2^2 - b_3^2) - d_3(b_1 b_2 - b_2 b_3)$$

$$h_2 = -2d_1 k b_1 - 2d_2 h b_2 + d_3(k b_2 + h b_1)$$

$$h_3 = d_1(b_2^2 + k^2) + d_2(b_3^2 + h^2) - d_3(b_2 b_3 + h k) - \frac{a^2}{a^2}$$

$$h_4 = 2b_1 b_2 d_1 + 2b_2 b_3 d_2 - d_3(b_2^2 + b_1 b_3)$$

$$h_5 = -2k b_2 d_1 - 2h b_3 d_2 + d_3(k b_3 + h b_2)$$

$$A_0 = h_1^2 + h_4^2$$

$$A_1 = 2h_1 h_2 + 2h_4 h_5$$

$$A_2 = h_2^2 + 2h_3 h_1 - h_4^2 + h_5^2$$

$$A_3 = 2h_3 h_2 - 2h_4 h_5$$

$$A_4 = h_3^2 - h_5^2$$

$$S^* = A_0 \cos^4 F + A_1 \cos^3 F + A_2 \cos^2 F + A_3 \cos F + A_4 = 0$$

### Derivatives of F and S

The derivative of F with respect to  $\bar{z}$  is needed to evaluate the costate equation. It can be obtained implicitly from the shadow equation.

$$\frac{dF}{d\bar{z}} = - \frac{\partial S}{\partial \bar{z}} / \frac{\partial S}{\partial F} \quad (G. 5)$$

These partials are listed in Table G-2. Note that in calculating  $\partial S/\partial p$  and  $\partial S/\partial q$  we have taken into account the fact that the sun's direction is given in equinoctial coordinates and therefore made use of the partial given in Appendix D.

Table G-2 Partial of the Shadow Function

$$\frac{\partial S}{\partial F} = 2 \left[ (1-X_s^2)X_1 - X_s Y_s Y_1 \right] \frac{\partial X_1}{\partial F} + 2 \left[ (1-Y_s^2)Y_1 - X_s Y_s X_1 \right] \frac{\partial Y_1}{\partial F}$$

$$\frac{\partial X_1}{\partial F} = a \left[ -(1-h^2 \beta) \sin F + hk \beta \cos F \right]$$

$$\frac{\partial Y_1}{\partial F} = a \left[ -hk \beta \sin F + (1-k^2 \beta) \cos F \right]$$

$$\frac{\partial S}{\partial a} = \frac{2a_e^2}{a}$$

$$\frac{\partial S}{\partial h} = 2 \left[ (1-X_s^2)X_1 - X_s Y_s Y_1 \right] \frac{\partial X_1}{\partial h} + 2 \left[ (1-Y_s^2)Y_1 - X_s Y_s X_1 \right] \frac{\partial Y_1}{\partial h}$$

$$\frac{\partial S}{\partial k} = 2 \left[ (1-X_s^2)X_1 - X_s Y_s Y_1 \right] \frac{\partial X_1}{\partial k} + 2 \left[ (1-Y_s^2)Y_1 - X_s Y_s X_1 \right] \frac{\partial Y_1}{\partial k}$$

$$\frac{\partial S}{\partial p} = -4 \left[ X_1^2 X_s + X_1 Y_1 Y_s \right] \left[ \frac{q Y_s + Z_s}{1+p^2+q^2} \right] - 4 \left[ Y_1^2 Y_s + X_1 Y_1 X_s \right] \left[ \frac{q X_s}{1+p^2+q^2} \right]$$

$$\frac{\partial S}{\partial q} = -4 \left[ X_1^2 X_s + X_1 Y_1 Y_s \right] \left[ \frac{p Y_s}{1+p^2+q^2} \right] - 4 \left[ Y_1^2 Y_s + X_1 Y_1 X_s \right] \left[ \frac{-p X_s + Z_s}{1+p^2+q^2} \right]$$

## LIST OF REFERENCES

1. Cake, J. E., and J. D. Regetz, Jr., Development of a Unified Guidance System for Geocentric Transfer, NASA Technical Memorandum, NASA TMX-7-648, March 1975.
2. Sackett, L. L., H. L. Malchow, T. N. Edelbaum, The Computation of Time Optimal Geocentric Transfers Using Solar or Nuclear Electric and High Thrust Propulsion, Report No. R-880, The Charles Stark Draper Laboratory, Inc., May 1975.
3. Jasper, T. P., "Low-Thrust Trajectory Analysis for the Geosynchronous Mission", AIAA Paper 73-1073, Lake Tahoe, 1973.
4. William, D. F., MOLTOP Users Manual, Northrup Service, Inc., Report No. M-240-1224, October 1973.
5. Horsewood, J. L., P. F. Flanagan, F. I. Mann, Program Manual for the Systems Evaluation of Orbit Raising (SEOR), Report No. 74-11, The Analytical Mechanics Associates, Inc., March 1974.
6. SERT-C Project Study, NASA Technical Memorandum, NASA TMX-71508, January 1974.
7. Sackett, L. L., T. N. Edelbaum, H. L. Malchow, A Users Manual for a Computer Program which Calculates Time Optimal Geocentric Transfers Using Solar or Nuclear Electric and High Thrust Propulsion, Report No. R-827, The Charles Stark Draper Laboratory, Inc., June 1974.
8. Edelbaum, T. N., L. L. Sackett, H. L. Malchow, "Optimal Low Thrust Geocentric Transfer", AIAA Paper No. 73-1074, Lake Tahoe, 1973.
9. Sackett, L. L., and T. N. Edelbaum, "Optimal High- and Low-Thrust Geocentric Transfer", AIAA Paper 74-801, Anaheim, 1974.
10. Kryloff, N., and N. Bogoliuboff, Introduction to Non-Linear Mechanics, Princeton University Press, 1947.
11. Broucke, R. A., and P. J. Cefola, "On the Equinoctial Orbital Elements", Celestial Mechanics, Vol. 5, pp. 303-310, 1972.
12. Edelbaum, T. N., "Optimal Thrust-Limited Orbit Transfer in Strong Gravitational Fields", Lecture Notes in Mathematics, 132 Symposium on Optimization, Springer Verlag, Berlin, 1970.
13. Edelbaum, T. N., "Optimal Power Limited Orbit Transfer in Strong Gravity Fields", AIAA J., Vol. 3, No. 6, 1965.

14. Cefola, P. J., "Equinoctial Orbit Elements -- Application to Artificial Satellite Orbits", AIAA Paper No. 72-937, Palo Alto, 1972.
15. Uphoff, C., "Numerical Averaging in Orbit Prediction", AIAA Paper No. 72-934, Palo Alto, September 1972.
16. Kaufman, B., "Variation of Parameters and Long-Term Behavior of Planetary Orbiters", AIAA Paper 70-1055, Santa Barbara, August 1970.
17. Small, H. W., Minimum Fuel Time-Free Transfer Between Elliptic Orbits, Ph.D. Dissertation, Stanford University, 1972.
18. Small, H. W., "Minimum N-Impulse Time-Free Transfers between Elliptic Orbits", AIAA Journal, Vol. 9, No. 4, April 1971.
19. Edelbaum, T. N., "The Use of High- and Low-Thrust Propulsion in Combination for Space Missions", J. Astronautical Sciences, Vol. 9, No. 2, pp. 49-60, 1962.
20. Fimple, W. R., "An Improved Theory of the Use of High and Low Thrust Propulsion in Combination", J. Astro. Sci., Vol. 10, No. 10, 1963.
21. Grodzovsky, G. L., Y. N. Ivanov, V. V. Tolkaref, Mechanics of Low-Thrust Spaceflight, NASA TTF-507, 1969.
22. Haxelrigg, G. A., "Optimal Space Flight with Multiple Propulsion Systems", J. Spacecraft and Rockets, October 1968.
23. Vahlberg, C. J., and T. N. Edelbaum, "Transfers Between Coplanar Coaxial Ellipses Using the Combination of High- and Low Thrust Propulsion", AIAA Paper No. 71-368, Ft. Lauderdale, 1971.
24. Sackett, L. L., and T. N. Edelbaum, Solar Electric Geocentric Transfer With Attitude Constraints: Program Manual, Report R-902, The Charles Stark Draper Laboratory, Inc., August, 1975.
25. Sackett, L. L., and T. N. Edelbaum, "Effect of Attitude Constraints on Solar-Electric Geocentric Transfers", AIAA Paper 75-350, New Orleans, 1975.
26. Malchow, H. L. and C. K. Whitney, "A Radiation Model for Geocentric Trajectory Calculations", AIAA Paper 75-351, New Orleans, 1975.
27. System /360 Scientific Subroutine Package Version IV, Programmers Manual, GH20-0205-4, IBM Corp., 5th Ed., 1970
28. Cefola, P. J., A. C. Long, G. Holloway, Jr., "The Long-Term Prediction of Artificial Satellite Orbits", AIAA Paper No. 74-170, Washington, D. C., 1974.

29. Horsewood, J. L., F. F. Flanagan, F. I. Mann, Program Manual for the Systems Evaluation of Orbit Raising (SEOR) Computer Program, Report No. 75-23, Analytical Mechanics Associates, Inc., July 1975.
30. Obenschain, A. F., et al, The Solar Array Synthesis Computer Program, NASA TMX-63709, September 1969.
31. GEOTOP II. A Precision Low-Thrust Geosynchronous Optimization Program Rockwell International Corp., Space Division, SD 72-SA-0247-1, Jan. 5, 1973.
32. Ives, N. E., Power Decay Characteristics for a Solar Electrically Propelled Spacecraft During Orbit Expansion to Synchronous Heights, Royal Aircraft Establishment Report No. 71075, April 1971.
33. Stassinopoulos, E., and G. Mead, ALLMAG, GDALMG, LINTRA Computer Programs for Geomagnetic Field and Field Line Calculations, NSSDC 72-12, Feb. 1972.
34. Teague, J., and J. Vette, The Use of the Inner Zone Electron Model AE-5 and Associated Computer Programs, NSSDC 72-11, Nov. 1972.
35. Rasmussen, R., "Calculation of 1MEV Electron Flux and Irradiation Degradation of Solar Cell I-V Curves by Computer", Proceedings of the Sixth Photovoltaic Specialists Conference, Cocoa Beach, Florida, March 28, 1967.
36. Carter, J., and H. Y. Tada, Solar Cell Radiation Handbook, TRW Systems Group, June 1973.
37. Battin, R. H., Astronautical Guidance, McGraw-Hill, New York, 1964.
38. Escobal, P. R., Methods of Orbit Determination, Wiley, New York, 1965.

<b>REPORT DOCUMENTATION PAGE</b>			<i>Form Approved</i> <i>OMB No. 0704-0188</i>	
Public reporting burden for this collection of information is estimated to average 1 hour per response, including the time for reviewing instructions, searching existing data sources, gathering and maintaining the data needed, and completing and reviewing the collection of information. Send comments regarding this burden estimate or any other aspect of this collection of information, including suggestions for reducing this burden, to Washington Headquarters Services, Directorate for Information Operations and Reports, 1215 Jefferson Davis Highway, Suite 1204, Arlington, VA 22202-4302, and to the Office of Management and Budget, Paperwork Reduction Project (0704-0188), Washington, DC 20503.				
<b>1. AGENCY USE ONLY (Leave blank)</b>		<b>2. REPORT DATE</b> August 1975	<b>3. REPORT TYPE AND DATES COVERED</b> Final Contractor Report	
<b>4. TITLE AND SUBTITLE</b>  Solar Electric Geocentric Transfer With Attitude Constraints: Analysis			<b>5. FUNDING NUMBERS</b>  NAS3-18886	
<b>6. AUTHOR(S)</b>  Lester L. Sackett, Harvey L. Malchow, and Theodore N. Edelbaum				
<b>7. PERFORMING ORGANIZATION NAME(S) AND ADDRESS(ES)</b>  The Charles Stark Draper Laboratory, Inc. 68 Albany Street Cambridge, Massachusetts 02139			<b>8. PERFORMING ORGANIZATION REPORT NUMBER</b>  E-12239	
<b>9. SPONSORING/MONITORING AGENCY NAME(S) AND ADDRESS(ES)</b>  National Aeronautics and Space Administration Cleveland, Ohio 44135-3191			<b>10. SPONSORING/MONITORING AGENCY REPORT NUMBER</b>  NASA CR-134927	
<b>11. SUPPLEMENTARY NOTES</b>  Project Manager, James Cake, Spacecraft Technology Division, NASA Lewis Research Center, Cleveland, Ohio.				
<b>12a. DISTRIBUTION/AVAILABILITY STATEMENT</b>  Unclassified - Unlimited			<b>12b. DISTRIBUTION CODE</b>	
<b>13. ABSTRACT (Maximum 200 words)</b>  A time optimal or nearly time optimal trajectory program has been developed for solar electric geocentric transfer with or without attitude constraints and with an optional initial high thrust stage. The method of averaging reduces computation time. A nonsingular set of orbital elements is used. The constraints, which are those of one of the SERT-C designs, introduce complexities into the analysis and the solution yields possible discontinuous changes in thrust direction. The power degradation due to VanAllen radiation is modeled analytically. A wide range of solar cell characteristics may be assumed. Effects such as oblateness and shadowing may be included. This report contains the analysis and the results of many example runs.				
<b>14. SUBJECT TERMS</b>  Solar electric; Geocentric transfer; Optimal trajectories; Low thrust; Attitude constraints			<b>15. NUMBER OF PAGES</b> 138	
			<b>16. PRICE CODE</b> A07	
<b>17. SECURITY CLASSIFICATION OF REPORT</b> Unclassified	<b>18. SECURITY CLASSIFICATION OF THIS PAGE</b> Unclassified	<b>19. SECURITY CLASSIFICATION OF ABSTRACT</b> Unclassified	<b>20. LIMITATION OF ABSTRACT</b>	